PROTON AND ELECTRON EFFECTS IN THERMAL CONTROL MATERIALS

FINAL REPORT FOR THE PROGRAM :

Degradation Tests on Thermal Control Materials

May 1970

CONTRACT NO. NAS5-11219

PREPARED BY
THE BOEING COMPANY
AEROSPACE GROUP
SEATTLE, WASHINGTON

FOR

GODDARD SPACE FLIGHT CENTER
GREENBELT, MARYLAND

PROTON AND ELECTRON EFFECTS IN THERMAL CONTROL MATERIALS

FINAL REPORT FOR THE PROGRAM :

Degradation Tests on Thermal Control Materials

CONTRACT NO. NAS5-11219

GODDARD SPACE FLIGHT CENTER

CONTRACTING OFFICER: W.A. Landymore

TECHNICAL MONITOR: Charles H. Duncan, 713

PREPARED BY: Lawrence B. Fogdall
TECHNICAL LEADER

Sheridan S Cannaday
PRINCIPAL INVESTIGATOR

SUPERVISED BY: Richard A. Brown
PROGRAM LEADER

THE BOEING COMPANY
AEROSPACE GROUP
SEATTLE, WASHINGTON

FOR

GODDARD SPACE FLIGHT CENTER
GREENBELT, MARYLAND

ABSTRACT

This document is the final report of experimental and analytical work performed for NASA-Goddard Space Flight Center under Contract NAS5-11219. The effects of 35-keV electrons and 40-keV protons on the reflectance and degradation properties of selected specular and diffuse thermal control materials tested at room temperatures have been studied and compared. FEP Teflon, Alzak, Kapton, and diffuse white paints have been emphasized. Exposure rates on the order of 10^{10} particles/cm^2-second have been used. Reflectance measurements between 0.24 and 2.54 microns wavelength have been made in situ on test specimens at various exposure levels up to about 2×10^{16} particles/cm^2. Plots of the materials' reflectance properties as a function of wavelength have been obtained with computer processing of test data, and are presented. Comparison of the proton and electron exposure results shows that four different types of spectral reflectance degradation characteristics obtain in the 18 types of materials tested in both particle environments. Plots showing these damage classifications are included, and coatings offering best solar absorptance stability (such as 2-mil silvered Teflon) are identified. A coating temperature study, a proton energy study, combined particle-ultraviolet radiation studies, and in situ capability for coating emittance measurements following exposure to charged particles are recommended as being important for future effort and understanding.

KEY WORDS

Electron
Hemispherical spectral reflectance
In situ
Kilo electron volt (keV)
Proton
Radiation Effects
Solar absorptance
Spectrophotometer
Thermal control coatings
Vacuum

The following Boeing personnel have contributed to this program:

Richard R. Brown	Program Leader
Lawrence B. Fogdall	Technical Leader
Sheridan S. Cannaday	Principal Investigator
Loren D. Milliman and Marc Hansen	Computer Software and Data Processing
Edward D. Sullivan	Test Equipment and Monitoring
Betty Barry and C.R. Brittain, Jr.	Test Monitoring and Data Reduction

TABLE OF CONTENTS

LIST OF ILLUSTRATIONS

LIST OF ILLUSTRATIONS (Continued)

LIST OF ILLUSTRATIONS (Continued)

LIST OF ILLUSTRATIONS (Continued)

LIST OF TABLES

1.0 INTRODUCTION

This program, under Contract NAS5-11219 of NASA's Goddard Space Flight Center, has been essentially experimental testing and evaluation of proton and electron effects in thermal control coatings. This introduction is a general discussion of the work called for, and a summary of the findings in the program.

1.1 PROGRAM DESCRIPTION

Two separate exposure studies—one with 35-keV (kiloelectron-volt) electrons and the other with 40-keV protons—have been conducted. Particle energies have been selected to provide data useful in predicting performance of currently-used thermal control coatings in the near-Earth space environment. The electron energy of 35-keV is intermediate between earlier 20-keV and 50-keV electron tests done by Boeing for NASA-Goddard under Contract NAS5-11164 (Reference 1).

Eighteen types of thermal control materials have been evaluated as part of the electron study, providing reflectance performance and degradation information after exposures ranging from 5×10^{12} to 1×10^{16} electrons/cm^2 (35-keV). Further description of test parameters applying to this study are contained in Sections 2.2.1 and 2.3.1.

The performance and degradation of 23 types of thermal control materials have been evaluated after exposure to 40-keV proton fluences ranging from 1×10^{12} to nearly 2×10^{16} protons/cm^2. Test details for this study are to be found in Sections 2.2.2 and 2.3.2.

Test results (Section 2.5) for each type of thermal control coating or surface at each exposure fluence interval are in the form of plots of hemispherical spectral reflectance as a function of wavelength between 0.24 and 2.54 microns, and in the form of solar absorptance (α_s) tables. The plots presented in this final report document are the result of computer processing of original test data, employing a combination of *in situ* integrating sphere reflectometer, far UV Beckman DK-2A spectrophotometer, Datex data encoder/selector, and IBM 526 card punch. Assurance that processed data closely approximate absolute reflectance is discussed in Section 2.4.

1.2 SUMMARY OF PROGRAM RESULTS

Results obtained in the 35-keV electron study are about as expected and thus fit well with the sets of data obtained in earlier programs (NAS5-11164 and NAS5-9650) at electron energies of 20 keV, 50 keV, and 80 keV. The diffuse white paints sustain large amounts of reflectance degradation in the infrared wavelength region, whereas the specular coatings are more sensitive at the shorter wavelengths (ultraviolet and visible).

In some coatings 40-keV proton exposure yields degradation that is spectrally similar to electron degradation. In others (mostly white paints) reflectance damage characteristics as a function of wavelength are quite different as electron and proton data are compared. Each of the 18 coating types exposed both to electrons and to protons can be classified by one of four spectral damage characteristics (Figures 1 through 4). Figure 1 is a comparison of reflectance changes in 2-mil aluminized Kapton as a function of wavelength, after separate 35-keV electron and 40-keV proton exposures to 1×10^{15} and 1×10^{16} particles/cm^2. After both kinds of particle exposure, reflectance changes peak in the spectral band just longer than the wavelength of the material's dominant absorption edge. These damage characteristics also apply to 2-mil, 5-mil, and 10-mil silvered FEP Teflon.

Figure 2 is a comparison of proton and electron effects (same fluences as above) in 2-mil aluminized FEP Teflon. The same spectral damage characteristics also apply to 5-mil and 10-mil aluminized FEP Teflon; to 3 thicknesses of Alzak anodized aluminum studied(0.15-mil, 0.22-mil, and 0.34-mil); to vapor-deposited SiO_2 over aluminum; and to one of the white paints having a wide band gap pigment, aluminum oxide in potassium silicate. In all these materials, reflectance damage peaks at or near the shortest wavelengths measured.

The remaining six types of white paints can properly be divided into two categories. One, in which reflectance damage is broad-band, extending throughout most or all of the visible and infrared wavelength region measured, applies to the other two potassium silicate-bound coatings studied. Both these coatings have another pigment besides aluminum oxide. Figure 3 compares proton and electron

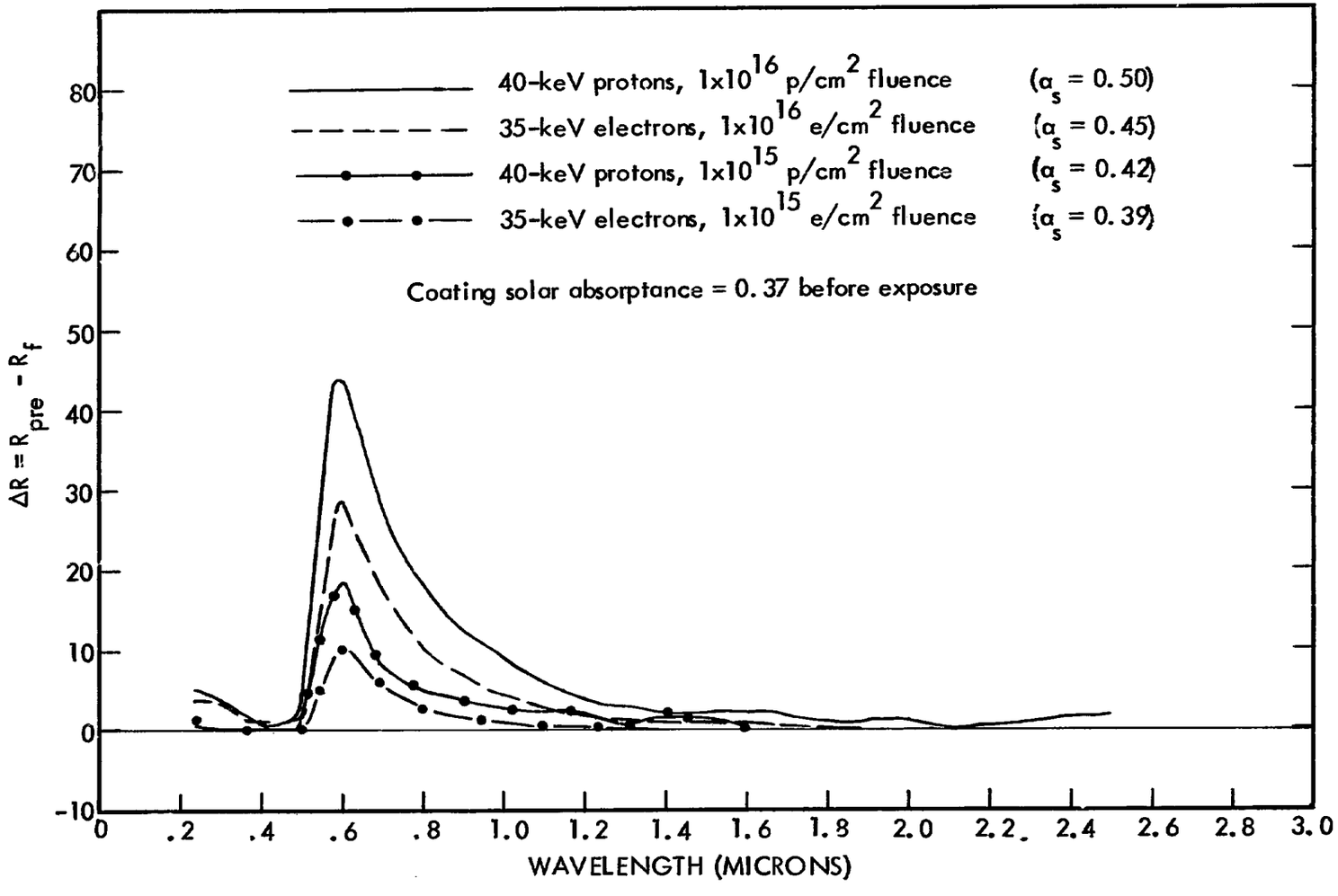

Figure 1. Comparison of Proton and Electron Effects in 2-mil Aluminized Kapton

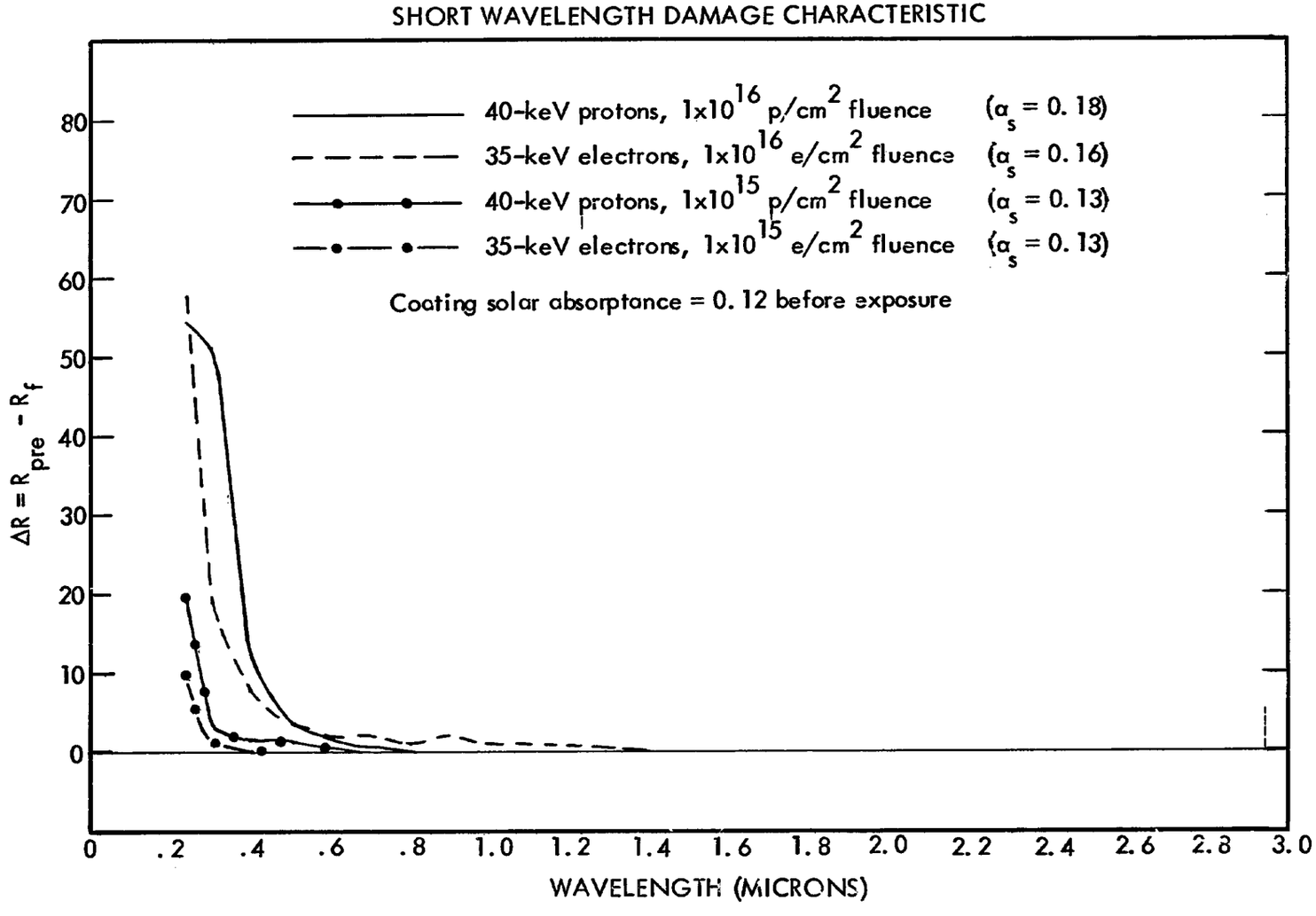

Figure 2. Comparison of Proton and Electron Effects in 2-mil Aluminized Teflon

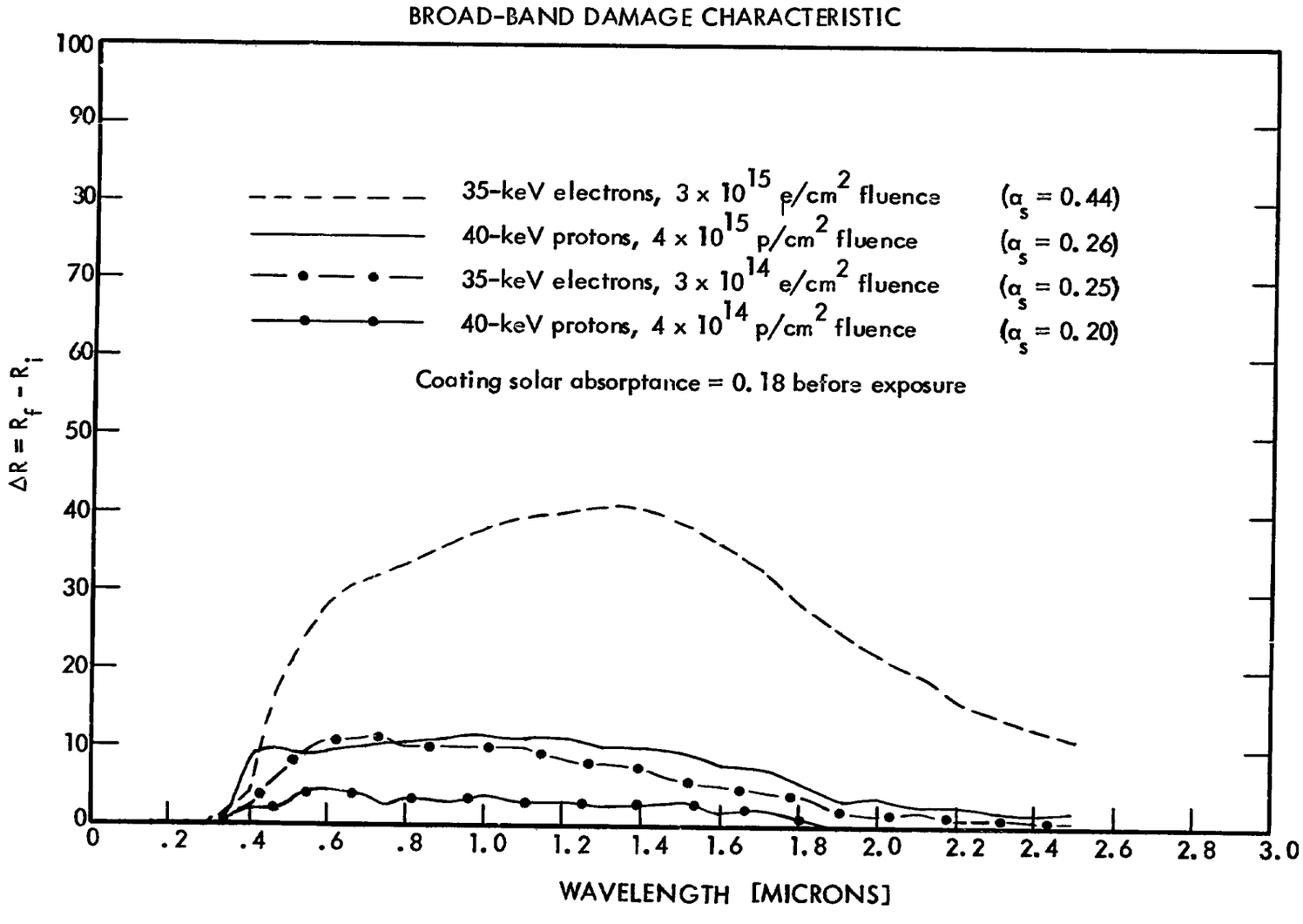

Figure 3. Comparison of Proton and Electron Effects in TiO_2 / Al_2O_3 — K_2SiO_3

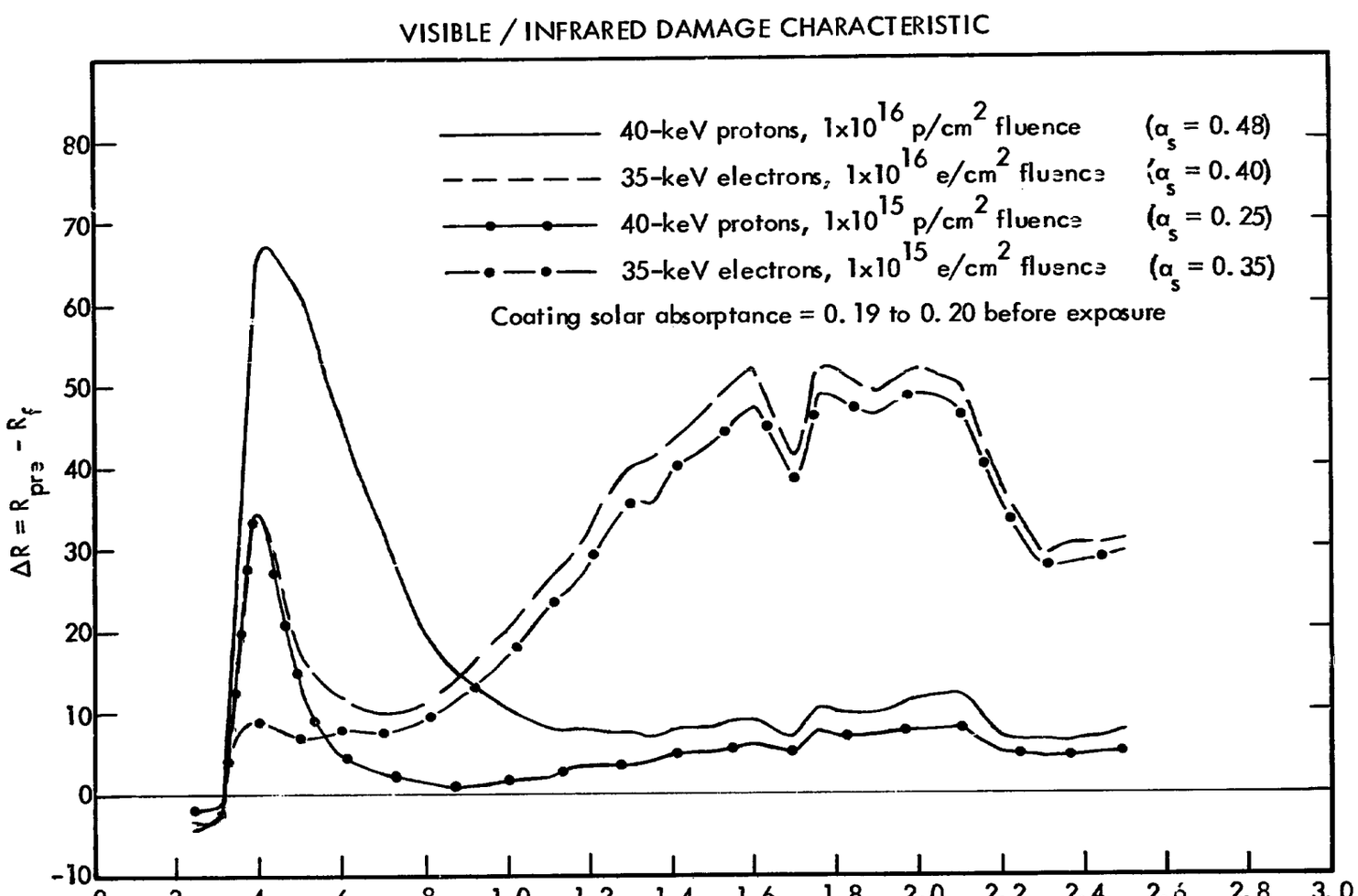

Figure 4. Comparison of Proton and Electron Effects in an Early S-13G Formulation

effects at similar fluences (3 or 4 times 10^{14} and 10^{15} particles/cm^2) in titanium dioxide/aluminum oxide—potassium silicate. These spectral characteristics also apply to zinc oxide/aluminum oxide—potassium silicate.

Four white coatings employing methyl silicone binders yield spectral damage characteristics similar to those in Figure 4 for an early formulation of S-13G (treated zinc oxide in methyl silicone) after separate 35-keV electron and 40-keV proton exposures to fluences of 1×10^{15} and 1×10^{16} particles/cm^2. In this fourth damage category, proton-induced effects are concentrated in the visible, whereas electron-induced effects peak in the infrared wavelength region. The other coatings showing this type of degradation are Goddard Series 101-7 treated zinc oxide, anatase titanium dioxide, and rutile titanium dioxide, all in methyl silicone binders.

The electron and proton damage characteristics can be related to the ranges these particles are expected to penetrate into the exposed sample materials. Electrons of 35-keV energy have a range on the order of 10 microns, which means that they pass through the vapor-deposited overcoatings on the various specular materials showing short-wavelength damage, but are stopped in the metallized organic coatings and diffuse paints, which are several mils thick. Protons of 40-keV energy/nucleon have an even shorter range, on the order of one-half micron, their greater dE/dx (loss of energy with distance) causing them to be stopped even in the thinnest overcoating studied, 11,000 Å Al_2O_3.

Damage characteristics 1 and 2 (Figures 1 and 2) indicate heavier proton damage per particle than occurs after electron exposure, for cases showing damage primarily at shorter wavelengths. The ratio of reflectance changes due to proton and electron damage, however, is far less than the dE/dx ratio between protons and electrons. This may mean that reflectance changes are only weakly dependent upon defect concentration or upon the actual mechanisms of proton and electron damage (types of defects). A more definite implication is that short wavelength solar energy (and monochromatic energy used in measuring sample reflectance) penetrates the exposed materials a distance intermediate between the proton and electron ranges. Then the relation between "light" penetration and defect type

and concentration, both as functions of depth in test materials, would predict how damage is manifested as reflectance changes. Studies to obtain this kind of information have been recommended previously in Section 4.2 of Reference 1.

Damage characteristics 3 and 4 (Figures 3 and 4) indicate heavier electron damage per particle for damage manifested in reflectance changes at long wavelengths. This implies penetration of the coating materials by infrared solar radiation (or measuring radiation) to a greater depth, coinciding with the greater electron penetration depth. In the visible wavelength region protons definitely ought to exceed by at least 1000 the effectiveness of electrons in creating color centers by atomic displacements (Reference 2). Yet the study results (summarized in Figure 4) show protons having only a ten-fold greater effectiveness for damage that is manifested in reduced visible-region spectral reflectance. Electrons of 35-keV energy each are capable of displacing only weakly bound low-Z atoms, implying chiefly ionization damage by electrons. It seems that electron damage and proton damage are not fully separable into ionization and displacement mechanisms (respectively).

Summarizing this information, it appears that short-wavelength damage is more a displacement-induced surface effect, whereas damage manifested at longer wavelengths is more of an ionization effect.

2.0 DETAILED REPORT OF PROGRAM RESULTS

This section details the test parameters applicable to the electron and proton studies conducted for this program, and presents the results obtained on each type of coating or surface tested.

2.1 TEST MATERIALS

The types of coatings and surfaces studied are described in Table 1. The listing is approximately in order of decreasing emphasis placed on a given coating. All specimens were held in a clean environment prior to the beginning of tests, and were handled carefully (on edge) when being installed in sample holders for testing.

Table 1. Types of Coatings and Radiation Environments in Which Studied

Type Code	Description of Coating	Exposed to	
		35-keV Electrons	40-keV Protons
TA-2	2-mil FEP Teflon, aluminized to opacity on unirradiated side and bonded to an aluminum substrate	x	x
TA-5	5-mil FEP Teflon, aluminized to opacity on unirradiated side and bonded to an aluminum substrate	x	x
TA-10	10-mil FEP Teflon, aluminized to opacity on unirradiated side and bonded to an aluminum substrate	x	x
TS-2	2-mil FEP Teflon, silvered to opacity on unirradiated side and bonded to an aluminum substrate	x	x
TS-5	5-mil FEP Teflon, silvered to opacity on unirradiated side and bonded to an aluminum substrate	x	x
TS-10	10-mil FEP Teflon, silvered to opacity on unirradiated side and bonded to an aluminum substrate	x	x
Z_3	0.15-mil anodized aluminum (Alzak)	x	x
Z_4	0.22-mil anodized aluminum (Alzak)	x	x
Z_5	0.34-mil anodized aluminum (Alzak)	x	x
N	2-mil aluminized Kapton film (type H) on an aluminum substrate	x	x
R	Treated zinc oxide—methyl silicone Goddard Series 101-7-1	x	x
M S-13G	Treated zinc oxide—methyl silicone Approximately 10 to 12 mils of an early formulation of S-13G, over S54044 primer	x	x

Table 1 (Concluded). Types of Coatings and Radiation Environments in Which Studied

Type Code	Description of Coating (Pigment—binder)	Exposed to	
		35-keV Electrons	40-keV Protons
O	Rutile titanium dioxide—GE RTV 602 methyl silicone, mixed 2 parts pigment to 1 part vehicle	×	×
L_1	Anatase titanium dioxide—Dow Corning Q92-0090 methyl silicone, mixed 3 parts paint to 1 part catalyst. Approximately 5 mils of paint on top of 2 mils of Cat-a-Lac white primer.	×	×
E_3	Rutile titanium dioxide/aluminum oxide—PS-7 potassium silicate. Approximately 4 mils of paint, applied directly on substrate.	×	×
F_3	Zinc oxide/aluminum oxide—PS-7 potassium silicate. Approximately 5 mils of paint, applied directly on substrate.	×	×
D_3	Alpha-phase aluminum oxide—PS-7 potassium silicate. Approximately 11 mils of paint, applied directly on substrate.	×	×
B S-13	Zinc oxide—methyl silicone. Approximately 9 mils of S-13 on top of a thin coat of GES54044 primer.		×
I	Leafing aluminum—mixed Dow Corning 805 and 806A phenylated silicones. Approximately 3 mils total, in 3 coats.		×
H	Silicon dioxide deposited in air on an aluminized substrate, to 25,000 Å thickness.	×	×
J	Vapor-deposited aluminum on a lacquered aluminum substrate.		×
K	Buffed and vapor-degreased aluminum substrate.		×
G	Vapor-deposited aluminum oxide (11,000 Å) on top of 1000 Å of aluminum evaporated onto a buffed, chemically cleaned, and glow discharge cleaned, substrate. (Prepared by Dr. Georg Hass of Fort Belvoir.)		×

2.2 EXPOSURE PARAMETERS

The experimental work for this program has been performed with Boeing's combined radiation effects test chamber (CRETC). The CRETC has internally an electron gun designed to accelerate electrons to energies as high as about 120 keV. This system has been used for the 35-keV electron study. An external positive-charge particle accelerator recently designed for generation of particles with energies from about one to about 100 keV has been used for the 40-keV proton study. Figure 5 is an overall photograph of this experimental equipment.

2.2.1 Electron Beam Properties

The electron beam which (after scattering) is used to expose the coating samples being studied, is formed by accelerating and focusing potentials within a two-stage electron gun. Before scattering, the energy of the electrons for the 35-keV electron study is 40±1 keV as set by the power supply accelerating potential difference. A 2.5μ-thick aluminum foil degrades the electron energy by approximately 5 keV as angular scattering takes place in the foil. Falloff in scattered beam intensity with angle from the unscattered beam axis is 10 percent at 9° and 30 percent at 18°. Samples are in two azimuthal rings 5° and 9° from the unscattered beam axis. These rate or intensity falloff values are based, not on calculations, but on dosimetry measurements with movable Faraday cups before each exposure. During an exposure the electron rate is continually monitored by a Faraday cup mounted on the beam axis behind the sample array, and by another cup mounted at an off-axis angle between foil and samples. This latter cup gives assurance of the continued integrity of the thin scattering foil by detecting and measuring scattered electrons. Measured electron rate is not appreciably altered by Faraday cup bias or by biasing a cup's outer guard ring, implying effective collection of electrons. During an exposure the electron flux or rate (electrons/cm^2-sec) may vary by ±5 percent, and the total exposure time required to reach the desired electron fluence (electrons/cm^2) is adjusted (recalculated) accordingly. There are no impurities in the electron beam, scattered or unscattered, and energy drift with time during exposure is less than ±1 keV.

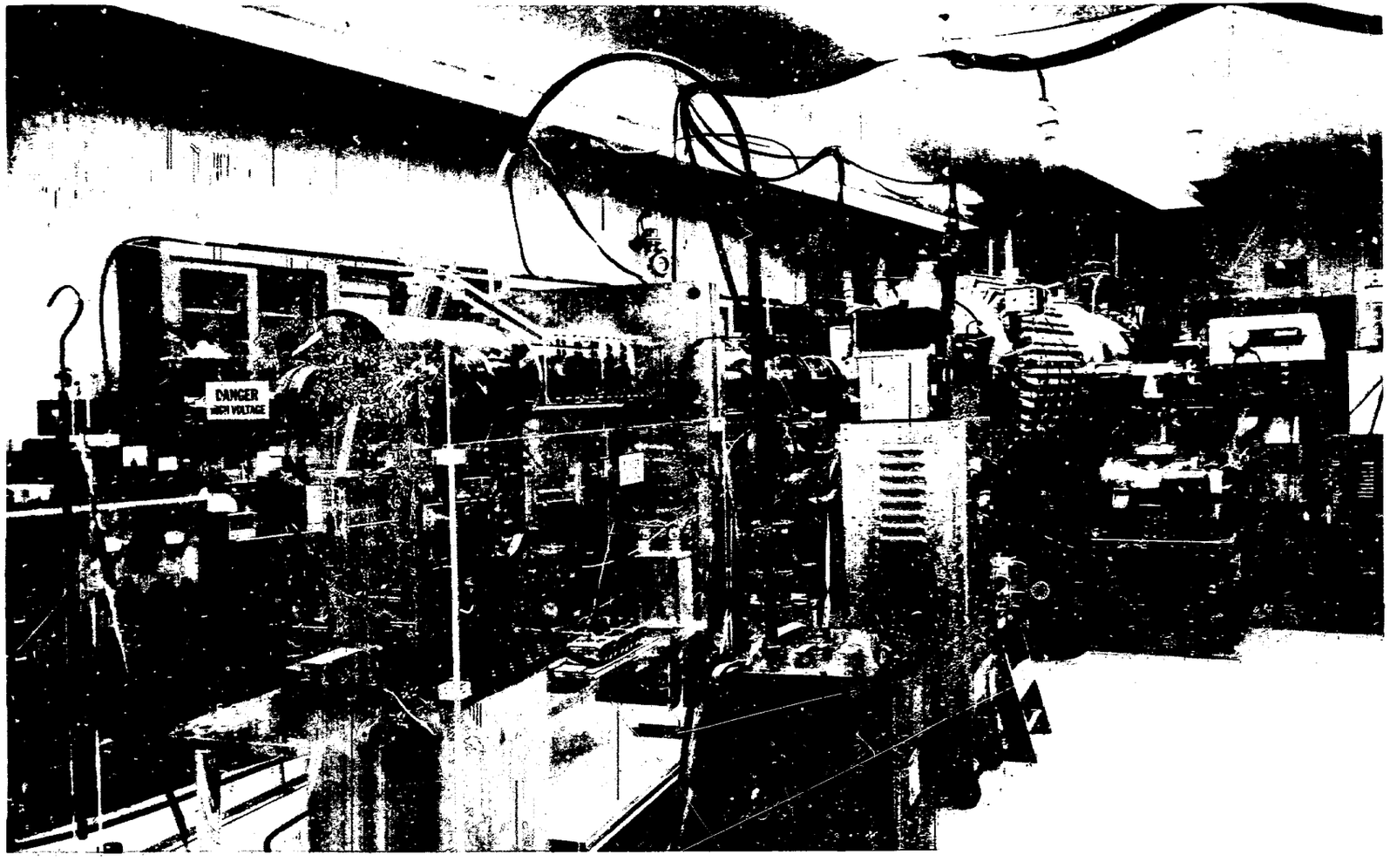

Figure 5. Experimental Facility for Combined Radiation Effects Studies

The electron fluences or exposure levels at which spectral reflectance measurements have been made during the 35-keV electron study, and the electron flux or rate used to reach each fluence level, are indicated in Table 2. From previous studies (Reference 3), no rate effects should be anticipated over this range.

Table 2. Test Points and Exposure Rates, 35-keV Electron Study

Electron Fluences for Measurements	Electron Flux
0 (Pre-irradiation)	- - - -
5×10^{12} electrons/cm^2	1×10^{10} electrons/cm^2-second
5×10^{13}	1×10^{10}
1×10^{14}	1×10^{10}
3×10^{14}	2×10^{10}
1×10^{15}	2×10^{10}
3×10^{15}	4×10^{10}
1×10^{16}	7×10^{10}

2.2.2 Proton Beam Properties

The proton beam originates with electrostatic extraction from a plasma within an Ortec 501 RF ion source, part of the positive particle accelerator in the foreground of Figure 5. The beam is magnetically analyzed to separate mass-one hydrogen nuclei for injection into the CRETC, and to reject particles with mass greater than one. It is not feasible to use foil scattering to obtain a large, uniform proton beam for concurrent exposure of a great number of test specimens. A three stage Einzel lens within the CRETC (in addition to a similar one employed adjacent to the proton extraction electrode) does provide a measure of defocusing for enlarging the beam size. Particle dosimetry is performed by Faraday cups and copper discs. As is done for electron exposures, two cups are moved in horizontal and vertical arc-swinging fashion to provide information about particle beam intensity as a function of angle or distance from beam axis. A third, fixed Faraday cup behind the sample plane continually determines particle intensity or flux at the

plane by virtue of its limiting apertures (one for each possible sample array) being in the sample wheel. Circular copper discs the same size as test samples are arranged in a dosimetry array at positions exactly equivalent to those occupied by coating specimens when exposed. The discs are insulated from the sample wheel (which is at chamber ground), and via feedthroughs allow monitoring of particle beam profile prior to exposure and periodically during each exposure (when rotated into proper position). It is recognized that because of backscatter and secondary emission, such discs provide flux information relative to each other (uniformity of exposure at various sample positions), while the fixed Faraday cup most accurately determines absolute particle flux or intensity. Throughout a days-long series of exposures that collectively constitute a test of several coating specimens, energy stability at the 40-keV level is about ±2 keV. Stability of beam uniformity is somewhat less with protons than with electrons (where scattering is feasible). Proton fluence values for Teflon, Alzak, and types I, J, and K (Table 4 and odd-numbered figures following) may be taken as correct within about ten per cent. Uncertainties up to about twenty percent obtain for some of the other coatings studied. Fluxes or exposure rates between about 1 and 5 x 10^{10} 40-keV protons/cm^2-second have been used in this program.

2.3 TEMPERATURE/VACUUM PARAMETERS

Each of the two radiation exposure studies conducted for this program has been performed with the substrates of the test specimens mounted in good thermal contact with the test chamber's temperature-controlled sample wheel. For "room temperature" studies as in this program, the most stable temperature-controlling fluid is externally supplied, unrecycled water whose temperature customarily varies throughout the year from about 20°C in the summer to about 10°C in the winter. The 35-keV electron study has been done with the sample wheel controlled to 18 ±1°C, whereas the 40-keV proton study has taken place with the sample wheel at 10 ±1°C. Neither the electron nor the proton study has involved particle arrival rates at the test specimen surfaces that would raise temperatures in the test materials by an appreciable amount.

Radiation exposure studies in the CRETC can employ any combination of cryogenic, turbomolecular, and ion pumping to obtain hard vacuum. In this program all three types have been used in concert to obtain the best vacuum levels possible. Measurements of vacuum level are based upon readings of ion pump currents and two ionization gauges at widely separated locations on the chamber. Values applicable to each study (electron and proton) are given below.

2.3.1 Electron Study Temperature/Vacuum Parameters

The temperature/vacuum history of each test sample in the 35-keV electron study is as follows: All samples were at room temperature (about 21°C) while being measured in air before exposure. Pumpdown to 10^{-8} torr occurred in stages, first with vacuum roughing to 5 microns, over a period of about 0.7 hour; second by turbomolecular pumping to 7×10^{-6} torr over a period of 12 hours; third, to 8×10^{-7} torr with the addition of liquid nitrogen to the cryogenic shroud; and fourth, to 1×10^{-7} torr during a period of 3 hours using ion pumping. Temperature-control water through the chamber sample wheel established the temperature of each sample substrate at 18°C, based upon water exit temperature from the chamber. By the time preirradiation, in-vacuum measurements were complete (about 48 hours), chamber pressure was 1.2×10^{-8} torr. Sample substrate temperature was maintained at 18 ±1°C throughout all subsequent exposure and measurement periods. Vacuum levels of 3 to 7×10^{-8} torr were maintained throughout all subsequent exposure periods, and 0.9 to 2×10^{-8} torr was maintained during subsequent measurement periods.

2.3.2 Proton Study Temperature/Vacuum Parameters

The temperature/vacuum history of each test sample during the 40-keV proton study is similar to that applicable to the electron study, pumpdown procedures being the same. The temperature of the coating substrates throughout the test period was 10 ±1°C, based upon water exit temperature from the chamber. Vacuum levels during exposures were 1 to 2×10^{-7} torr. During measurement periods, pressures as low as the low 10^{-8} torr range were achieved.

2.4 REFLECTANCE MEASUREMENT PROCEDURES

The reflectance measurement system used with the CRETC involves an integrating sphere in vacuum, a far UV Beckman DK-2A double-beam, ratio-recording spectrophotometer, a Datex SDS-1 automatic data collection system, and an IBM 526 card punch. Reflectance measurements made before and after each exposure are continuous-scan charts over the 0.24- to 2.54-micron wavelength region, resulting in very high resolution of reflectance structure with wavelength, as well as simultaneous punching of data onto cards for subsequent computer processing (using encoders and the Datex system).

For accurage determination of reflectance properties and coating solar absorptance (α_s) values, the following procedure has been established. Each specimen reflectance measurement is made relative to the reflectance of the magnesium oxide coating on the integrating sphere wall. This eliminates errors which otherwise could be present due to ability to "scale" any measurement using the 100 percent adjustment on the spectrophotometer. A comparison of this "normalized" reflectance characteristic is made with that obtained using an integrating sphere with sample-at-the-center technique, which is more widely regarded as approximating absolute reflectance more accurately if imperfections in sphere wall uniformity and diffusivity are ignored. This establishes a "normalization function" $k(\lambda)$ for reflectance versus wavelength. Separate, slightly different functions have been determined and are used for diffuse and for specular materials. In summary, then, each spectral reflectance value R_λ on plots presented in this report (Figures 6 through 66) is determined from the equation,

$$R_\lambda = k(\lambda) \frac{R_{sam}}{R_{ref}},$$

where R_{sam} is the spectral reflectance of the specimen measured in situ, and R_{ref} is the corresponding reference spectral reflectance measured at (nearly) the same time. R_λ values are then used for α_s determinations. Using 100 energy bands

(each one representing 1 percent of the solar radiant intensity),

$$\alpha_s = 1 - R_s = 1 - \frac{\sum_{100} R_\lambda}{100}$$

if reflectance R_λ is on a decimal scale from zero to unity. Otherwise, the denominator is 10^4 if reflectance is considered scaled from zero to 100.

Typical reproducibility of the reflectance measuring system is indicated by the stability of reflectance of control specimens. Repeated measurements made on specular and diffuse control specimens before and after each exposure result in nearly exact retracings of computer-processed output curves (Figures 6 and 7).

2.5 EXPERIMENTAL RESULTS

Both the solar absorptance (α_s) characteristics and the reflectance-wavelength characteristics of the materials indicated in Table I are presented in this Section. Solar absorptance values, as defined in Section 2.4 and weighted against solar radiant intensity through zero air mass, are given in Table 3 for samples exposed during the 35-keV electron study. Table 4 indicates solar absorptance values obtained for samples exposed in the 40-keV proton study. Figures 8 through 43 give reflectance degradation information on the 18 types of materials exposed in both studies. Even-numbered figures are electron results; odd-numbered figures show proton data. Figures 44 through 48 contain results for materials exposed only to 40-keV protons. S-13 is included (Figure 44) to provide a comparison with S-13G and Goddard Series 101-7. The zinc oxide pigment in the latter two types is presumed to be thoroughly encapsulated with potassium silicate for ultraviolet stability. S-13 pre-dates this silicate treatment process. Though the thickness of the encapsulating K_2SiO_3 is unknown, it is on the order of the range of 40-keV protons, thus altering the principal sample constituents in which proton deceleration occurs.

Finally, as part of the program scope, in air/in vacuum reflectance characteristics are presented in Figures 49 through 66. Unlabeled curves in Figures 8 through 66 correspond to measurement conditions listed in Tables 3 and 4.

FIGURE 6.
TYPE K ALUMINUM SUBSTRATE EXPOSED TO VACUUM AS A CONTROL

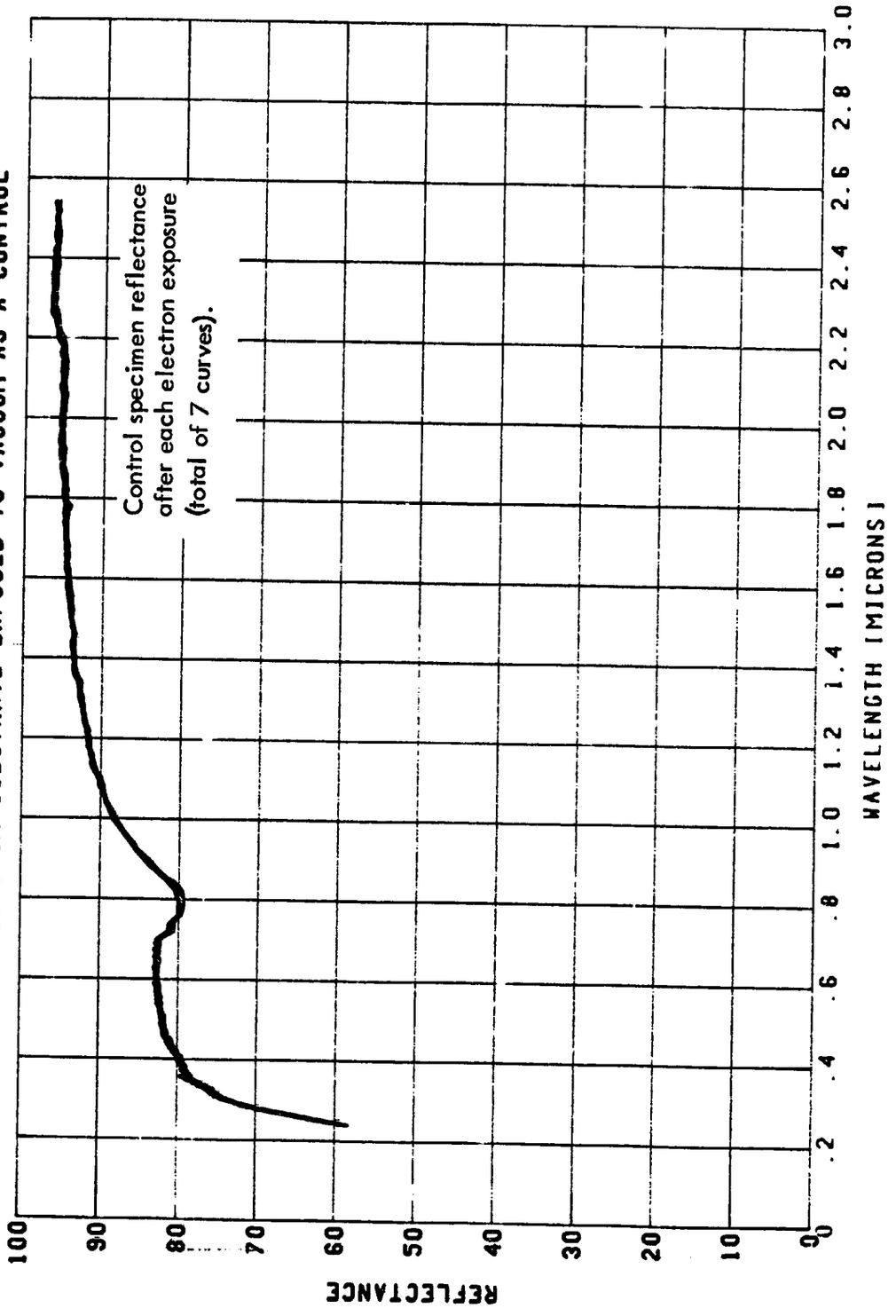

FIGURE 7.

TYPE D3 AL203—K2SI03 WHITE COATING EXPOSED TO VACUUM AS A CONTROL

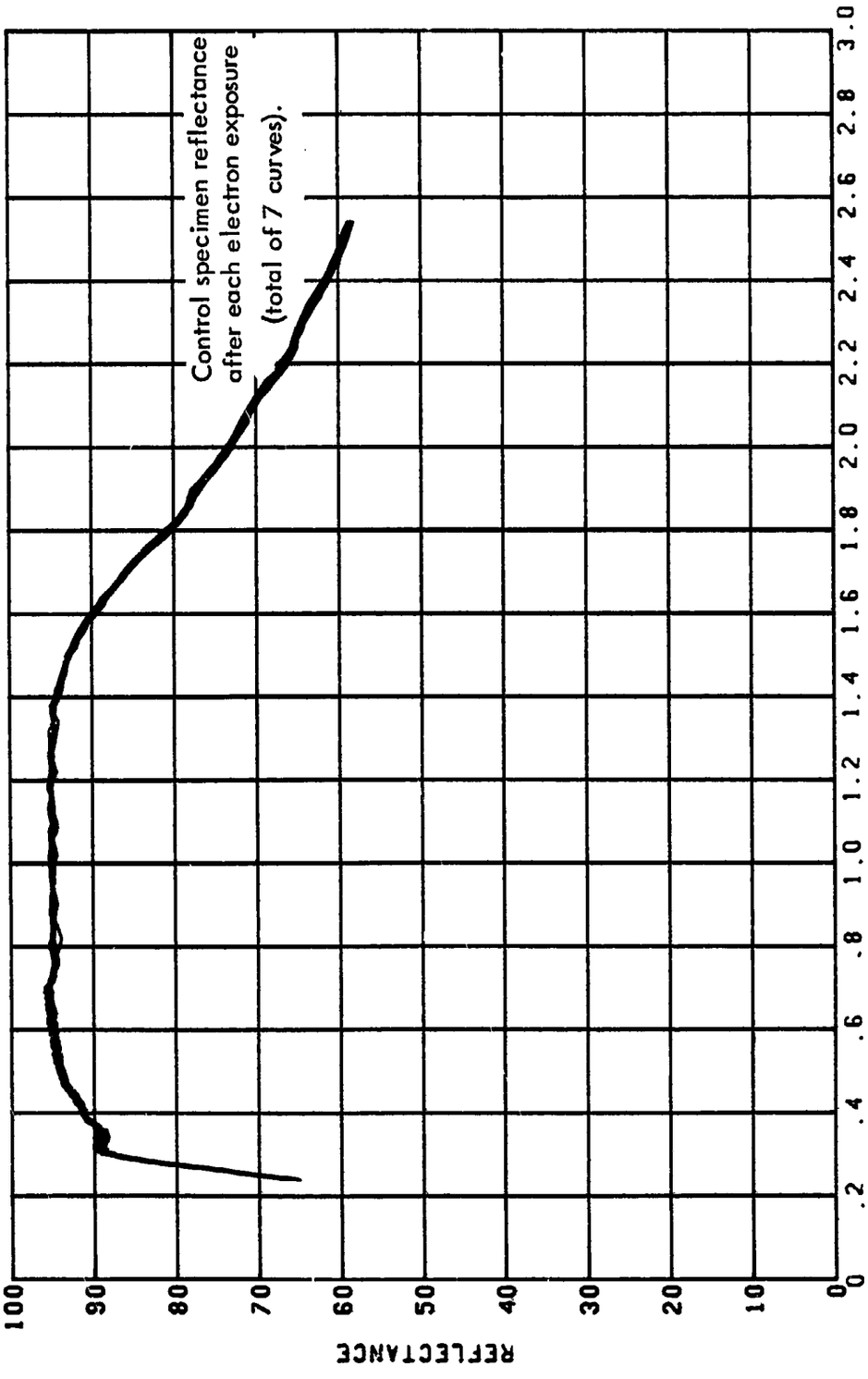

Table 3a. Solar Absorptance of NASA-Goddard Coatings Exposed to 35-keV Electrons

Coating or Surface			Measurement Conditions							
					In vacuum after exposure to 35-keV electron fluences of:						
Type Code		Principal Constituents	In air before Exposure	In vacuum before Exposure	5×10^{12}	5×10^{13}	10^{14}	3×10^{14}	10^{15}	3×10^{15}	10^{16} e/cm^2
TS-2	Silvered	2-mil FEP Teflon	0.06	0.06		0.06	0.06	0.06	0.06	0.07	0.08
TS-5	Silvered	5-mil FEP Teflon	0.08	0.07		0.07	0.07	0.07	0.08	0.08	0.10
TS-10	Silvered	10-mil FEP Teflon	0.10	0.10		0.10	0.10	0.10	0.10	0.11	0.12
TA-2	Aluminized	2-mil FEP Teflon	0.13	0.12		0.12	0.12	0.12	0.13	0.14	0.16
TA-5	Aluminized	5-mil FEP Teflon	0.14	0.13		0.14	0.14	0.14	0.14	0.15	0.17
TA-10	Aluminized	10-mil FEP Teflon	0.17	0.16		0.16	0.16	0.16	0.17	0.18	0.20
N		2-mil Kapton (H)	0.37	0.37		0.37	0.37	0.38	0.39	0.42	0.45
Z_3		0.15-mil Alzak	0.14	0.13	0.14	0.14	0.14	0.14	0.15	0.15	0.16
Z_4		0.22-mil Alzak	0.15	0.14	0.14	0.14	0.15	0.15	0.15	0.16	0.16
Z_5		0.34-mil Alzak	0.16	0.15	0.16	0.16	0.16	0.17	0.17	0.18	0.19

Table 3b. Solar Absorptance of NASA-Goddard Coatings Exposed to 35-keV Electrons

Coating or Surface		Measurement Conditions								
				In vacuum after exposure to 35-keV electron fluences of:						
Type Code	Principal Constituents	In air before Exposure	In vacuum before Exposure	5×10^{12}	5×10^{13}	10^{14}	3×10^{14}	10^{15}	3×10^{15}	10^{16} e/cm^2
R	GSFC Series 101-7 ZnO/KS--M Silicone	0.21	0.21	0.21	0.22	0.23	0.26	0.31	0.34	0.37
M	Early S-13G ZnO/KS--M Silicone	0.20	0.20	0.20	0.24	0.26	0.31	0.35	0.36	0.40
L_1	Anatase TiO_2--MS	0.18	0.18	0.19	0.22	0.23	0.26	0.30	0.35	0.43
O	Rutile TiO_2--MS	0.20	0.20		0.20	0.21	0.22	0.25	0.33	0.44
D_3	Al_2O_3--K_2SiO_3	0.10	0.09	0.10	0.11	0.11	0.11	0.12	0.12	0.13
E_3	TiO_2/Al_2O_3--K_2SiO_3	0.19	0.18	0.19	0.20	0.21	0.25	0.34	0.44	0.52
F_3	ZnO/Al_2O_3--K_2SiO_3	0.17	0.16	0.16	0.18	0.19	0.20	0.26	0.34	0.43
H	Vapor-deposited SiO_2 over Al	0.13	0.12		0.13	0.12	0.12	0.12	0.12	0.12

Table 4a. Solar Absorptance of NASA-Goddard Coatings Exposed to 40-keV Protons

Type Code	Coating or Surface: Principal Constituents	Measurement Conditions: In vacuum before Exposure	In vacuum after exposure to 40-keV proton fluences of: 3×10^{12}	5×10^{13}	3×10^{14}	8×10^{14}	3×10^{15}	1×10^{16} p/cm^2
TS-2	Silvered: 2-mil FEP Teflon	0.06	0.06	0.06	0.06	0.06	0.07	0.09
TS-5	Silvered: 5-mil FEP Teflon	0.07	0.07	0.07	0.07	0.07	0.08	0.10
TS-10	Silvered: 10-mil FEP Teflon	0.09	0.09	0.09	0.09	0.09	0.10	0.12
TA-2	Aluminized: 2-mil FEP Teflon	0.12	0.12	0.12	0.12	0.12	0.13	0.16
TA-5	Aluminized: 5-mil FEP Teflon	0.13	0.13	0.13	0.13	0.14	0.15	0.18
TA-10	Aluminized: 10-mil FEP Teflon	0.16	0.16	0.16	0.16	0.16	0.17	0.20
			After 2×10^{14}			8×10^{14}	3×10^{15}	1×10^{16} p/cm^2
Z_3	0.15-mil Alzak	0.13	0.14			0.14	0.15	0.20
Z_4	0.22-mil Alzak	0.13	0.14			0.14	0.16	0.19
Z_5	0.34-mil Alzak	0.16	0.16			0.17	0.20	0.25
K	Buffed Al substrate	0.14	0.14			0.14	0.14	0.15
J	Flash-aluminized lacquer	0.07	0.07			0.07	0.07	0.08
I	Leafing Al-mixed silicones	0.22	0.22			0.22	0.22	0.23

Table 4b. Solar Absorptance of NASA-Goddard Coatings Exposed to 40-keV Protons

Coating or Surface		Measurement Conditions										
Type Code	Principal Constituents	In vacuum before Exposure	In vacuum after exposure to 40-keV proton fluences of:									
			1×10^{12}	1x	2x	5×10^{13}	1x	3x	5×10^{14}	1x	2x	5×10^{15}	1×10^{16} p/cm^2
R	Series 101-7 ZnO/K_2SiO_3—M Silicone	0.19	0.19		0.19		0.20		0.21	0.23		0.36	
M	Early S-13 G ZnO/K_2SiO_3—M Silicone	0.19	0.19	0.19			0.20			0.25		0.38	0.48
B	S-13 ZnO—M Silicone	0.17					0.18[a]	0.19		0.24	0.26	0.33	
L_1	Anatase TiO_2—M Silicone	0.18					0.19		0.21	0.27	0.30	0.40[b]	
O	Rutile TiO_2—M Silicone	0.18				0.18	0.17		0.18		0.25	0.35	
D_3	Al_2O_3—K_2SiO_3	0.09	0.10	0.10			0.10	0.10		0.10[a]			0.13[a]
E_3	TiO_2/Al_2O_3—K_2SiO_3	0.18	0.18		0.18		0.19		0.20[a]	0.21		0.26[a]	
F_3	ZnO/Al_2O_3—K_2SiO_3	0.17					0.18			0.22	0.30[c]		0.36[a]
N	2-mil Kapton (H)	0.37						0.38		0.42		0.47[b]	0.50
H	SiO_2 over Al Vapor deposited	0.12				0.12[a]	0.12	0.12				0.13[a]	
G	Al_2O_3 over Al	0.14				0.14			0.14		0.14	0.15	

Measured at approximately [a]0.8, [b]1.2, [c]1.5 times the fluence value listed

FIGURE 8.
IN SITU EFFECTS OF 35-KEV ELECTRONS ON THE REFLECTANCE OF NASA-GODDARD SILVERED 2-MIL TEFLON (TS-2)

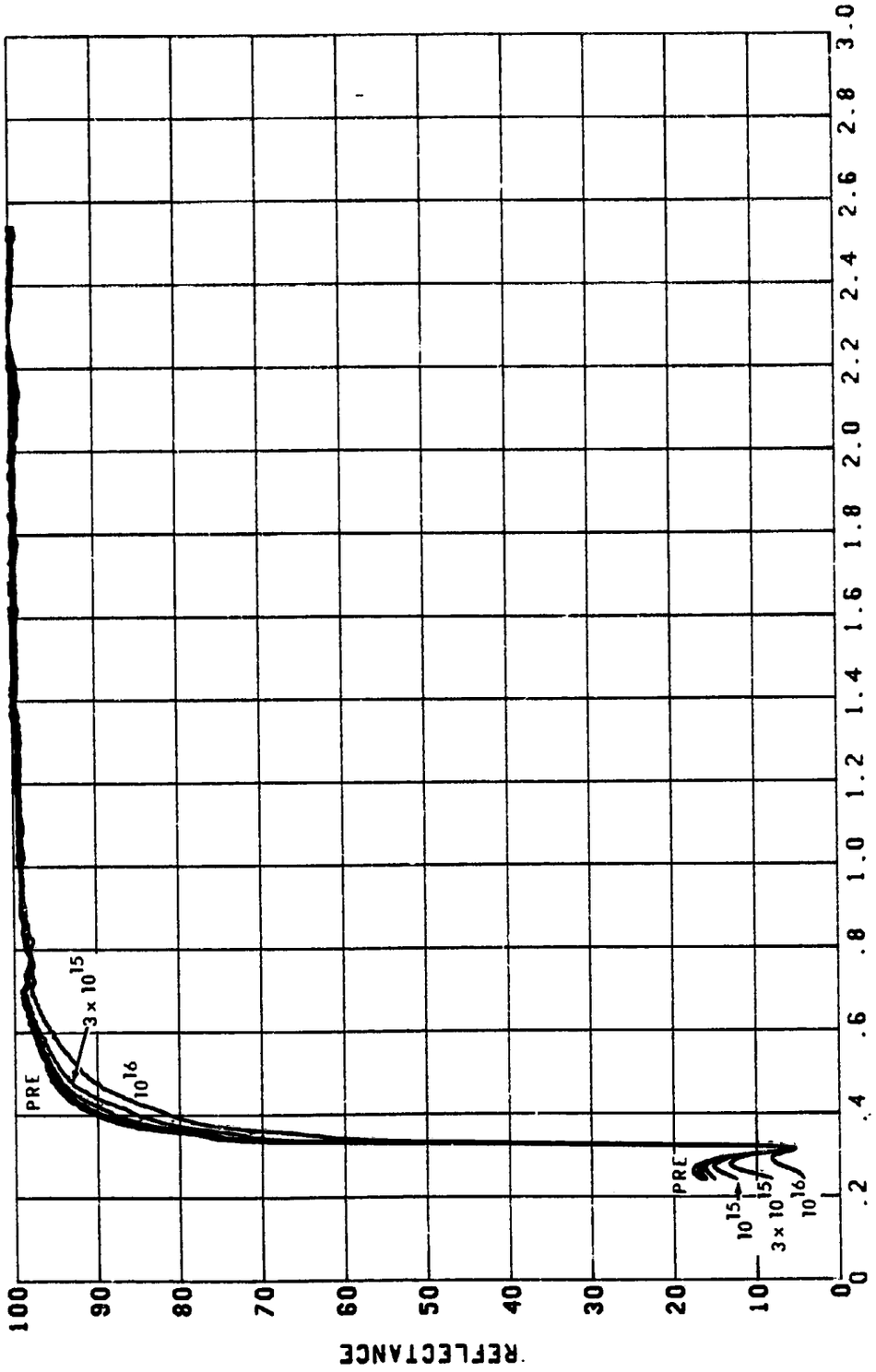

FIGURE 9.

IN SITU EFFECTS OF 40-KEV PROTONS ON THE REFLECTANCE OF NASA GODDARD SILVERED 2-MIL TEFLON [TS-2]

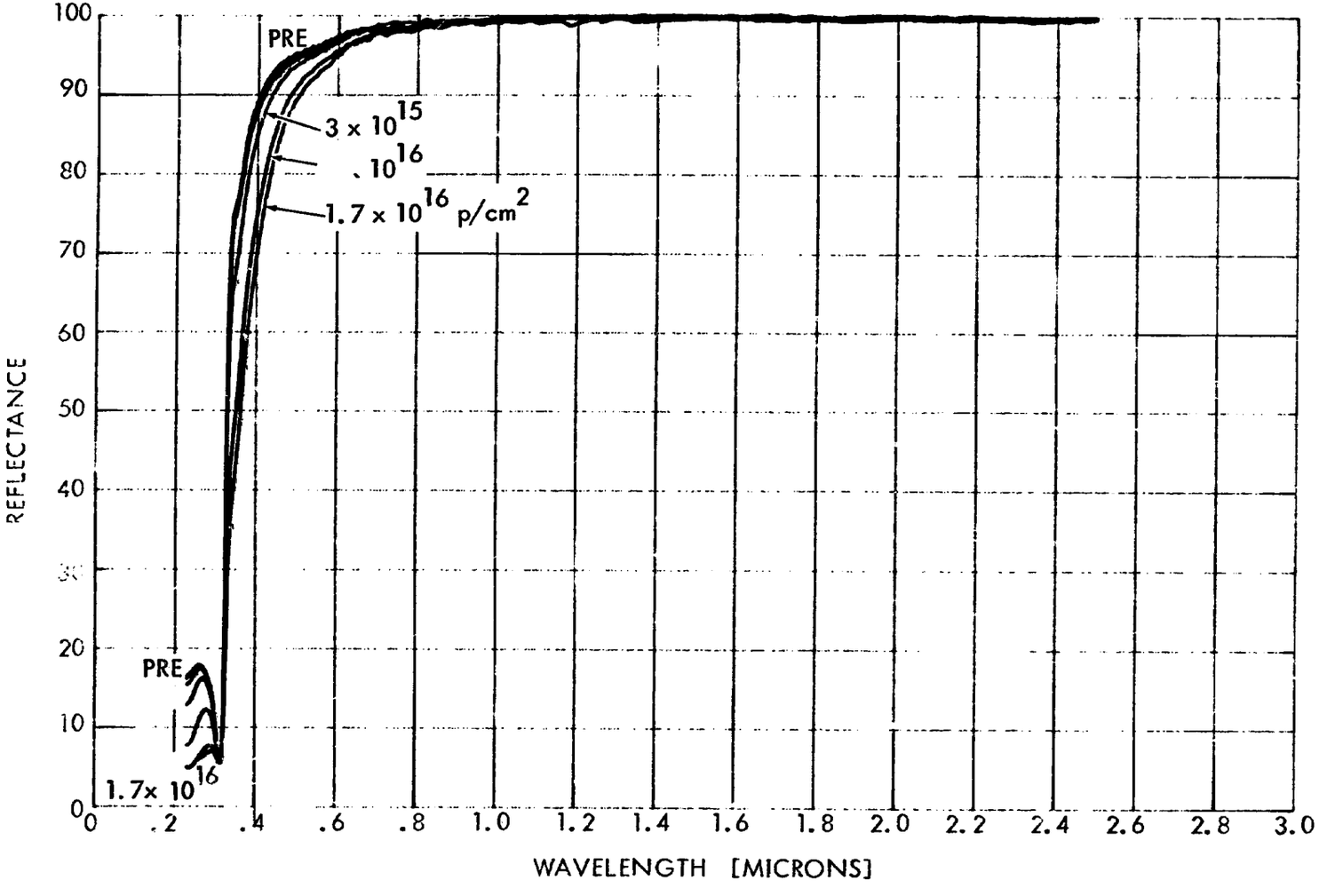

FIGURE 10.

IN SITU EFFECTS OF 35-KEV ELECTRONS ON THE REFLECTANCE OF NASA-GODDARD SILVERED 5-MIL TEFLON (TS-5)

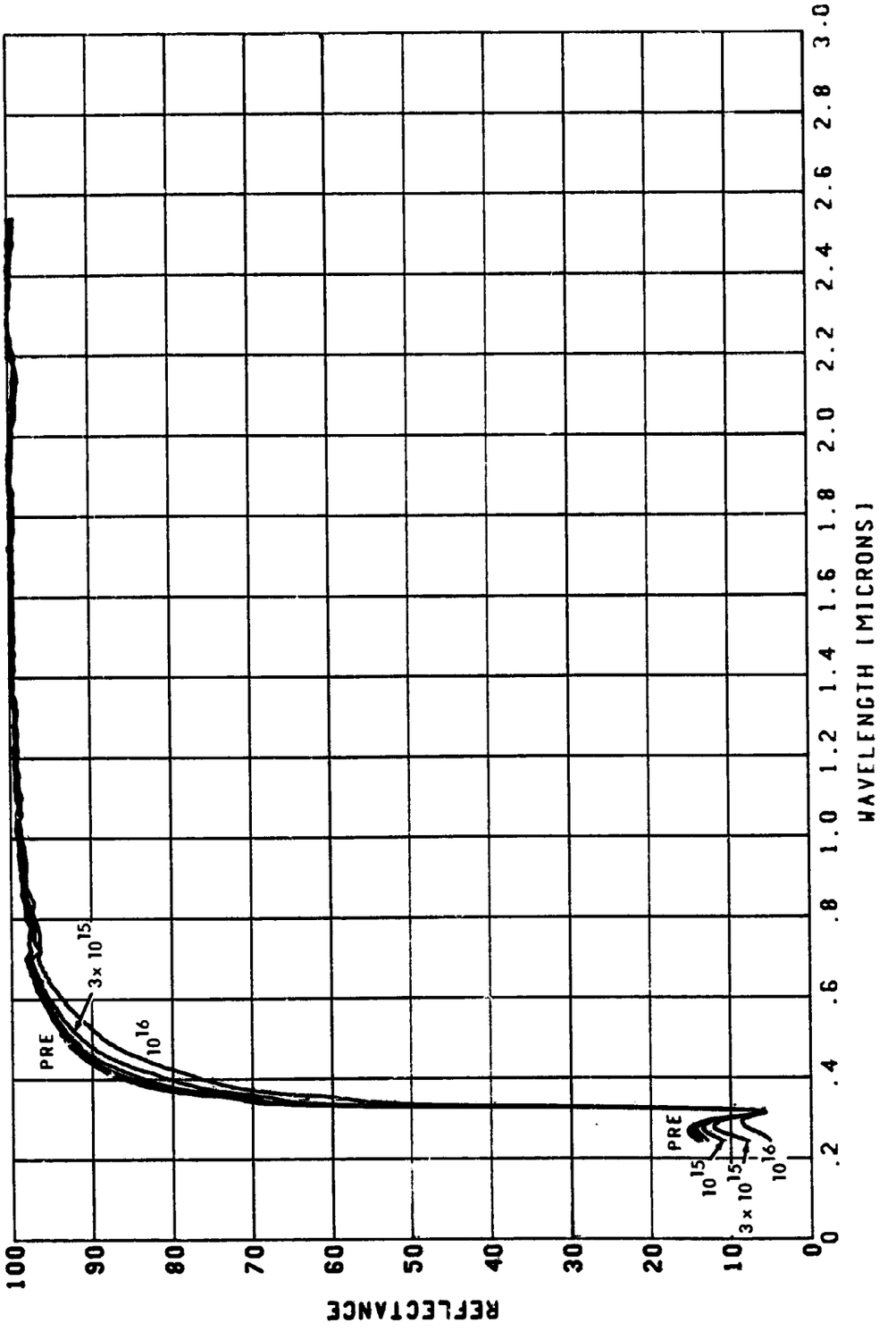

FIGURE 11.

IN SITU EFFECTS OF 40-KEV PROTONS ON THE REFLECTANCE OF NASA-GODDARD SILVERED 5-MIL TEFLON TS-5

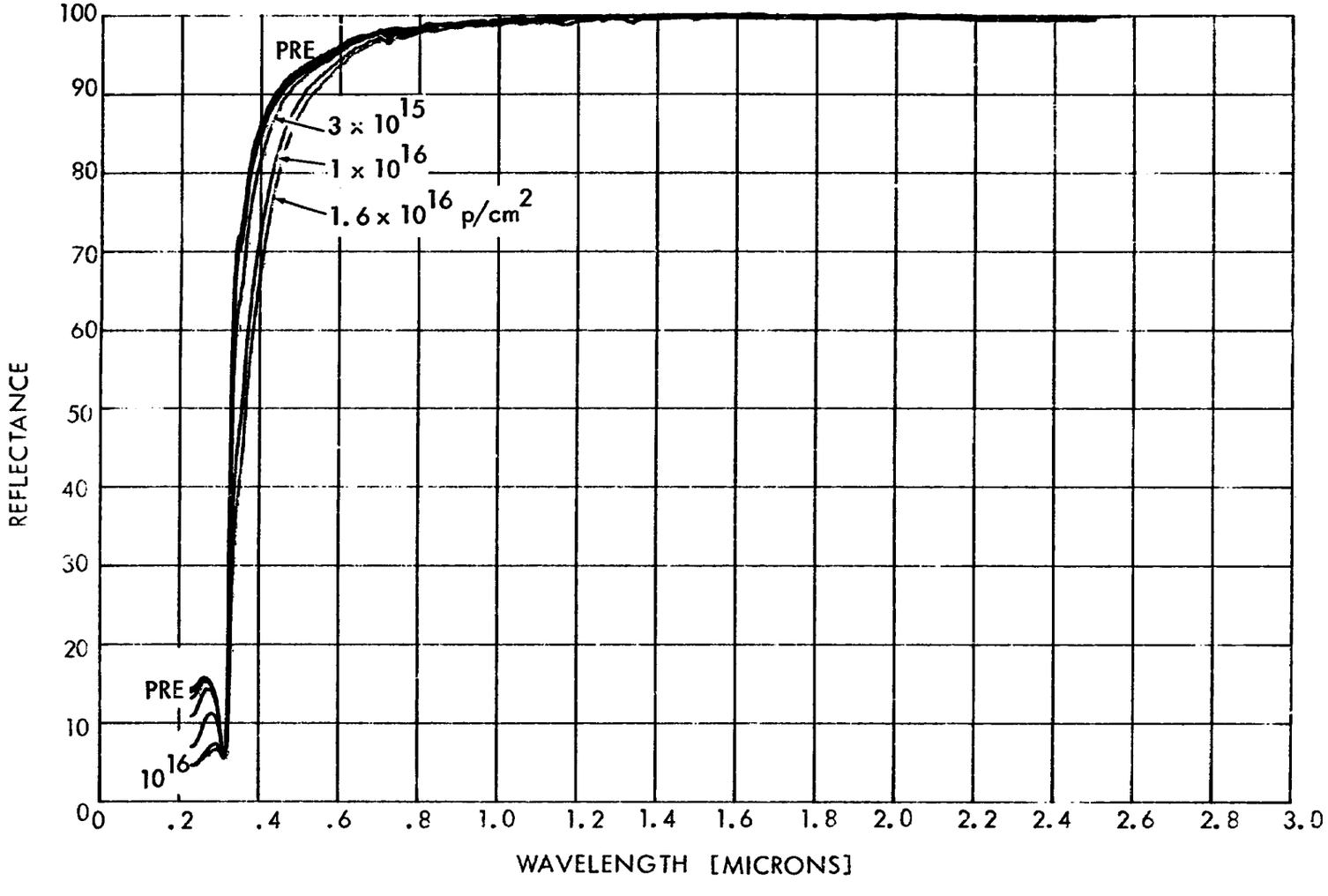

FIGURE12.

IN SITU EFFECTS OF 35-KEV ELECTRONS ON THE REFLECTANCE OF NASA-GODDARD SILVERED 10-MIL TEFLON (TS-10)

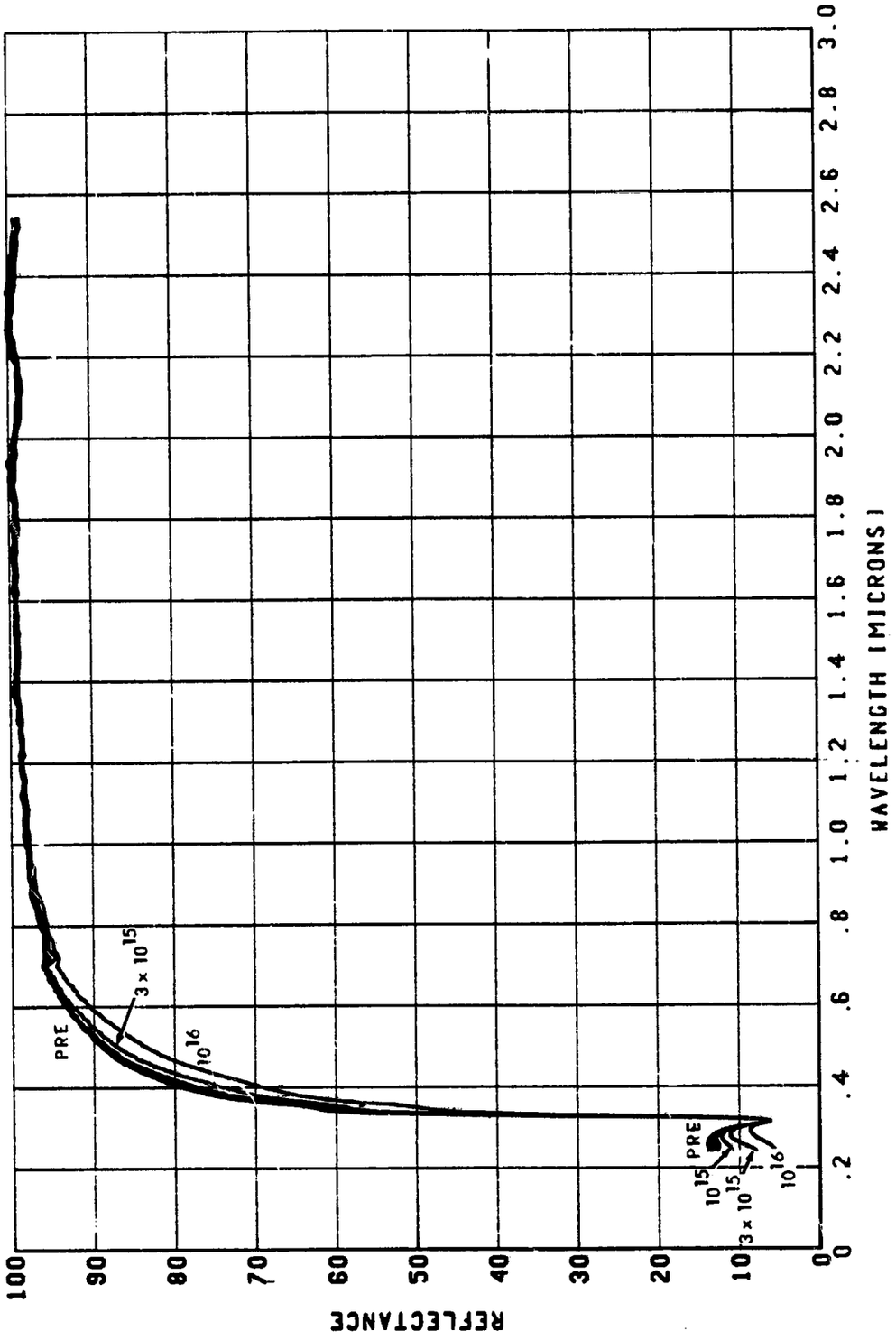

FIGURE 13.

IN SITU EFFECTS OF 40-KEV PROTONS ON THE REFLECTANCE OF NASA-GODDARD SILVERED 10-MIL TEFLON TS-10

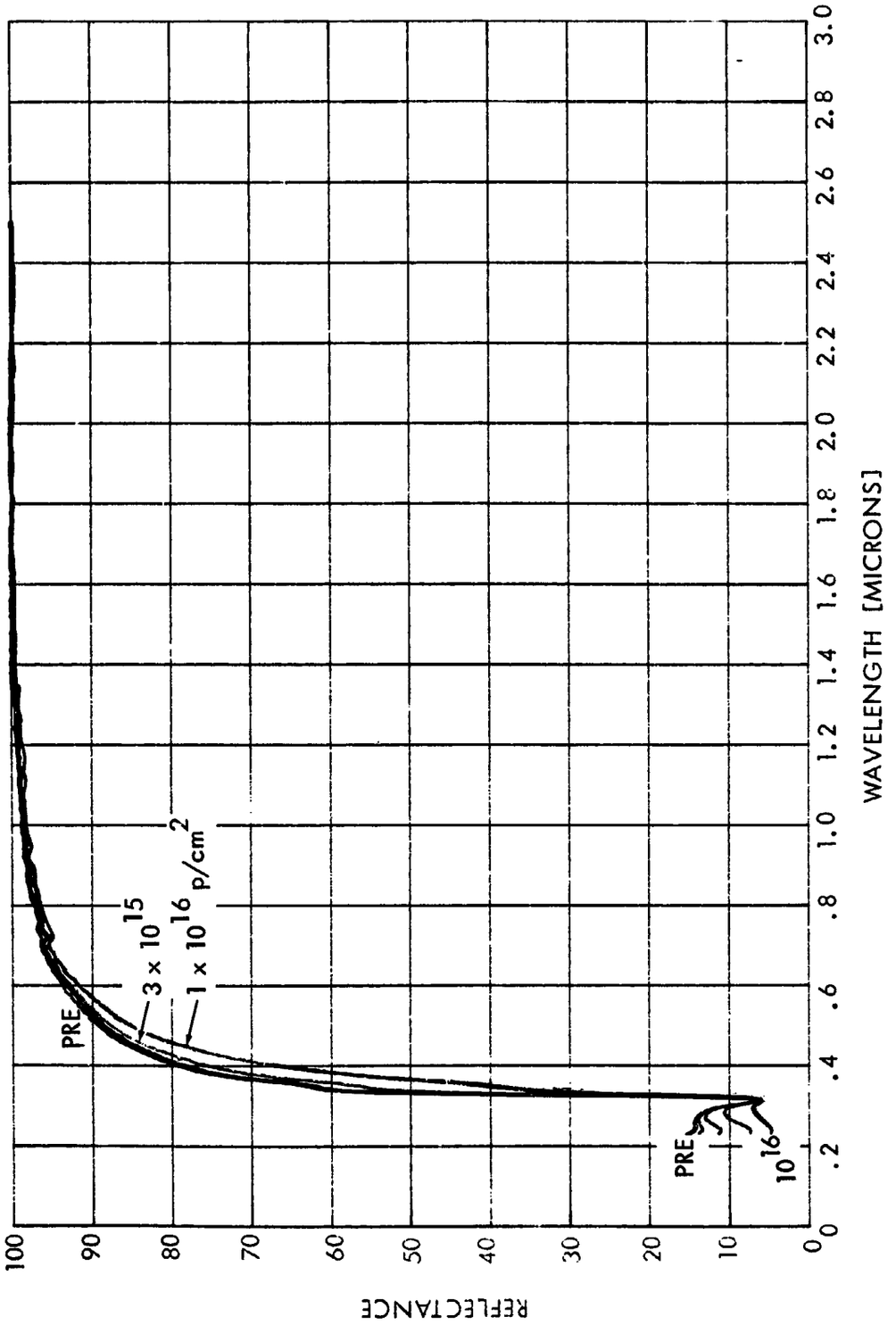

FIGURE 14.

IN SITU EFFECTS OF 35-KEV ELECTRONS ON THE REFLECTANCE OF NASA-GODDARD ALUMINIZED 2-MIL TEFLON (TA-2)

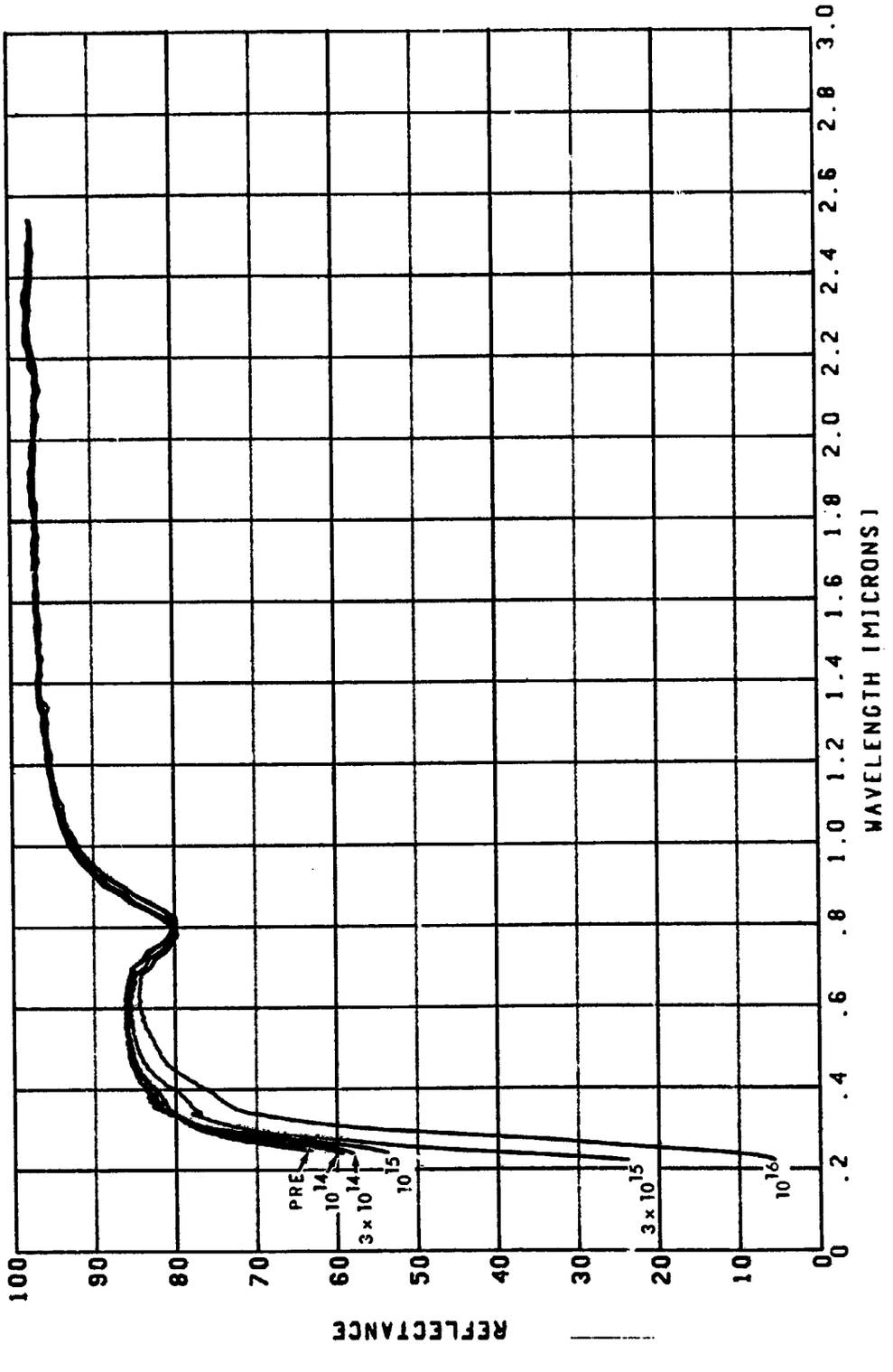

FIGURE 15.

IN SITU EFFECTS OF 40-KEV PROTONS ON THE REFLECTANCE OF NASA-GODDARD ALUMINIZED 2-MIL TEFLON TA-2

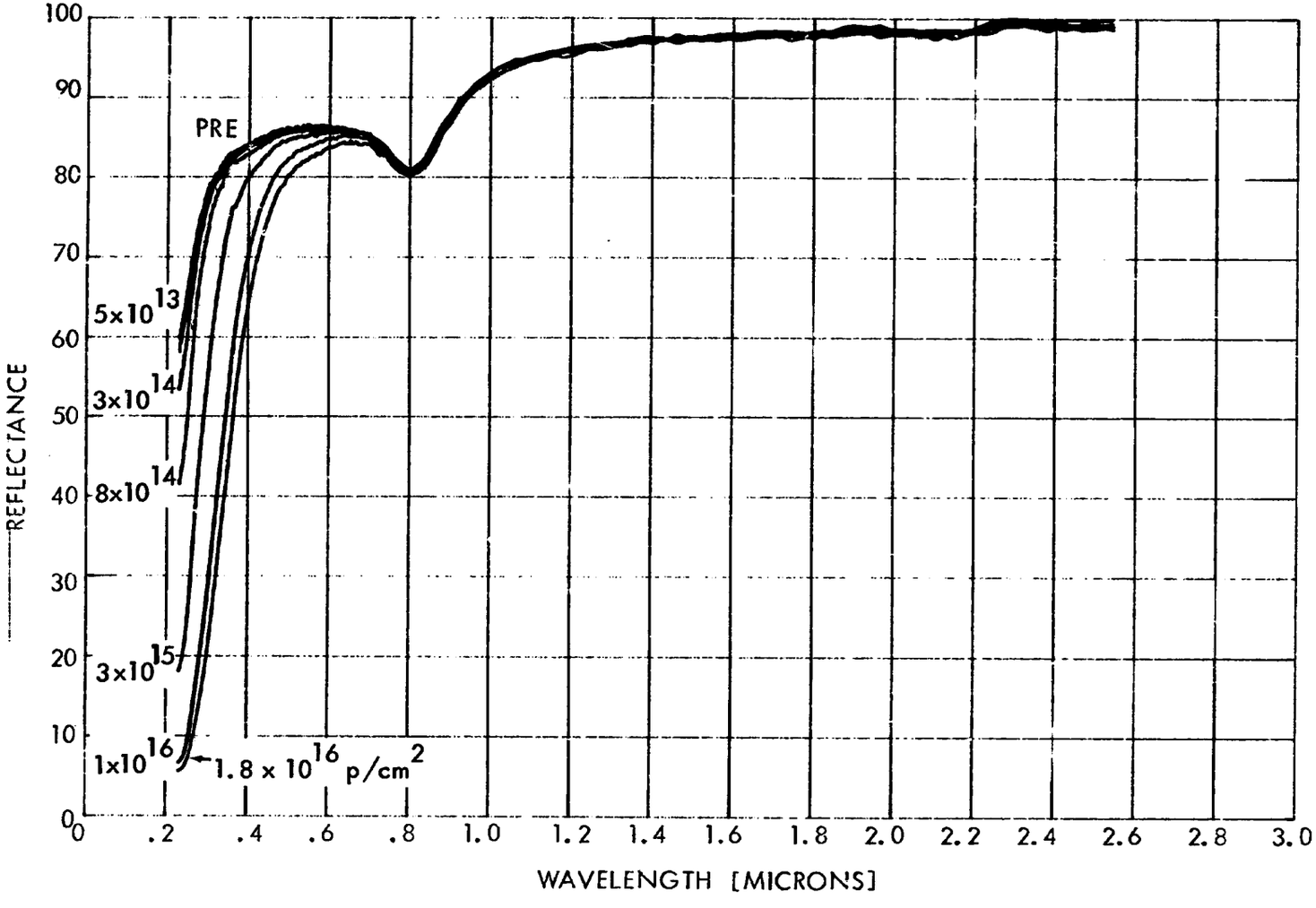

FIGURE 16.

IN SITU EFFECTS OF 35-KEV ELECTRONS ON THE REFLECTANCE OF NASA-GODDARD ALUMINIZED 5-MIL TEFLON (TA-5)

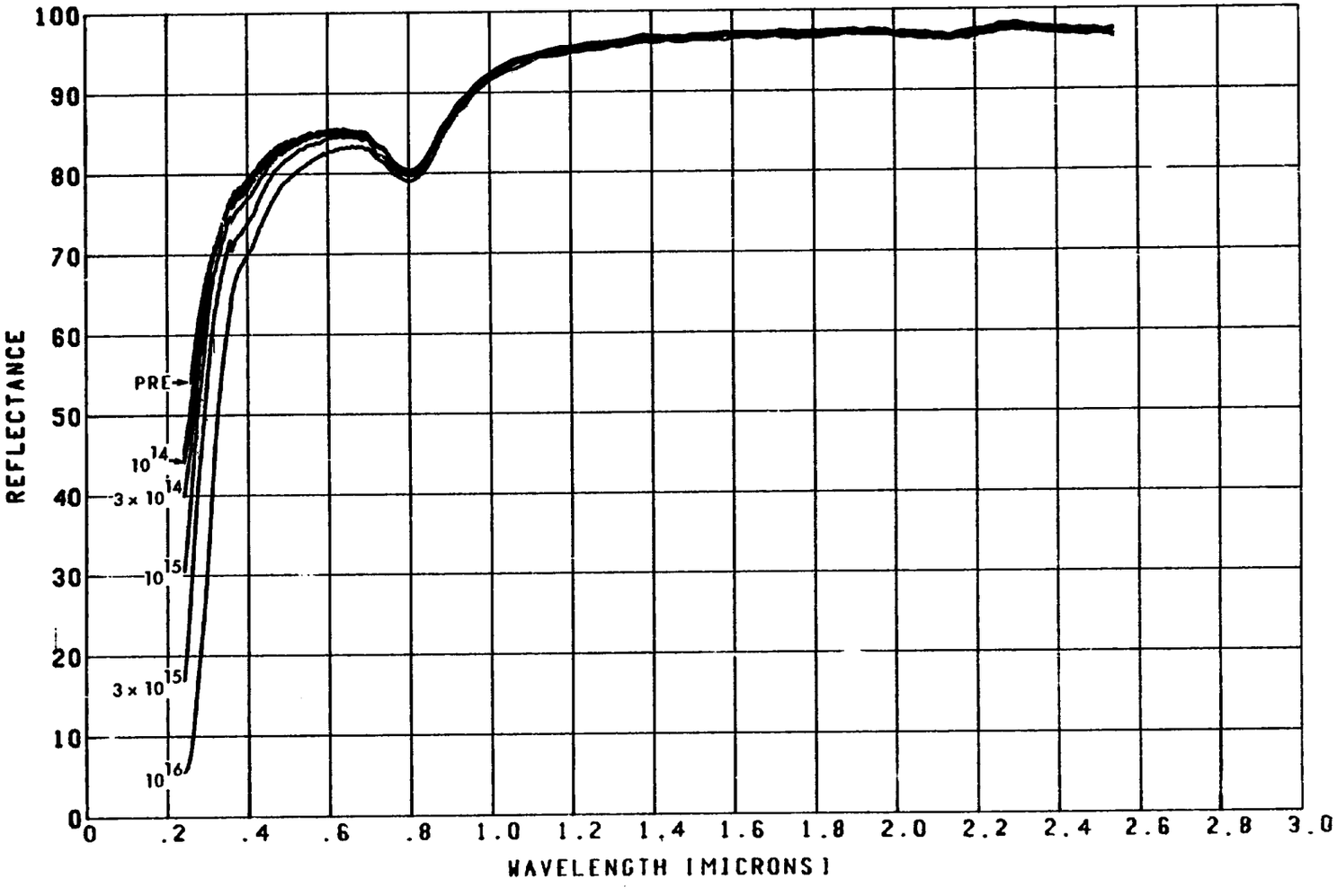

FIGURE 17.

IN SITU EFFECTS OF 40-KEV PROTONS ON THE REFLECTANCE OF NASA-GODDARD ALUMINIZED 5-MIL TEFLON TA-5

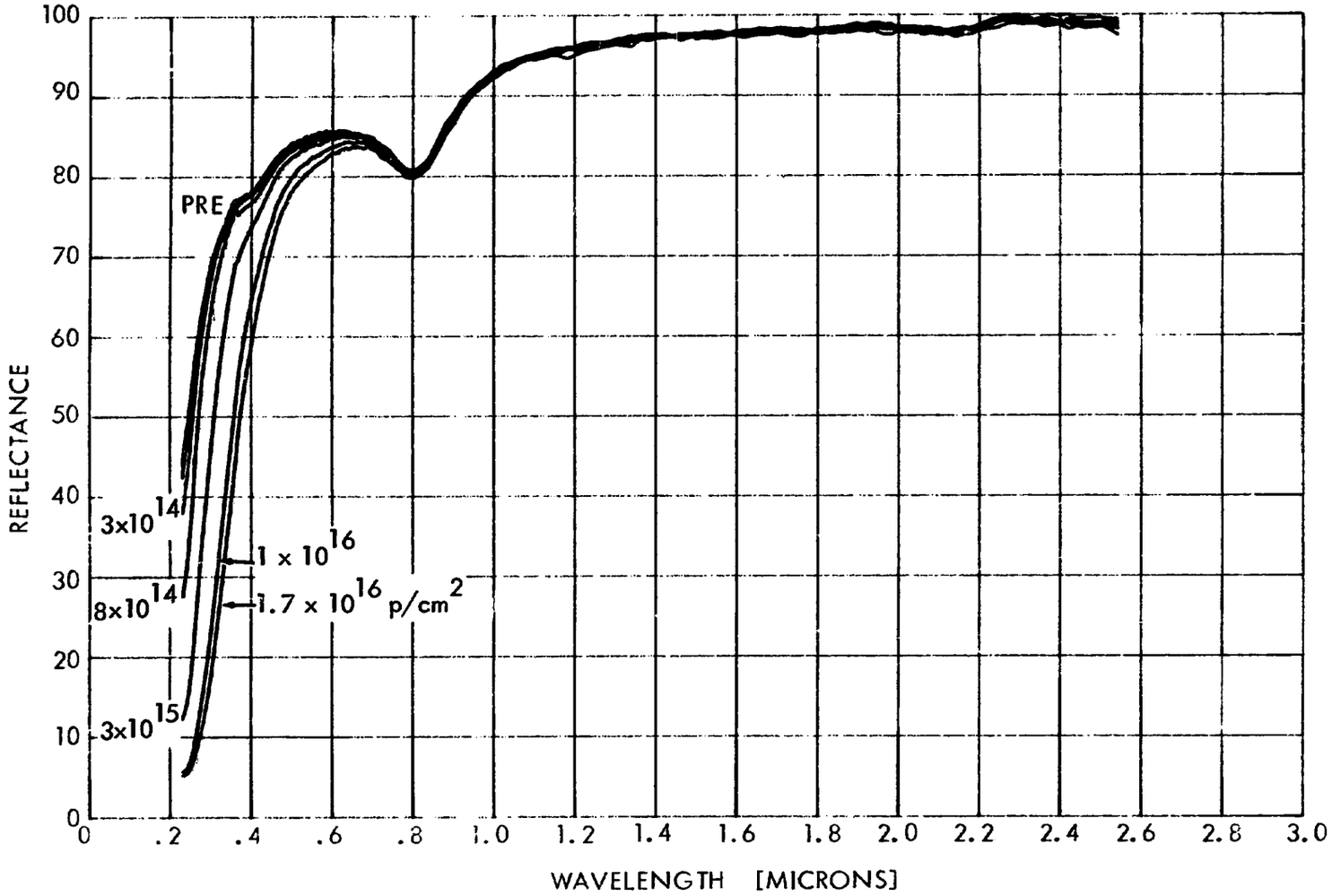

FIGURE 18.

IN SITU EFFECTS OF 35-KEV ELECTRONS ON THE REFLECTANCE OF NASA-GODDARD ALUMINIZED 10-MIL TEFLON [TA-10]

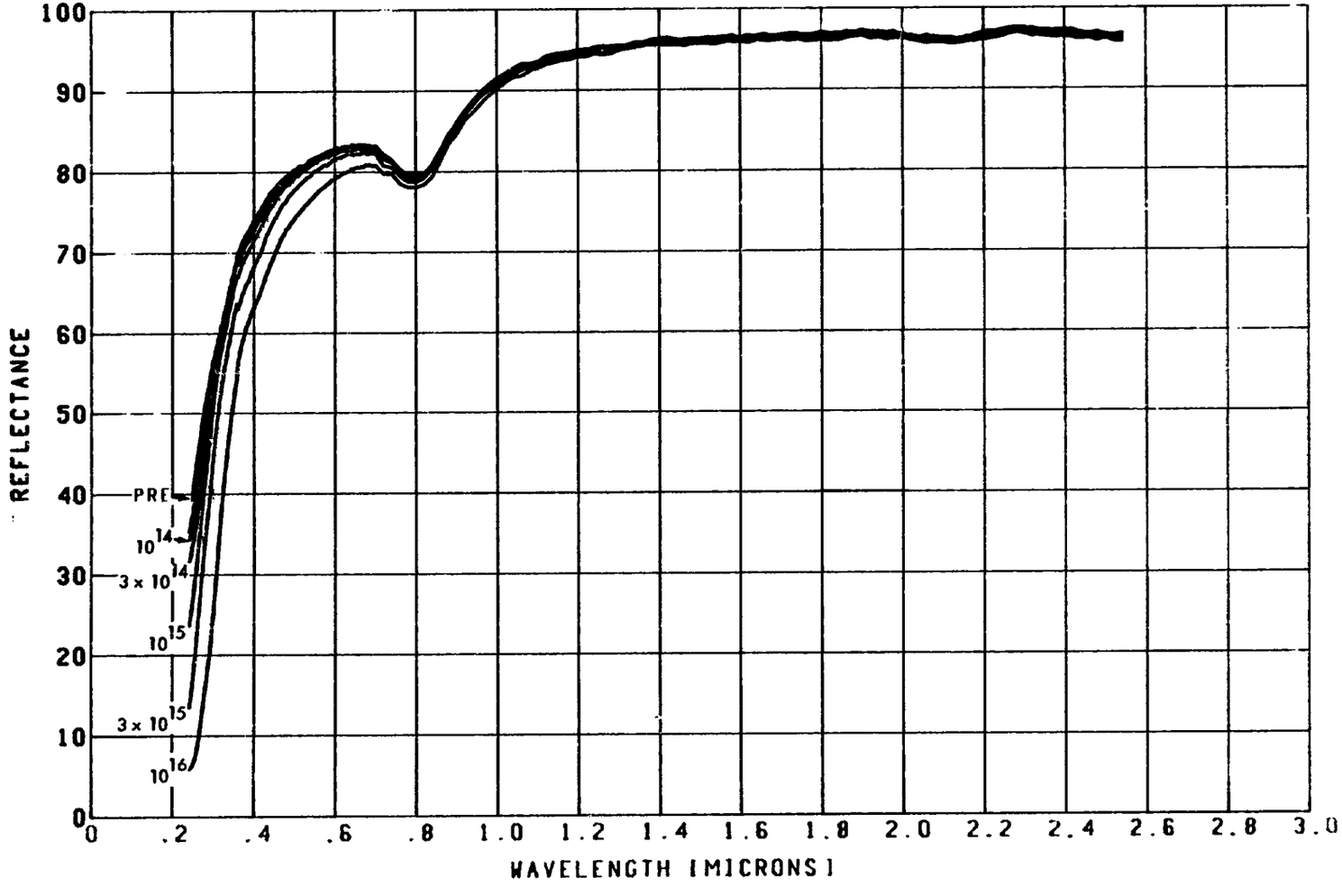

FIGURE 19.

IN SITU EFFECTS OF 40-KEV PROTONS ON THE REFLECTANCE OF NASA-GODDARD ALUMINIZED 10-MIL TEFLON TA-10

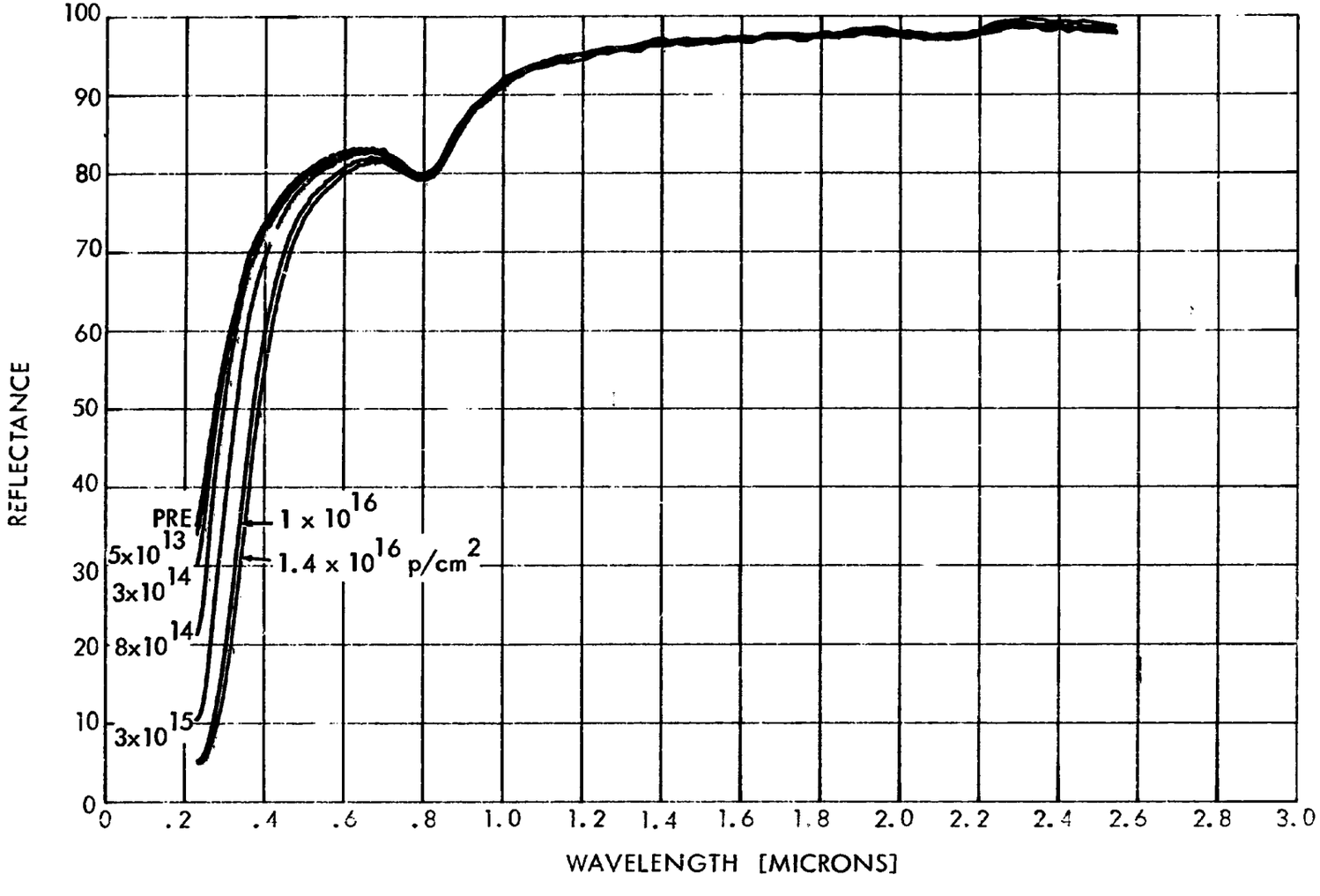

FIGURE 20.

IN SITU EFFECTS OF 35-KEV ELECTRONS ON THE REFLECTANCE OF NASA-GODDARD 0.15 MIL ALZAK [23]

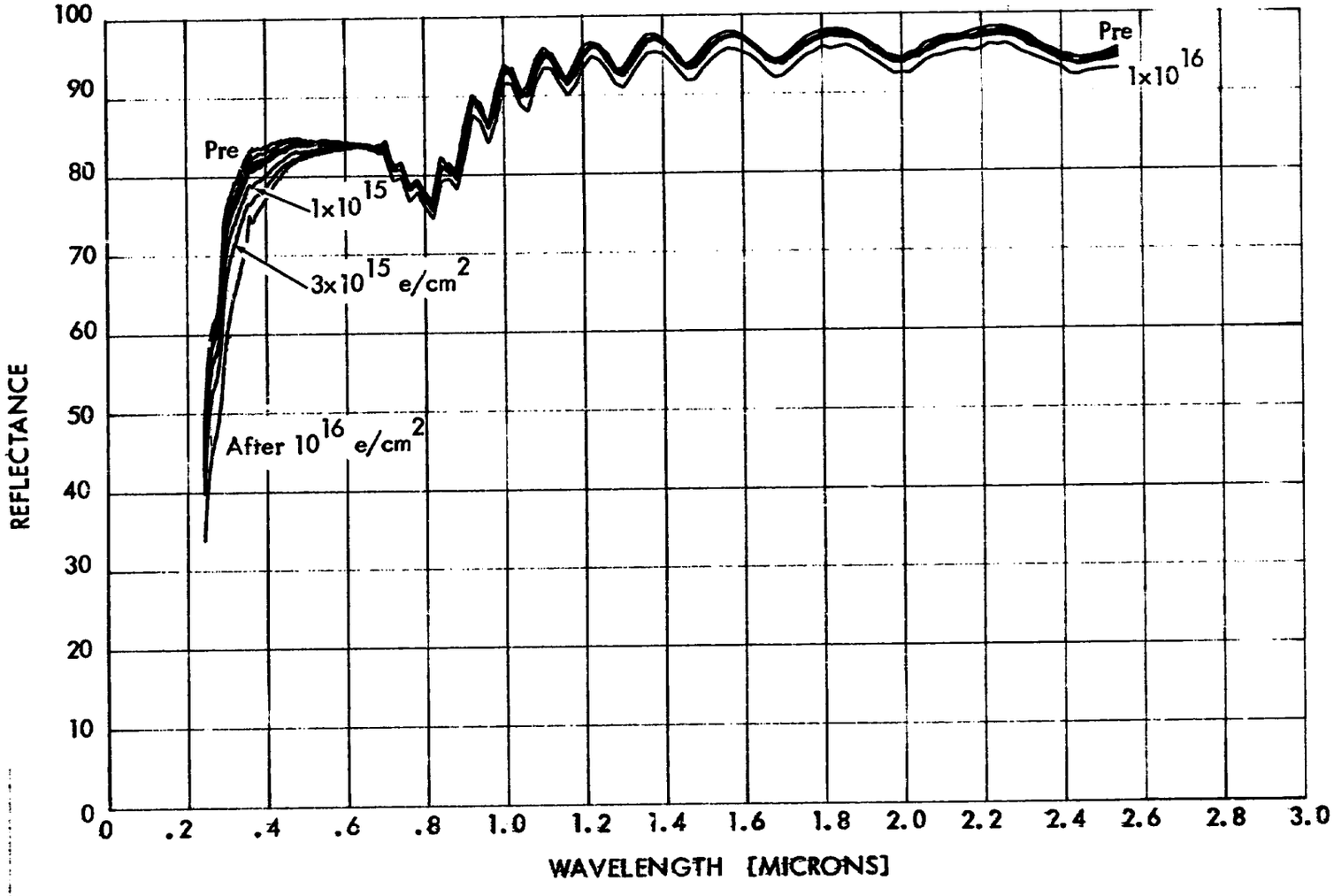

FIGURE 21.

IN SITU EFFECTS OF 40-KEV PROTONS ON THE REFLECTANCE OF NASA-GODDARD 0.15-MIL ANODIZED ALUMINUM [ALZAK, Z3]

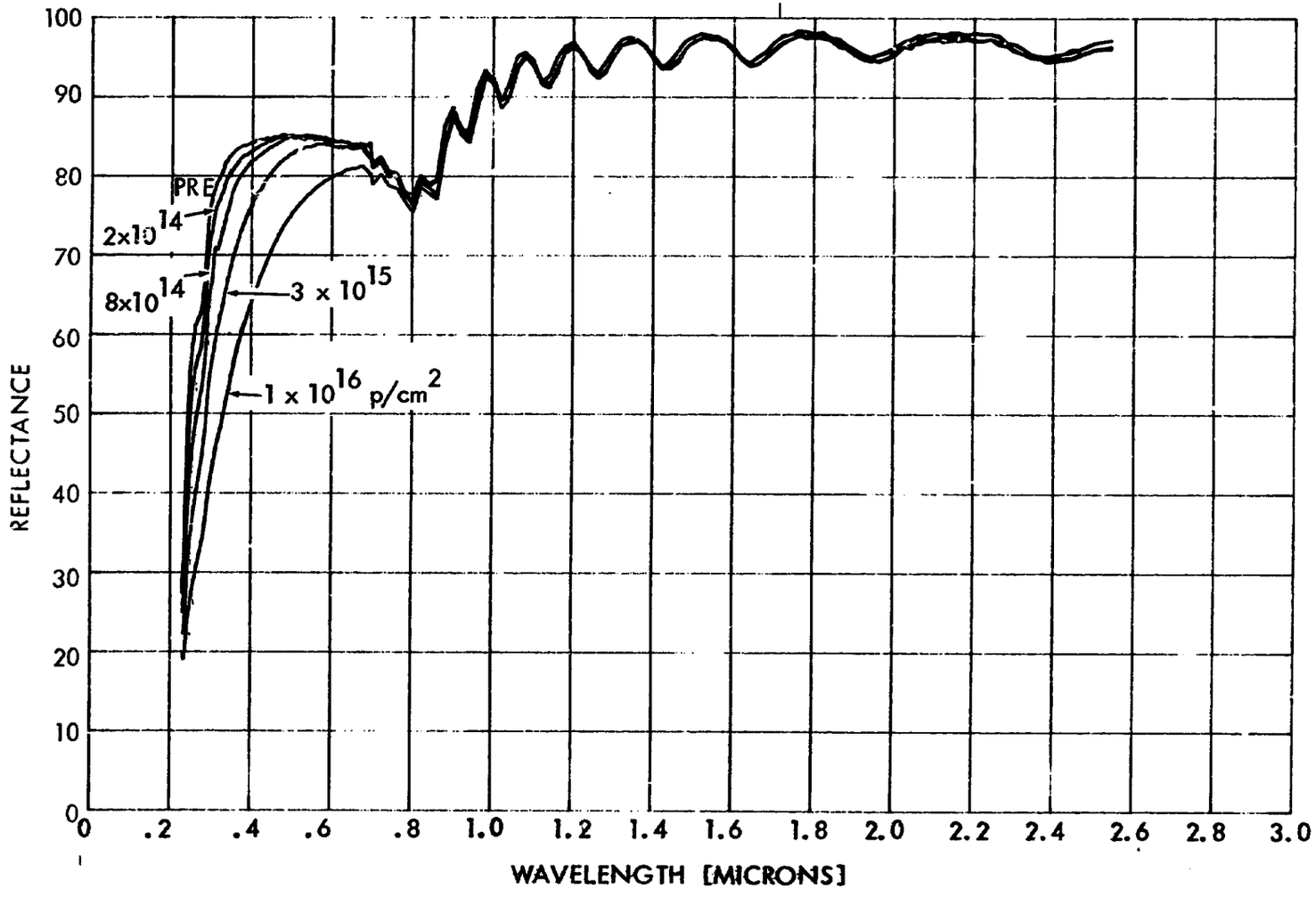

FIGURE 22.

IN SITU EFFECTS OF 35-KEV ELECTRONS ON THE REFLECTANCE OF NASA-GODDARD 0.22-MIL ALZAK [Z4]

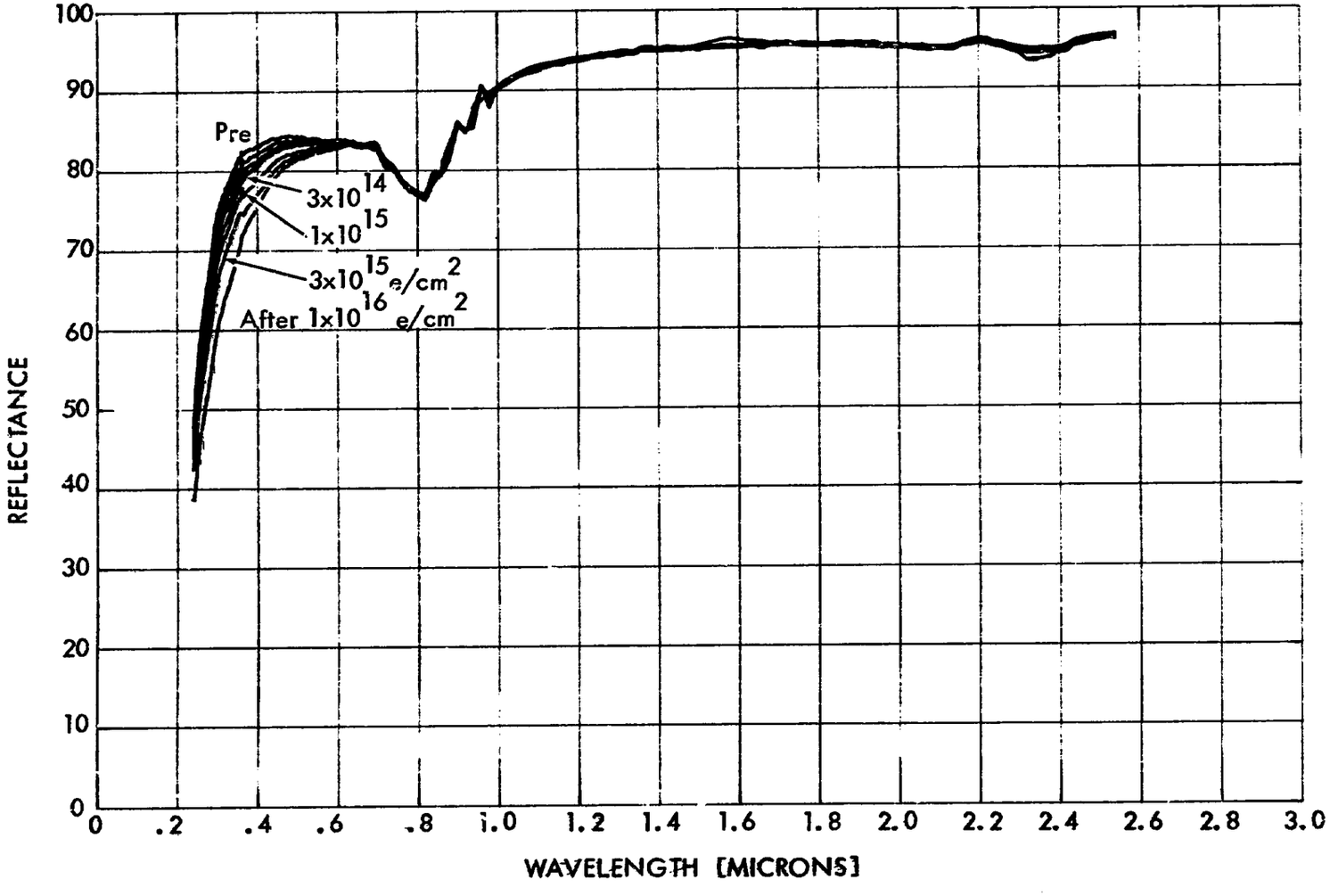

FIGURE 23.

IN SITU EFFECTS OF 40-KEV PROTONS ON THE REFLECTANCE OF NASA-GODDARD 0.22-MIL ANODIZED ALUMINUM [ALZAK, Z4]

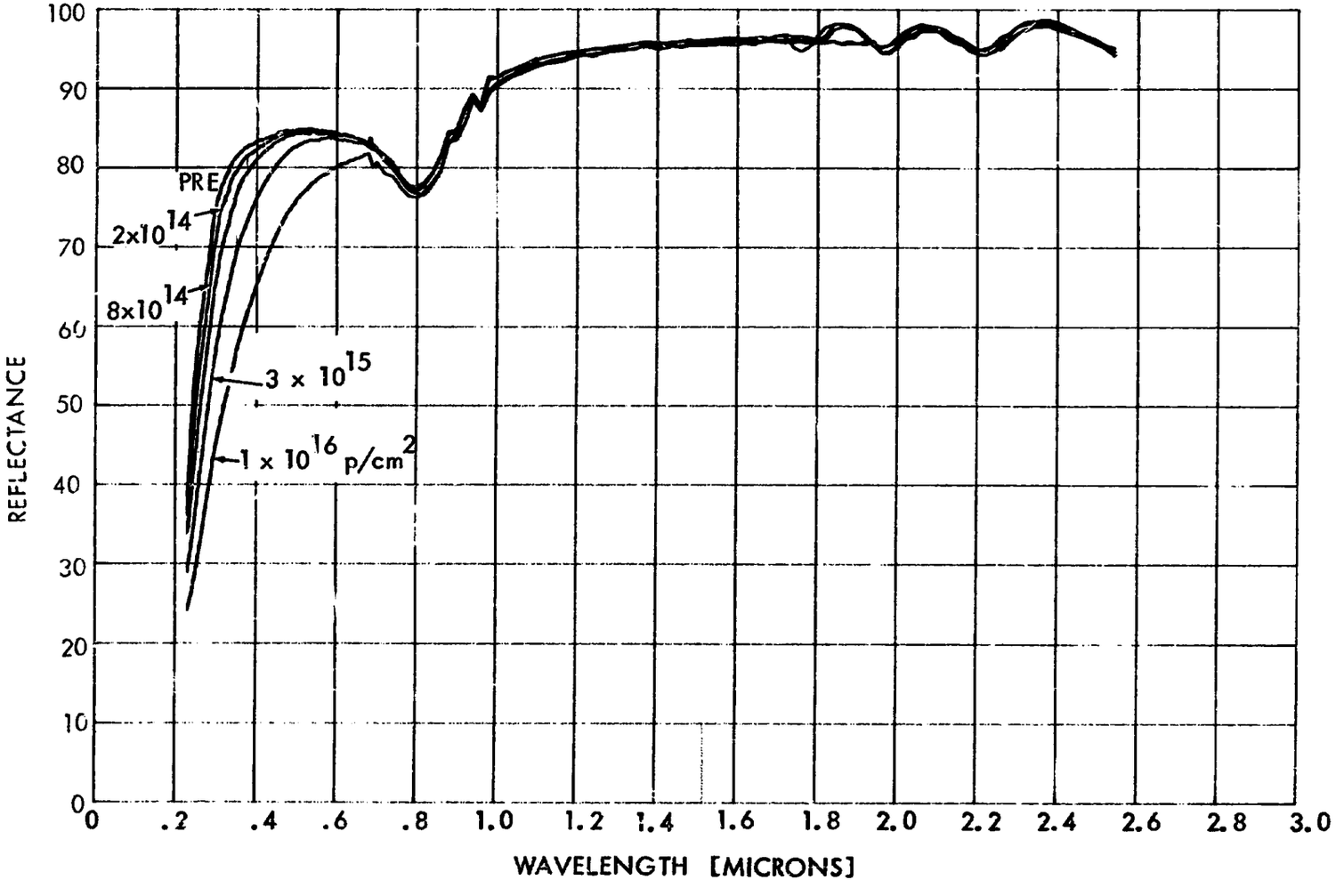

FIGURE 24.

IN SITU EFFECTS OF 35-KEV ELECTRONS ON THE REFLECTANCE OF NASA-GODDARD 0.34-MIL ALZAK [25]

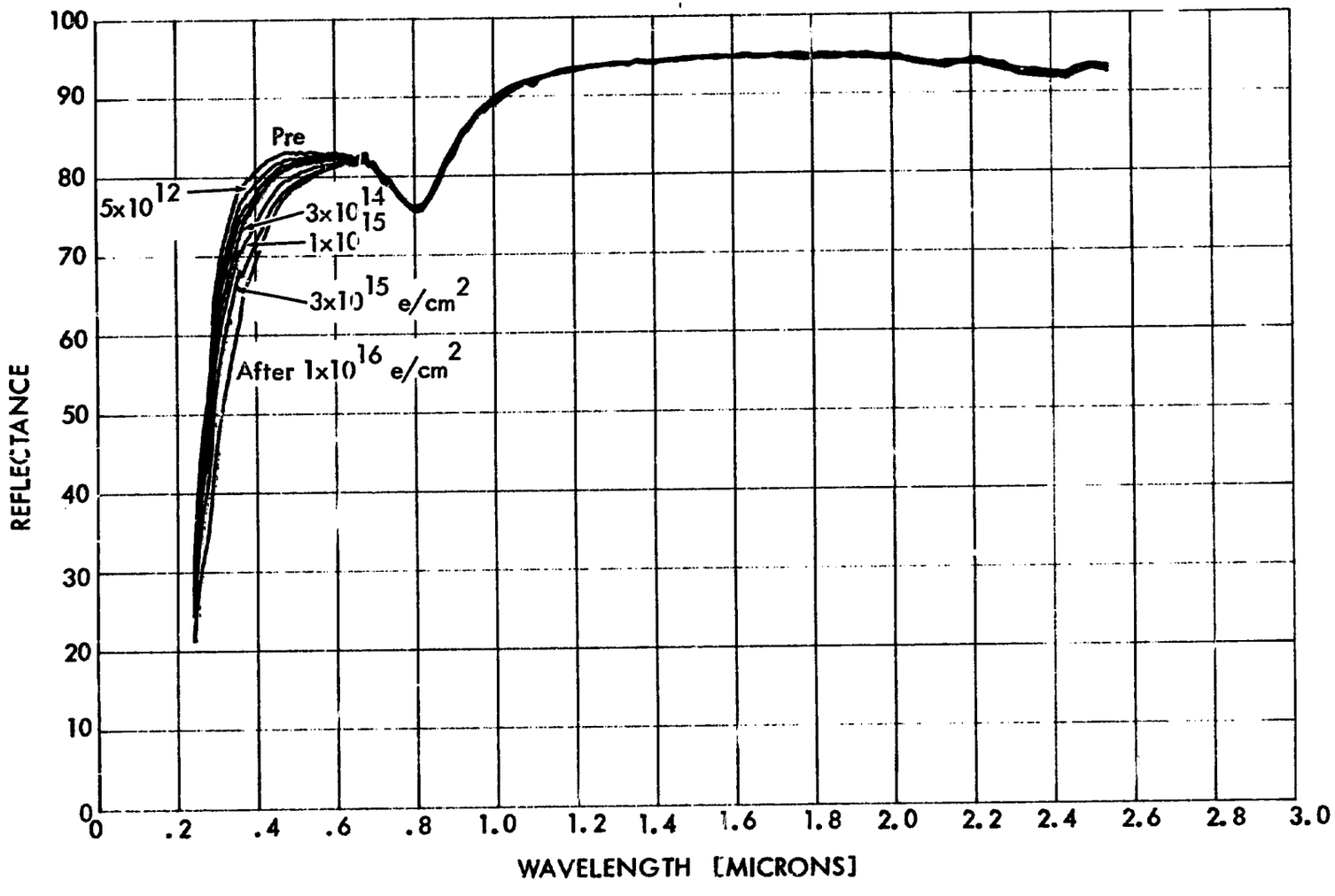

FIGURE 25.

IN SITU EFFECTS OF 40-KEV PROTONS ON THE REFLECTANCE OF NASA-GODDARD 0.34-MIL ANODIZED ALUMINUM [ALZAK, Z5]

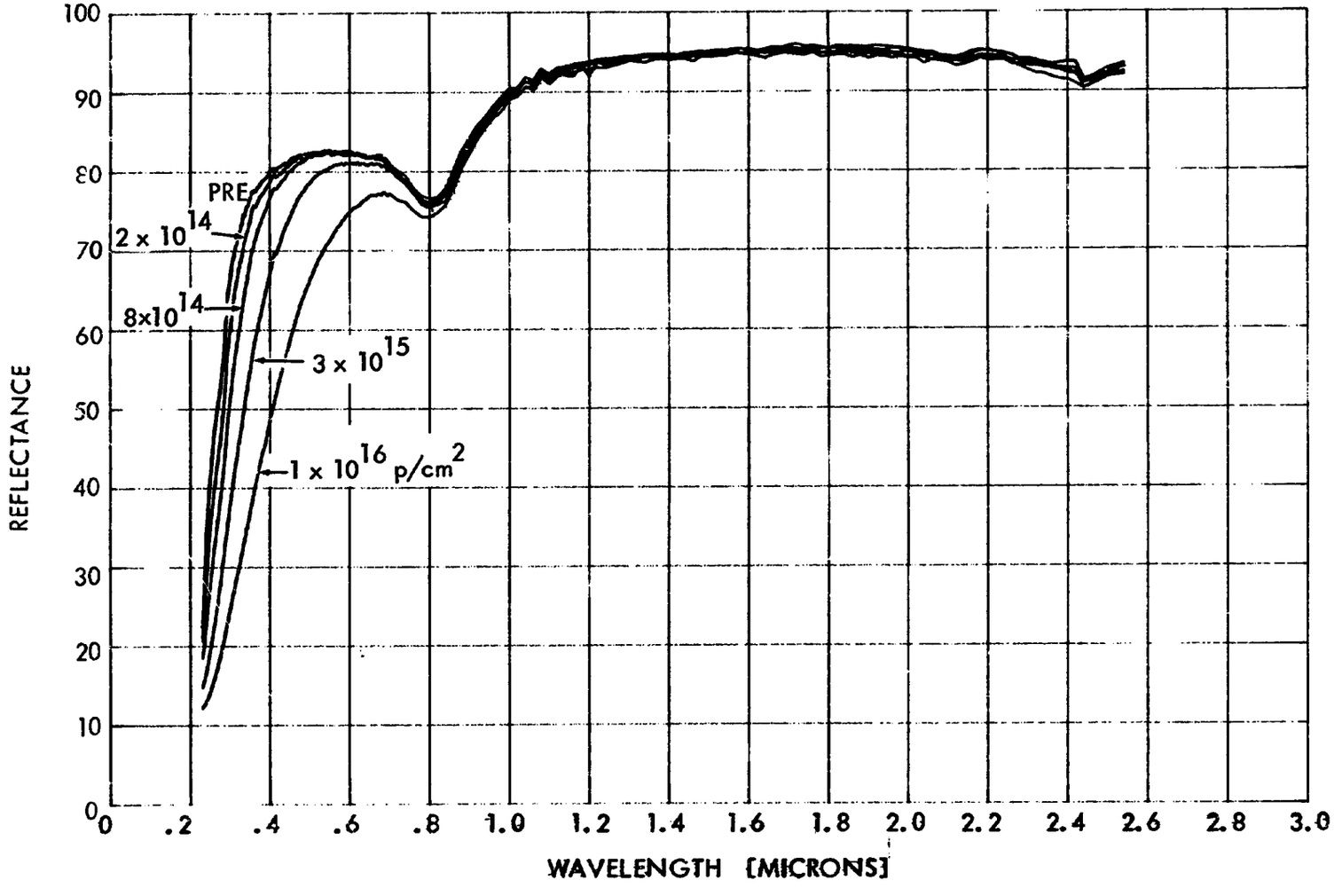

FIGURE 26.

IN SITU EFFECTS OF 35-KEV ELECTRONS ON THE REFLECTANCE OF NASA-GODDARD SILICON DIOXIDE VAPOR-DEPOSITED ON ALUMINUM [H]

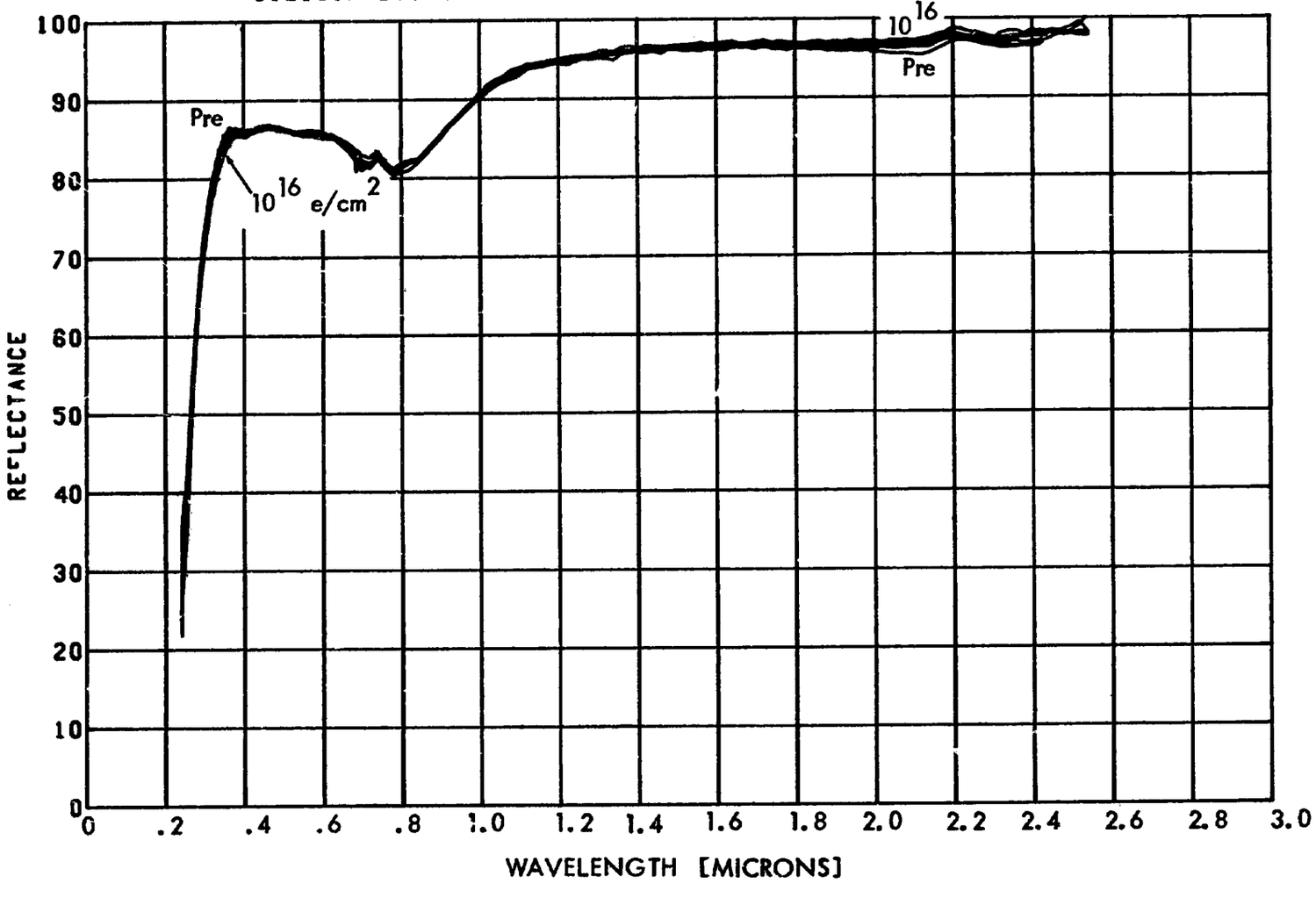

FIGURE 27.

IN SITU EFFECTS OF 40-KEV PROTONS ON THE REFLECTANCE OF NASA-GODDARD SILICON DIOXIDE EVAPORATED ONTO ALUMINUM [H]

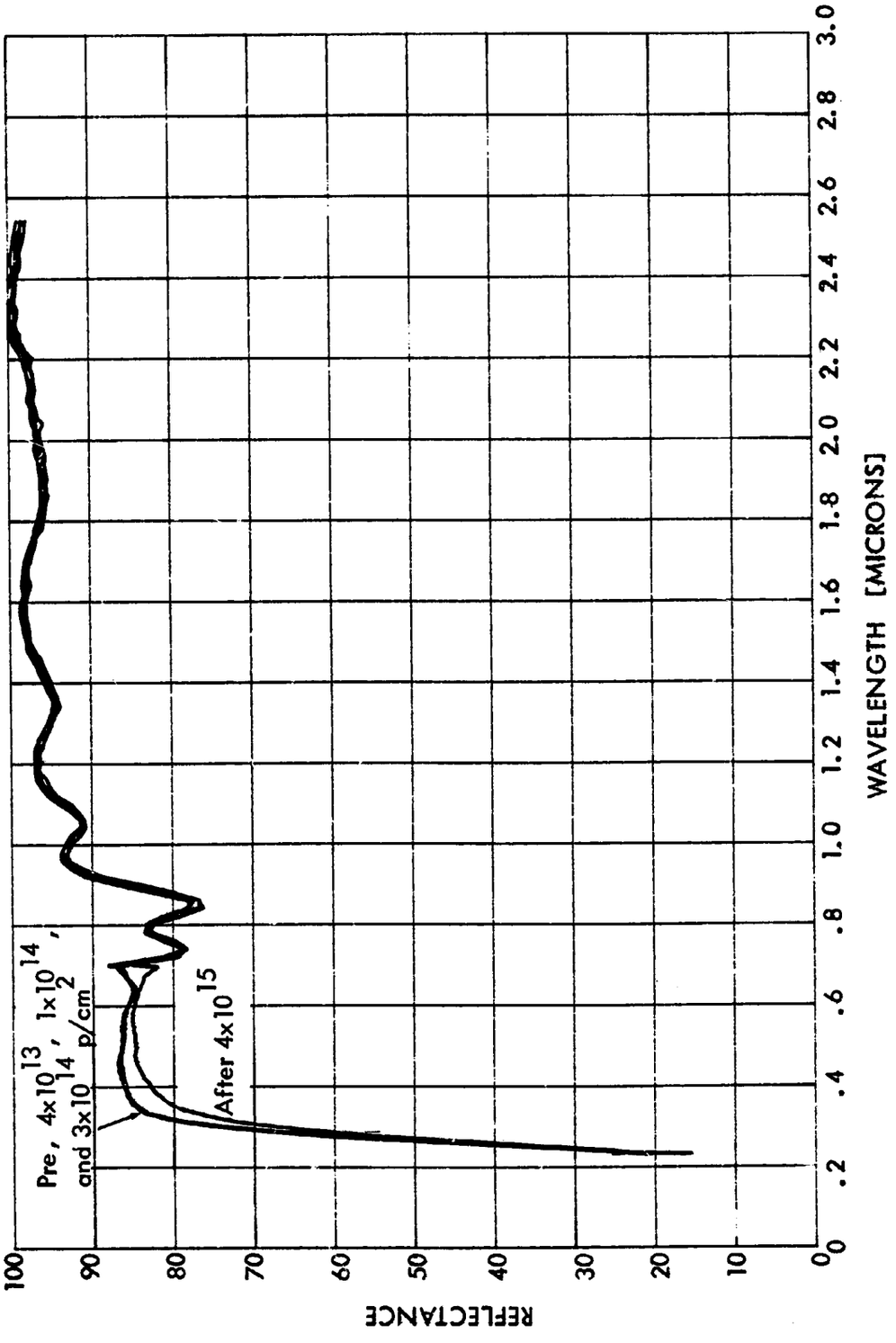

FIGURE 28.

IN SITU EFFECTS OF 35-KEV ELECTRONS ON THE REFLECTANCE OF NASA-GODDARD TYPE H KAPTON FILM (N)

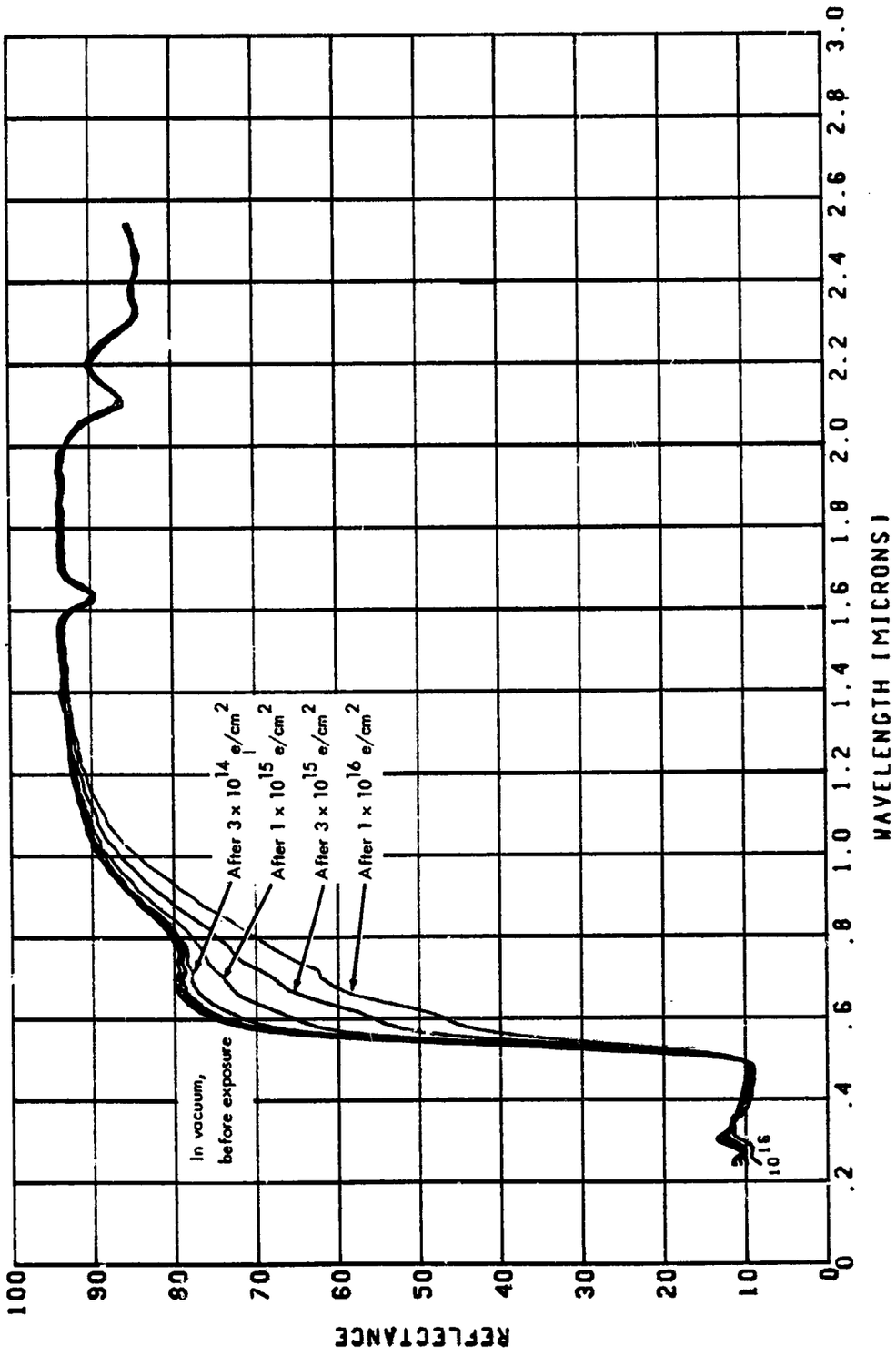

FIGURE 29.

IN SITU EFFECTS OF 40-KEV PROTONS ON THE REFLECTANCE OF NASA-GODDARD TYPE H KAPTON FILM [N]

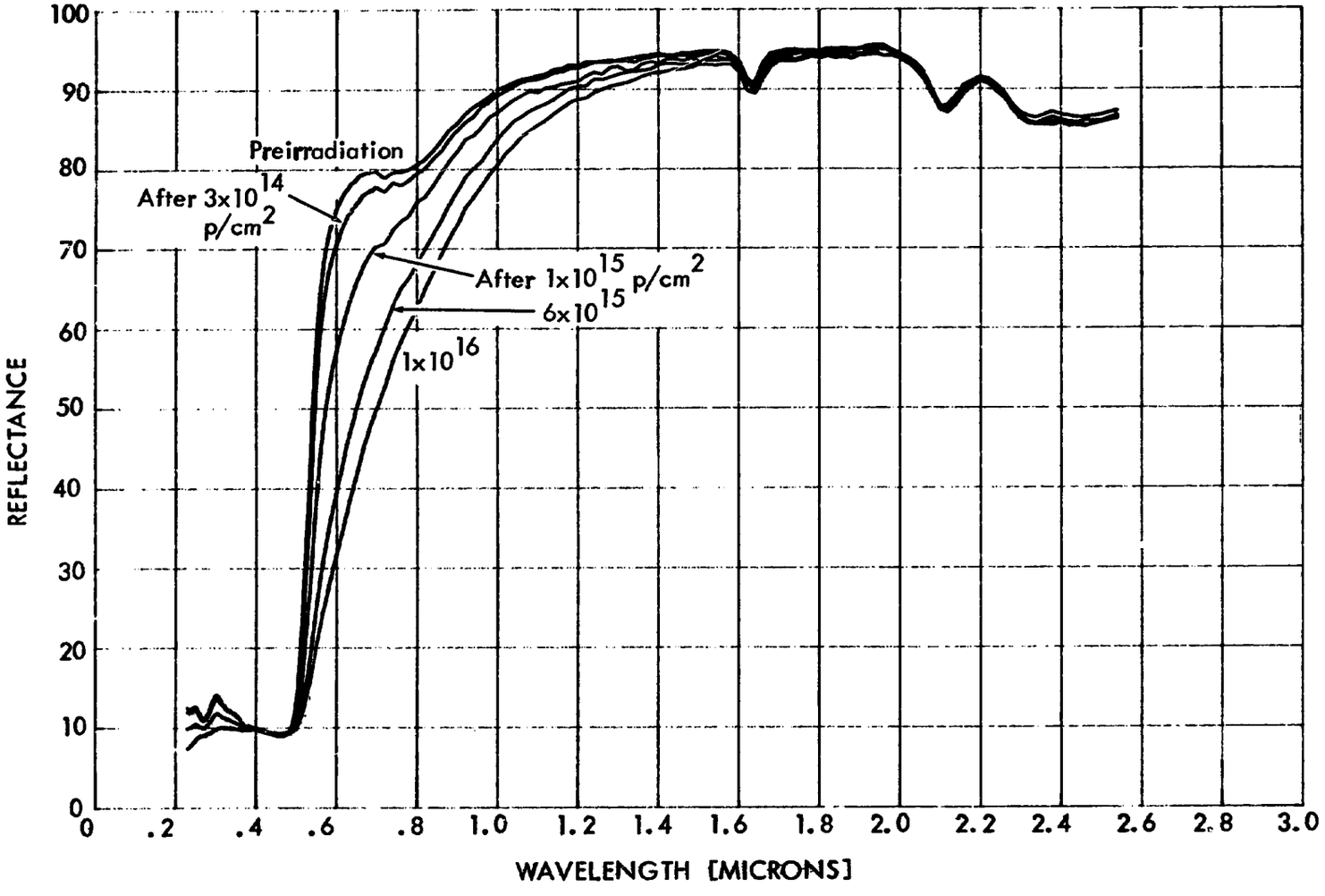

FIGURE 30.

IN SITU EFFECTS OF 35-KEV ELECTRONS ON THE REFLECTANCE OF NASA-GODDARD TREATED ZINC OXIDE — METHYL SILICONE (SERIES 101-7, R)

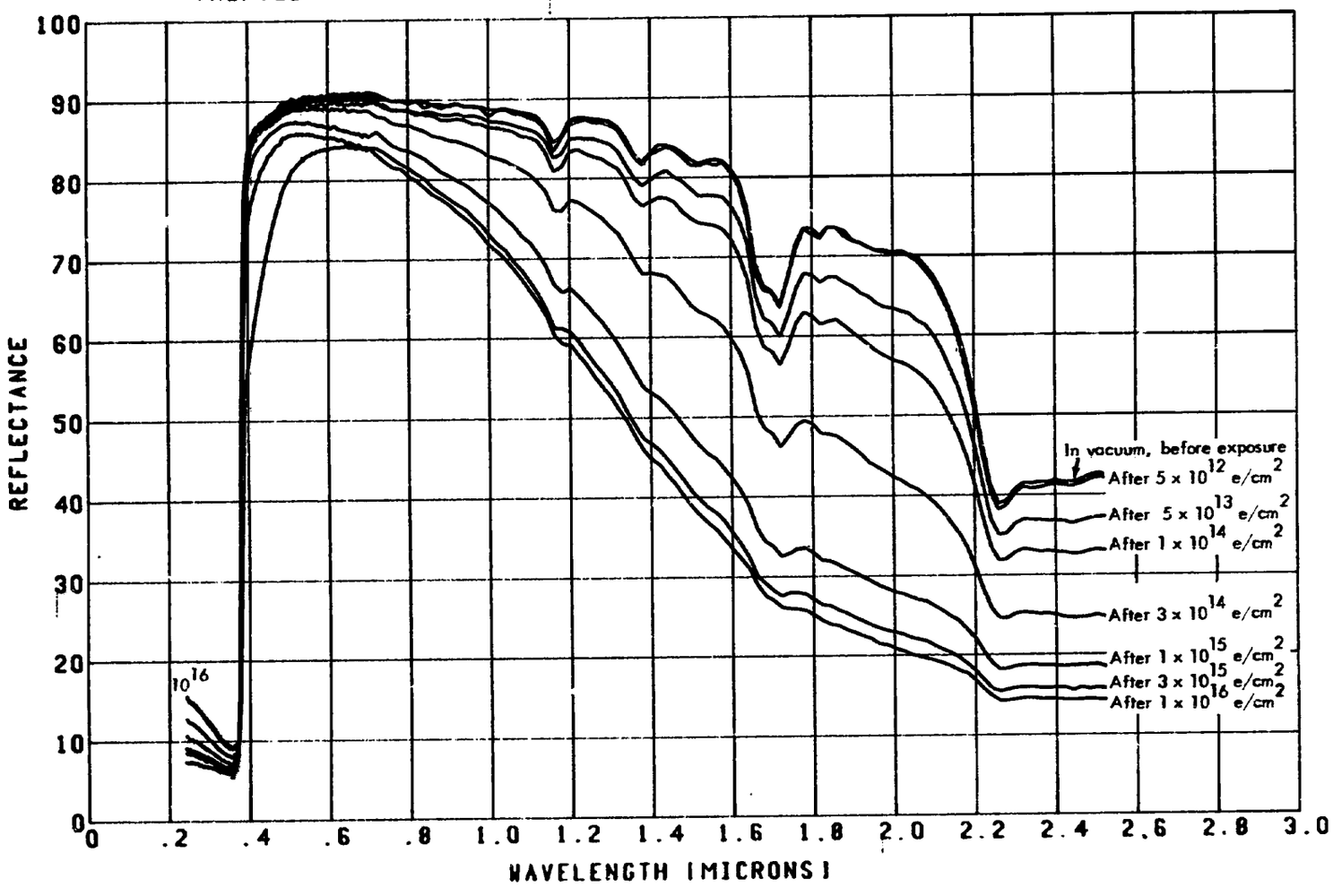

FIGURE 31.

IN SITU EFFECTS OF 40-KEV PROTONS ON THE REFLECTANCE OF NASA-GODDARD TREATED ZINC OXIDE-METHYL SILICONE [SERIES 101-7,R]

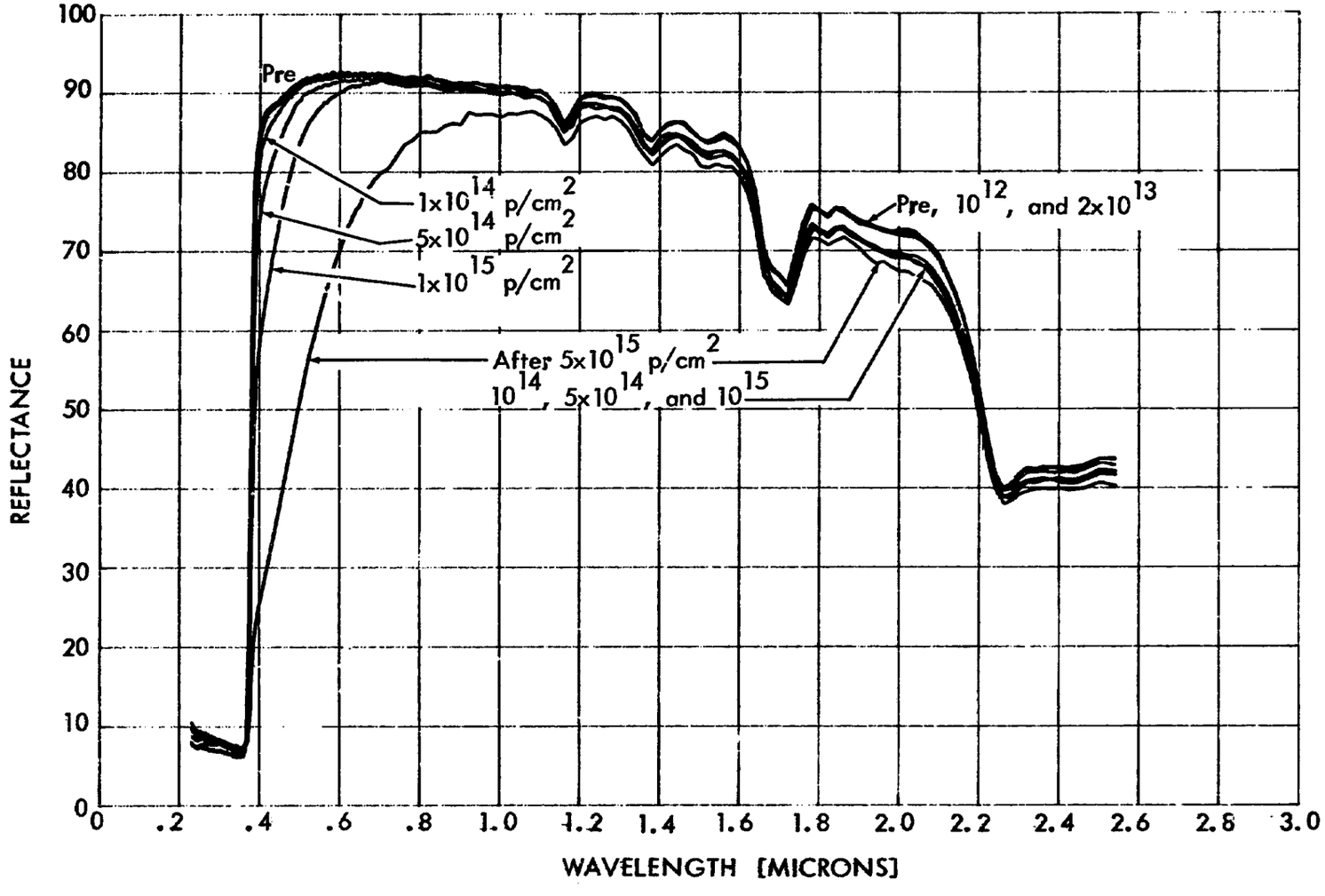

FIGURE 32.

IN SITU EFFECTS OF 35-KEV ELECTRONS ON THE REFLECTANCE OF NASA-GODDARD TREATED ZINC OXIDE — METHYL SILICONE (S-13G TYPE M)

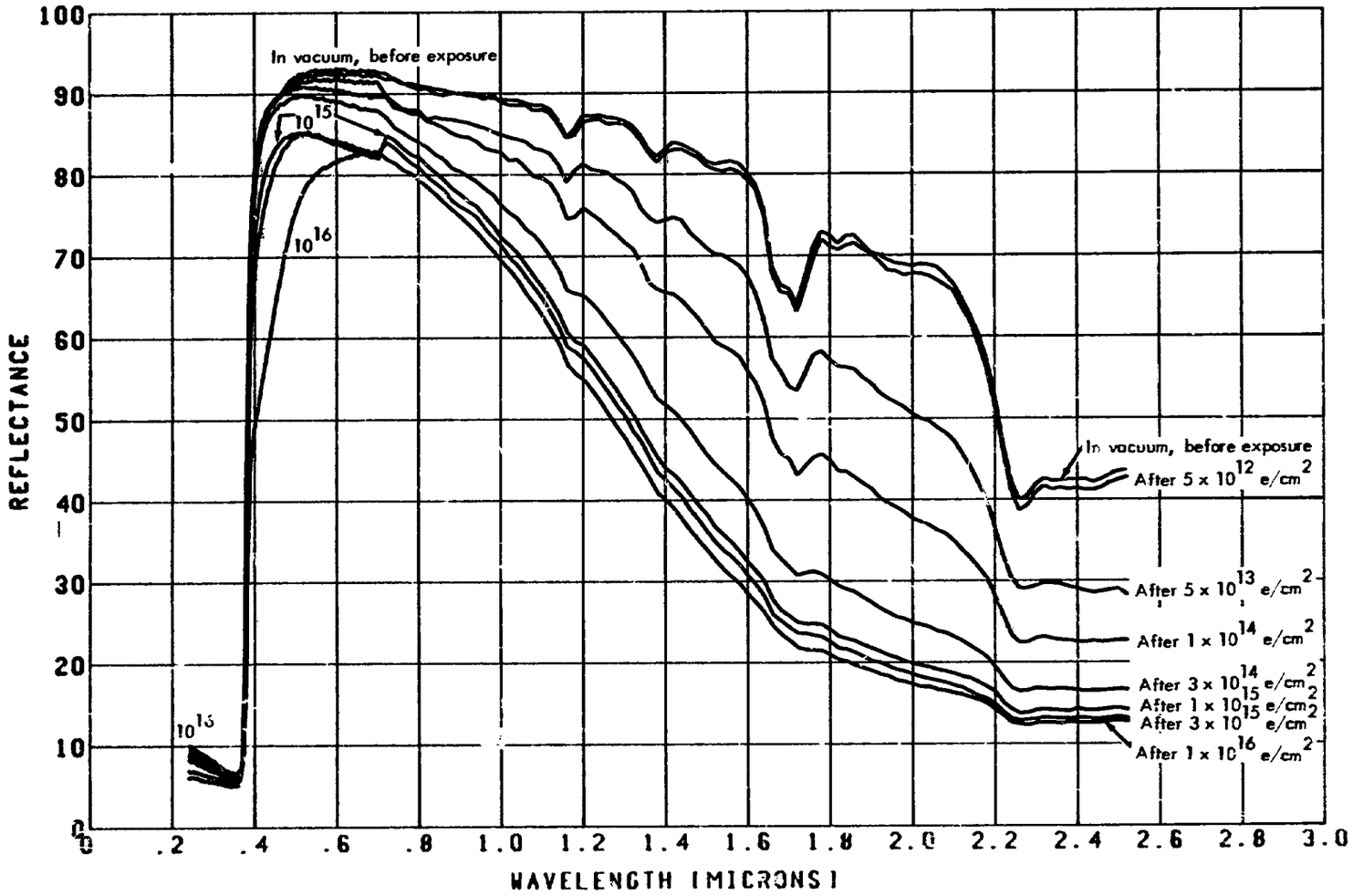

FIGURE 33.

IN SITU EFFECTS OF 40-KEV PROTONS ON THE REFLECTANCE OF NASA-GODDARD TREAT'D ZINC OXIDE-METHYL SILICONE [M]

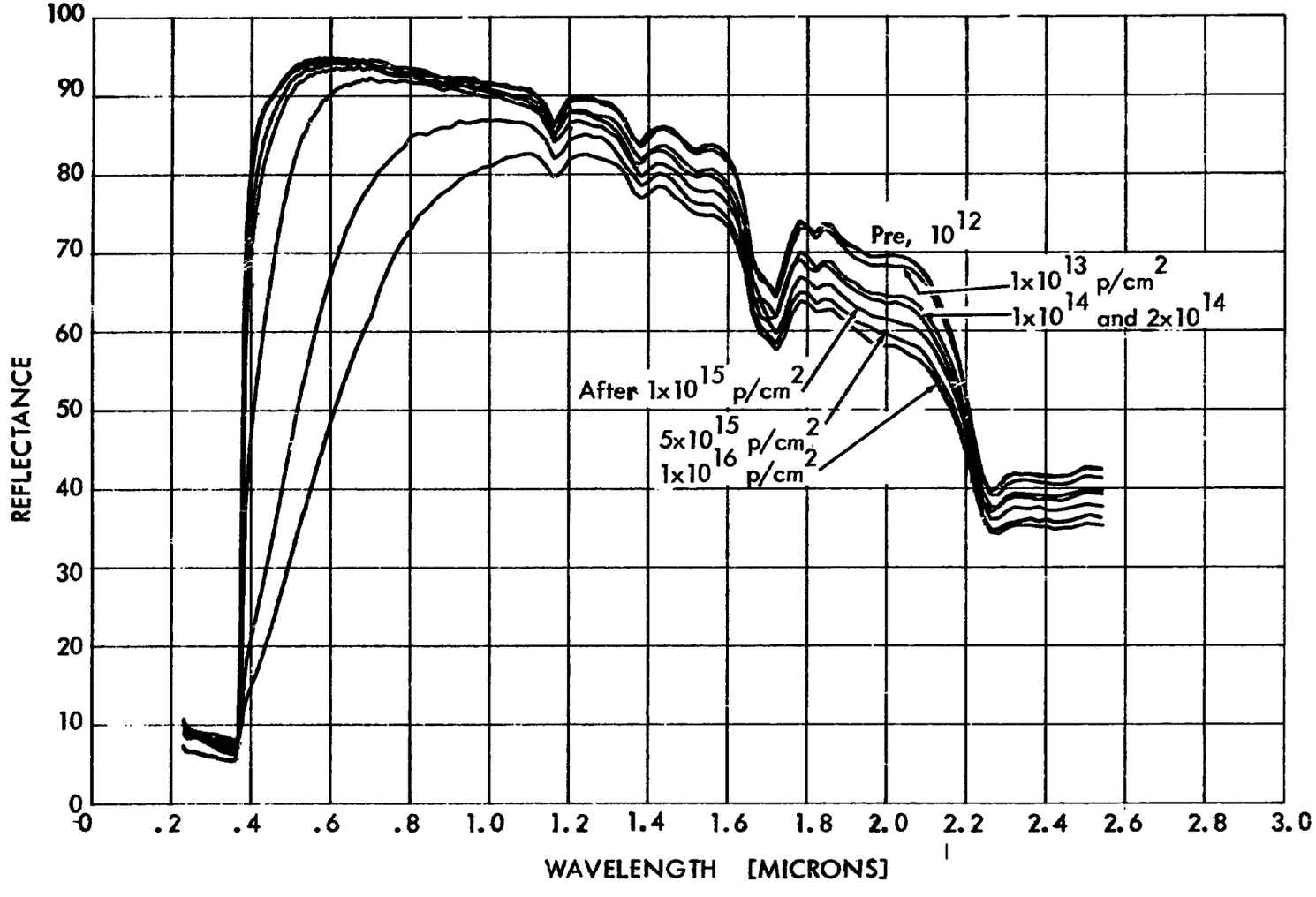

FIGURE 34.

IN SITU EFFECTS OF 35-KEV ELECTRONS ON THE REFLECTANCE OF NASA-GODDARD ANATASE TITANIUM DIOXIDE—METHYL SILICONE (L1)

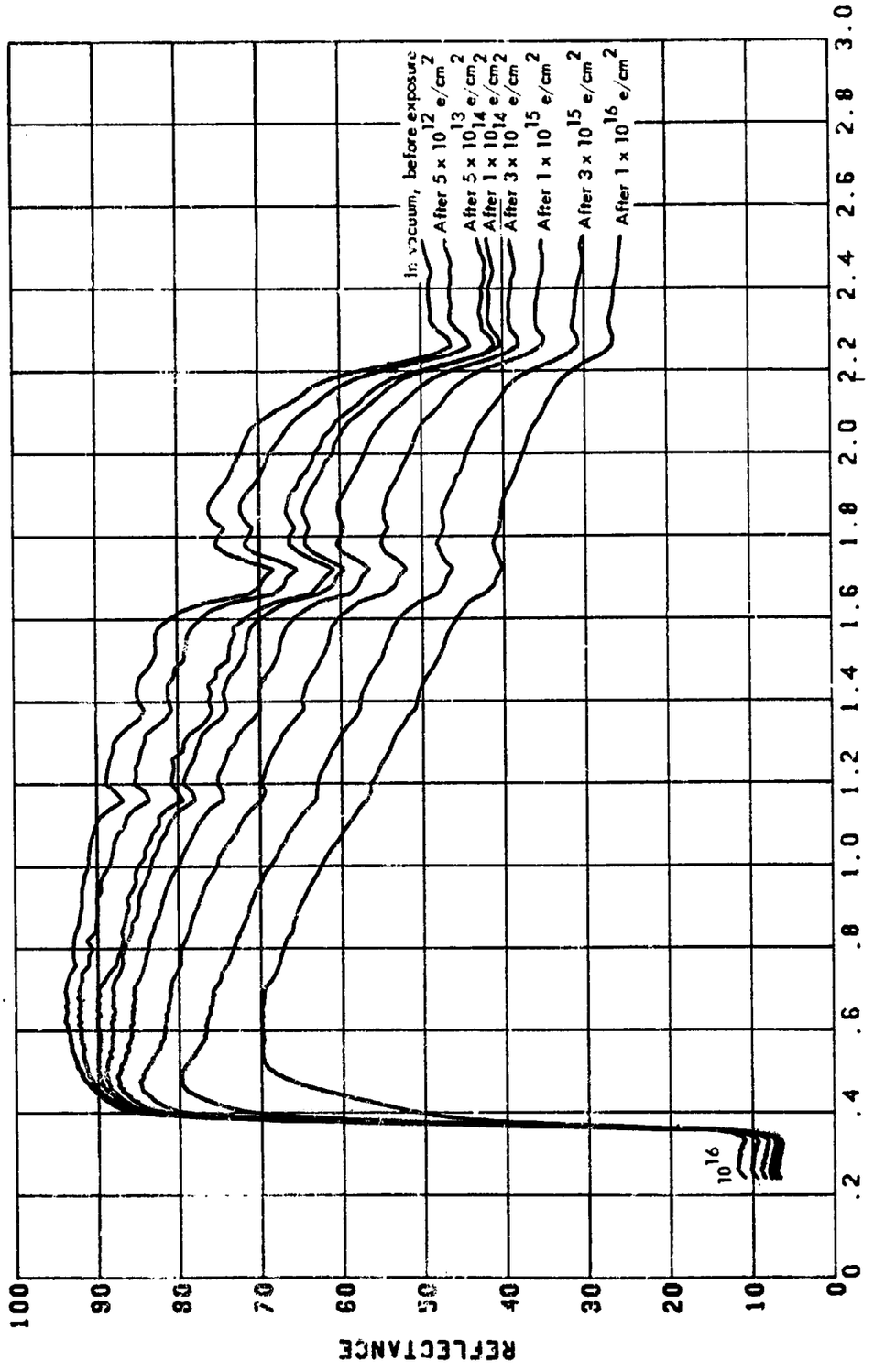

FIGURE 35.

IN SITU EFFECTS OF 40-KEV PROTONS ON THE REFLECTANCE OF NASA-GODDARD ANATASE TITANIUM DIOXIDE-METHYL SILICONE [illegible]

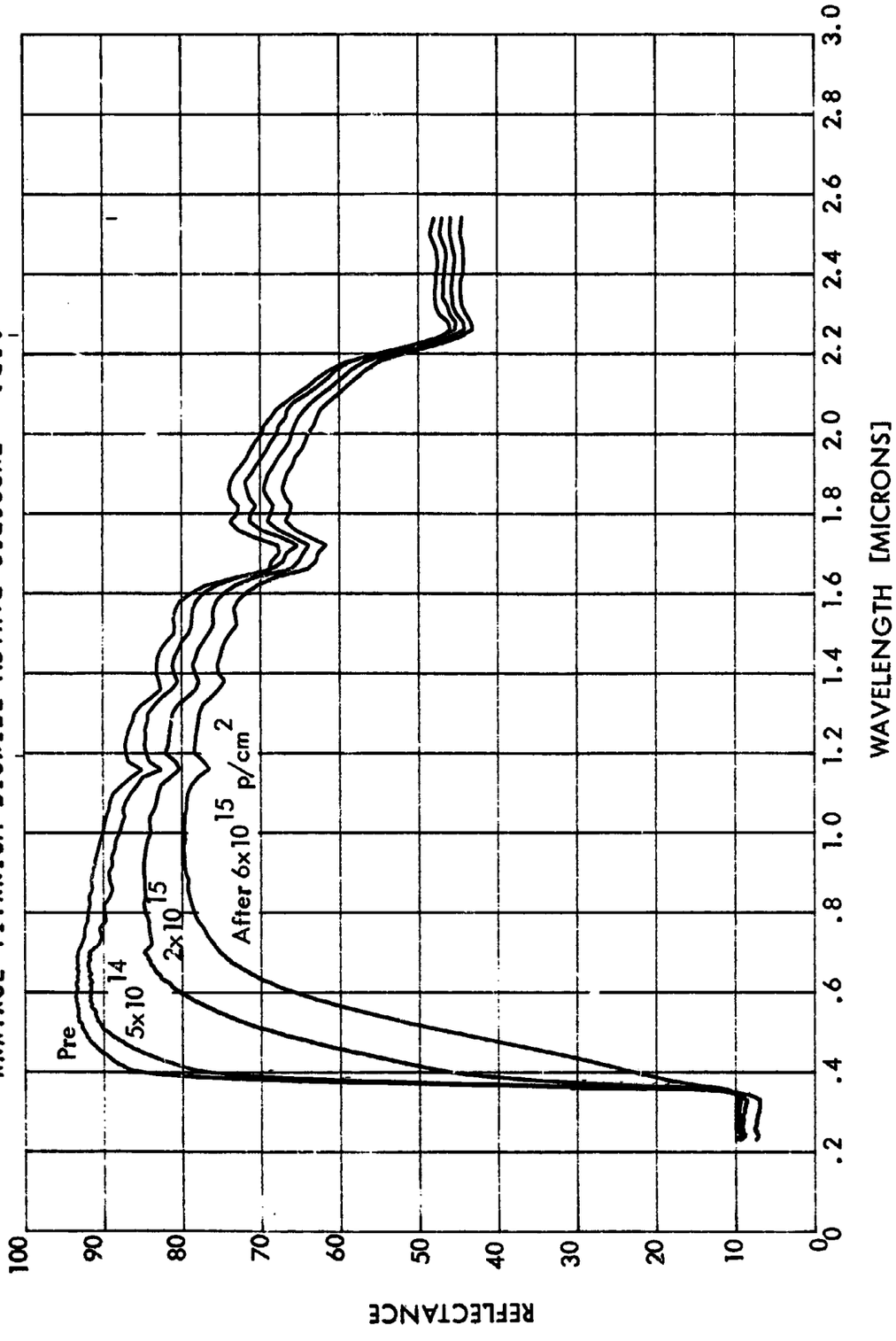

FIGURE 36.

IN SITU EFFECTS OF 35-KEV ELECTRONS ON THE REFLECTANCE OF NASA-GODDARD RUTILE TITANIUM DIOXIDE—METHYL SILICONE [O]

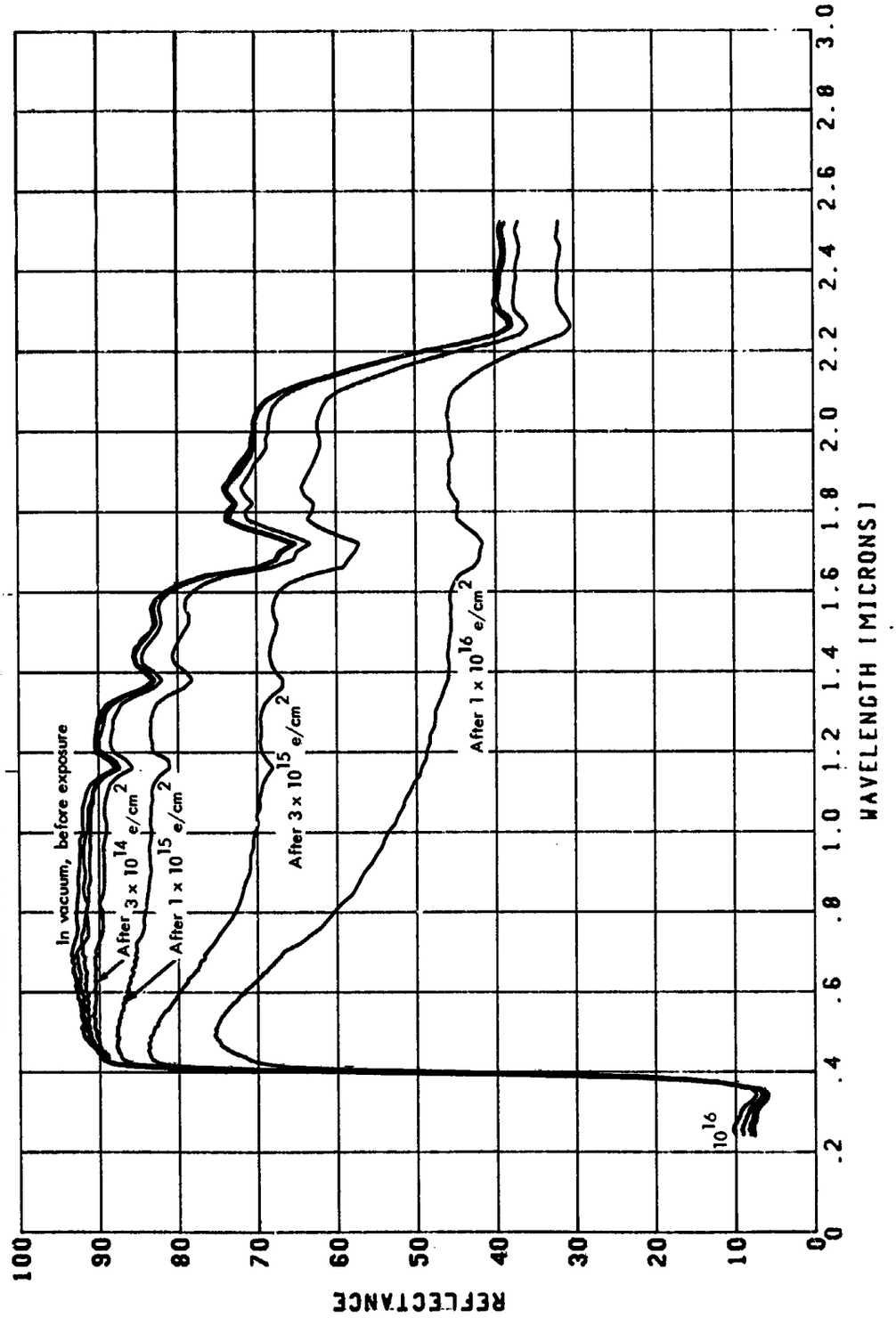

FIGURE 37.

IN SITU EFFECTS OF 40-KEV PROTONS ON THE REFLECTANCE OF NASA-GODDARD RUTILE TITANIUM DIOXIDE-METHYL SILICONE [0]

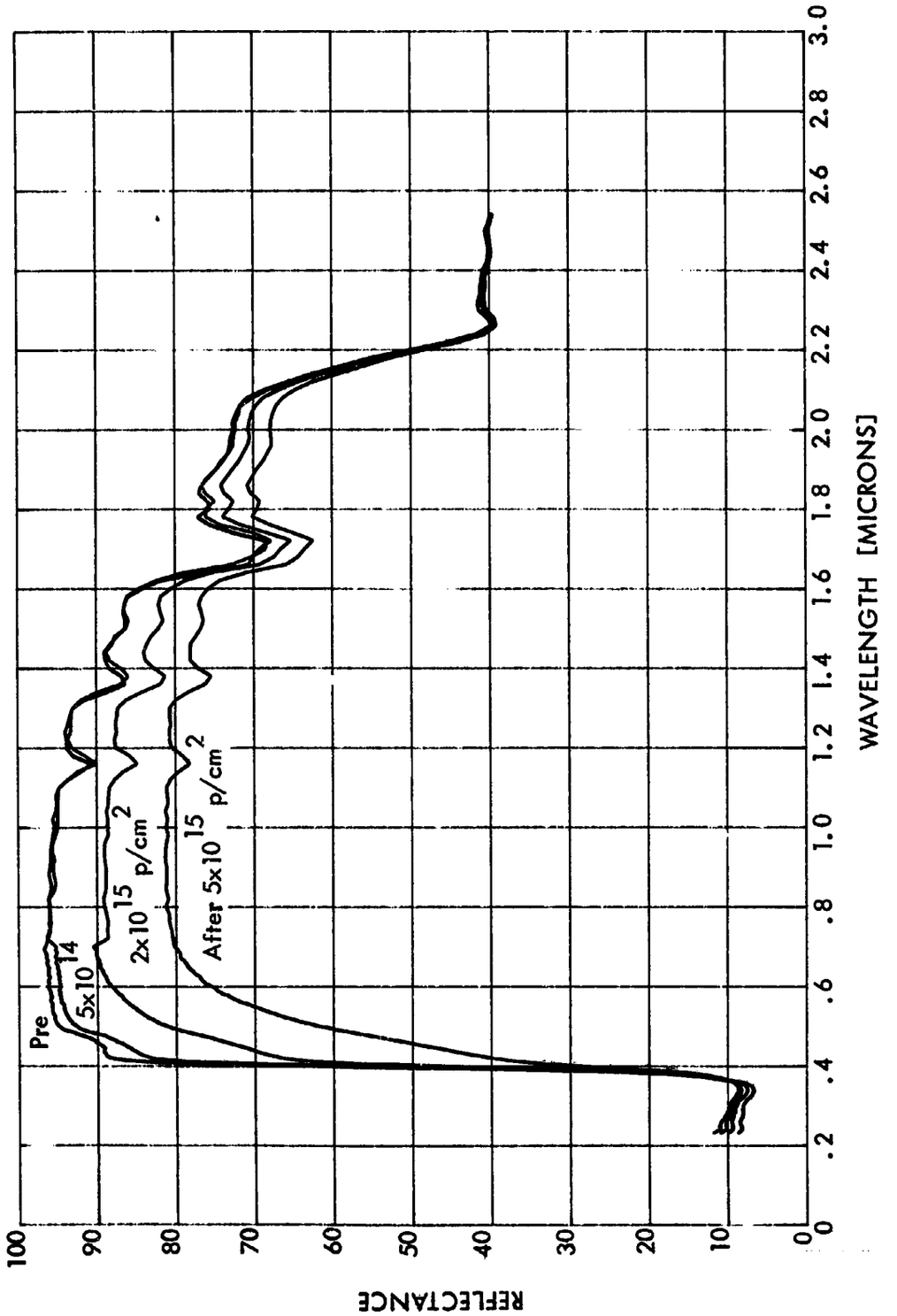

FIGURE 38.

IN SITU EFFECTS OF 35-KEV ELECTRONS ON THE REFLECTANCE OF NASA-GODDARD RUTILE TITANIUM DIOXIDE/ALUMINUM OXIDE — POTASSIUM SILICATE [E3]

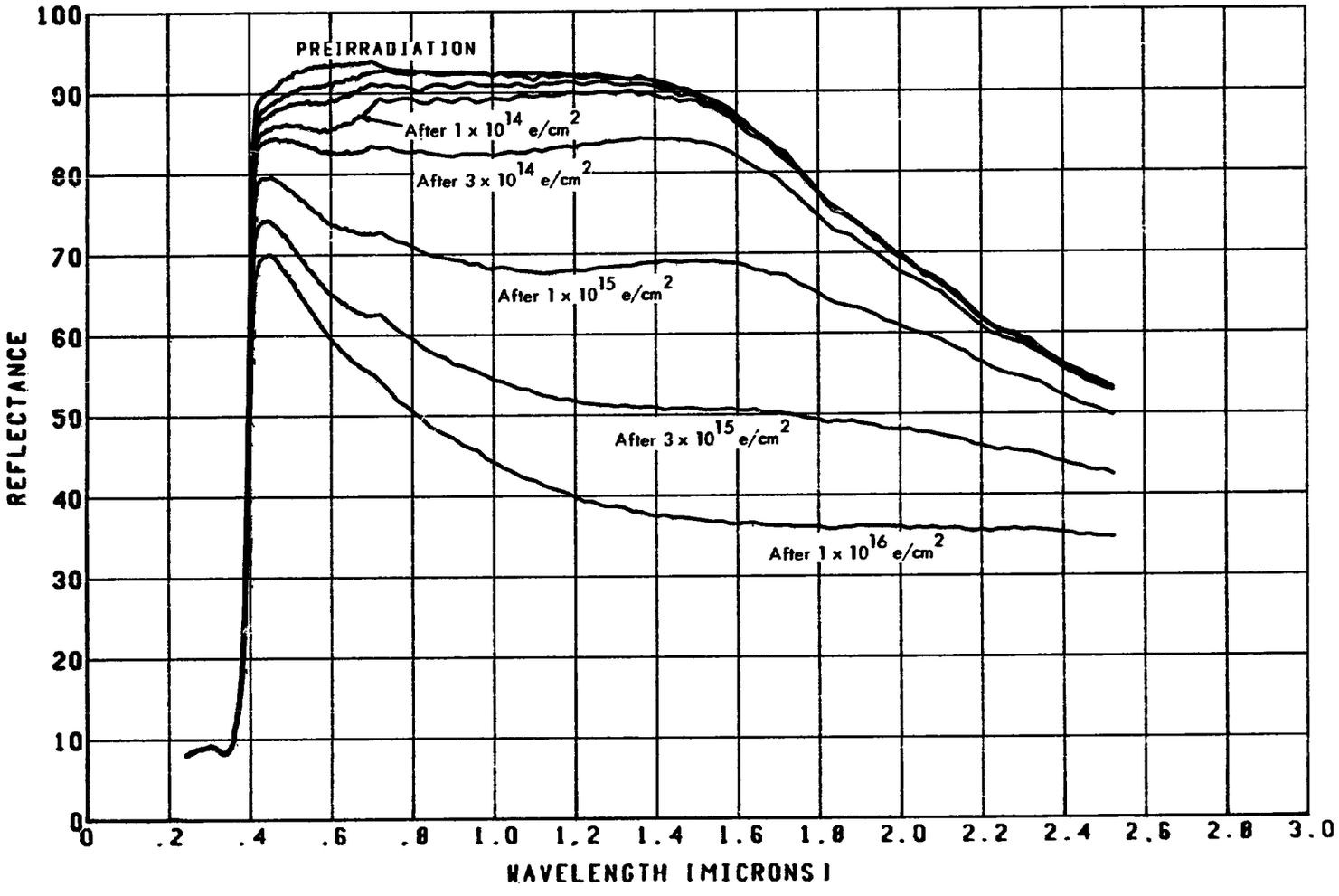

FIGURE 39.

IN SITU EFFECTS OF 40-KEV PROTONS ON THE REFLECTANCE OF NASA-GODDARD RUTILE TITANIUM DIOXIDE/ALUMINUM OXIDE-POTASSIUM SILICATE [E3]

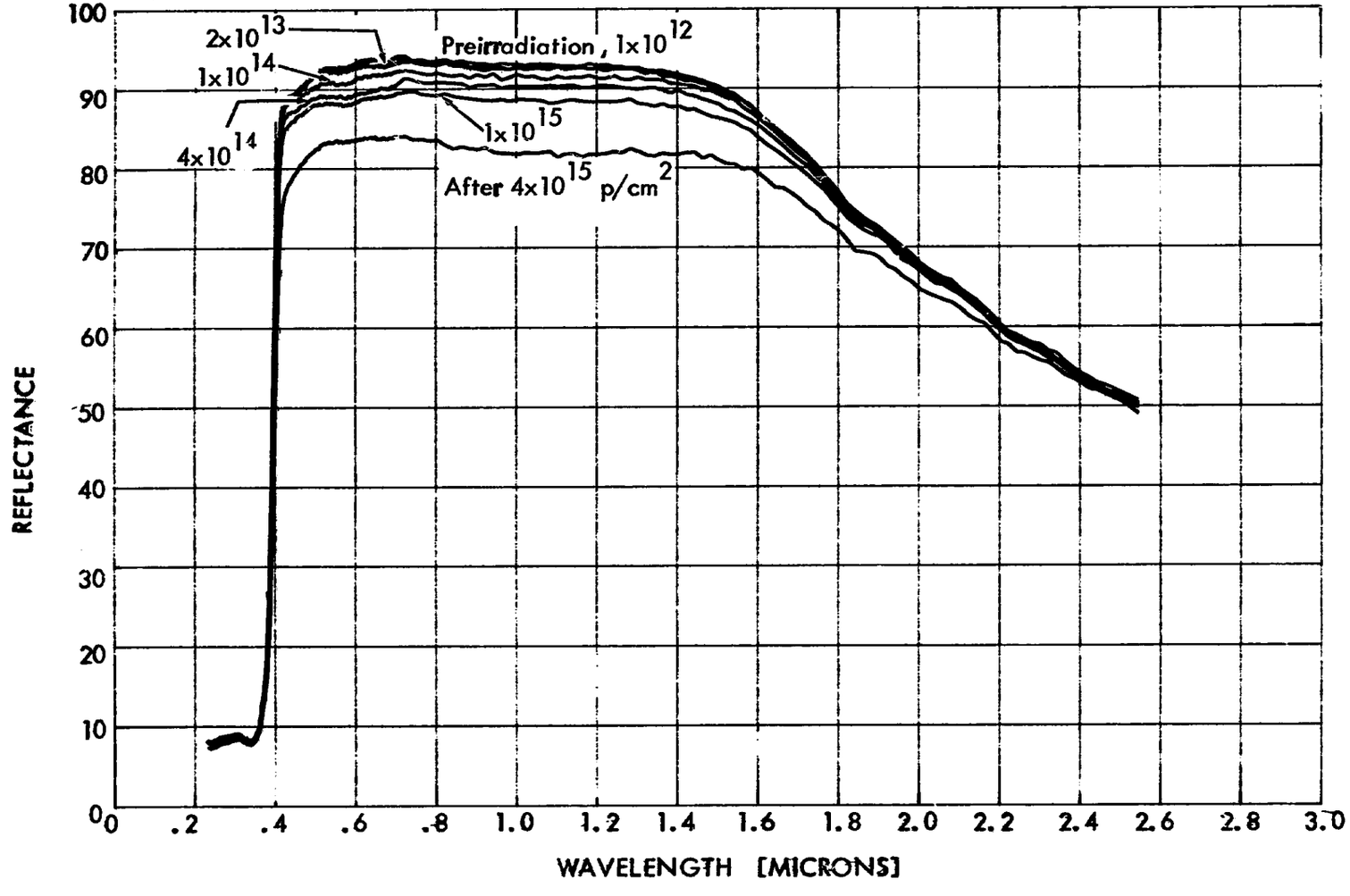

FIGURE 40.

IN SITU EFFECTS OF 35-KEV ELECTRONS ON THE REFLECTANCE OF NASA-GODDARD ZINC OXIDE/ALUMINUM OXIDE — POTASSIUM SILICATE [F3]

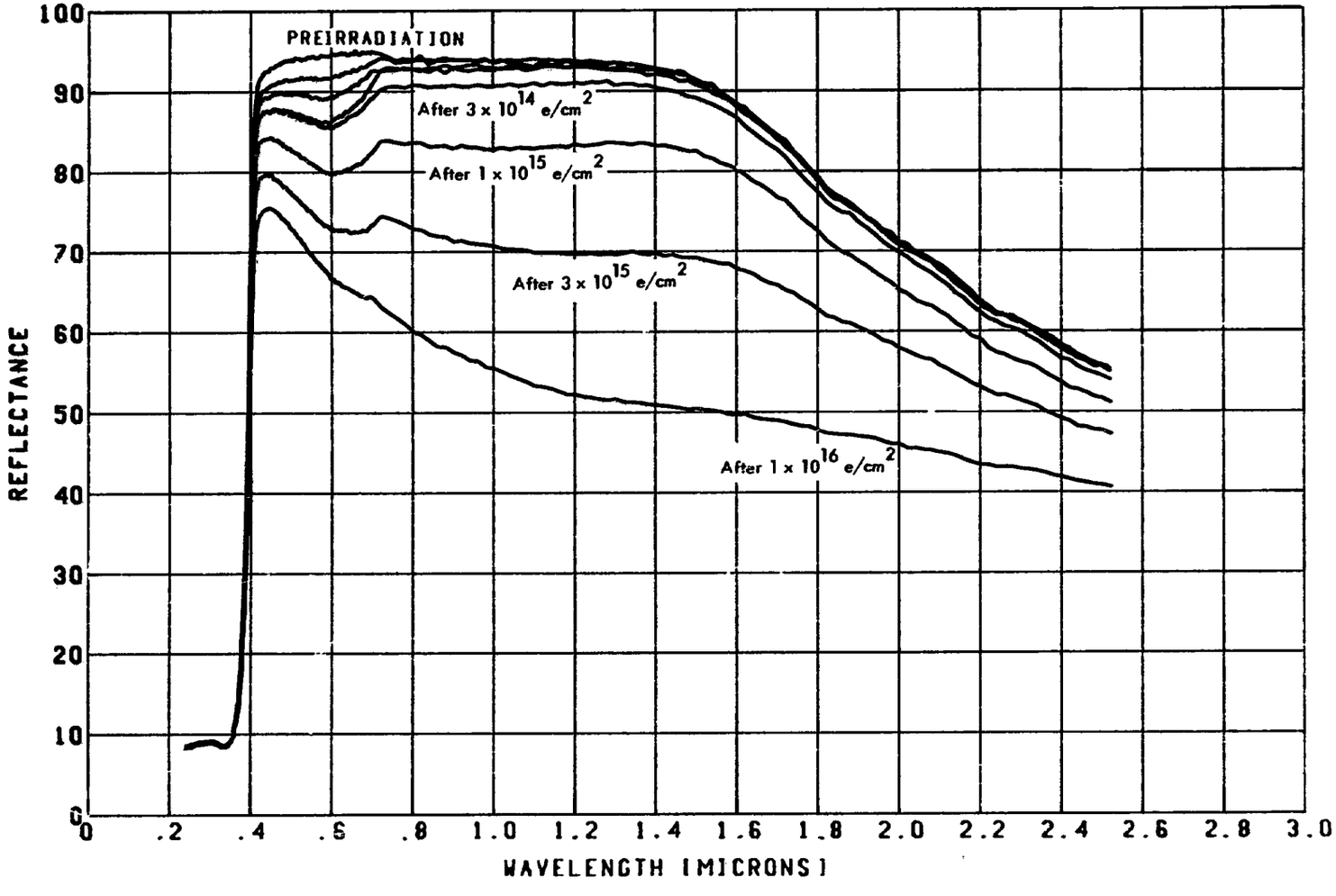

FIGURE 41.

IN SITU EFFECTS OF 40-KEV PROTONS ON THE REFLECTANCE OF NASA-GODDARD ZINC OXIDE/ALUMINUM OXIDE-POTASSIUM SILICATE [F3]

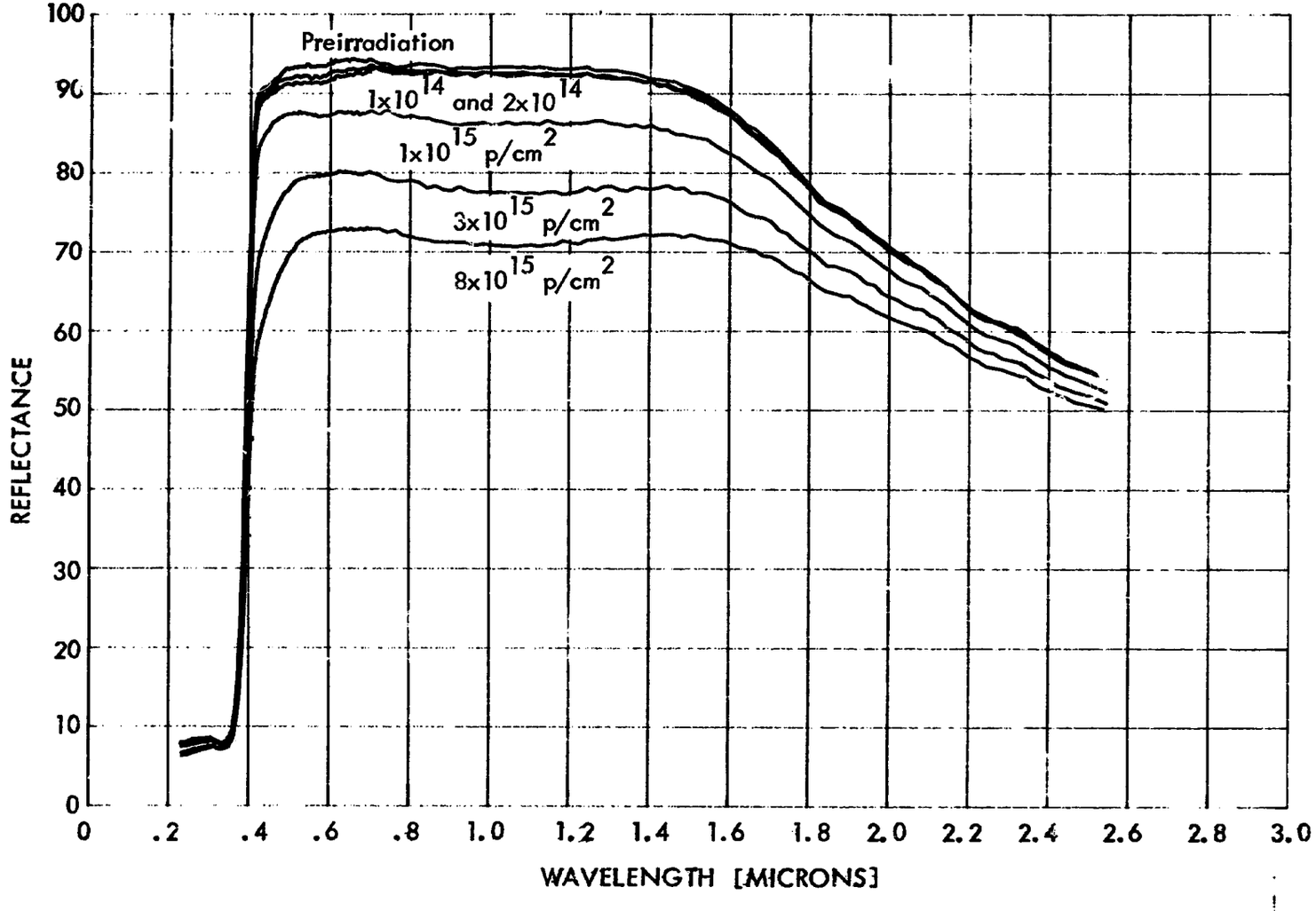

FIGURE 42.

IN SITU EFFECTS OF 35-KEV ELECTRONS ON THE REFLECTANCE OF NASA-GODDARD ALUMINUM OXIDE - POTASSIUM SILICATE (D31)

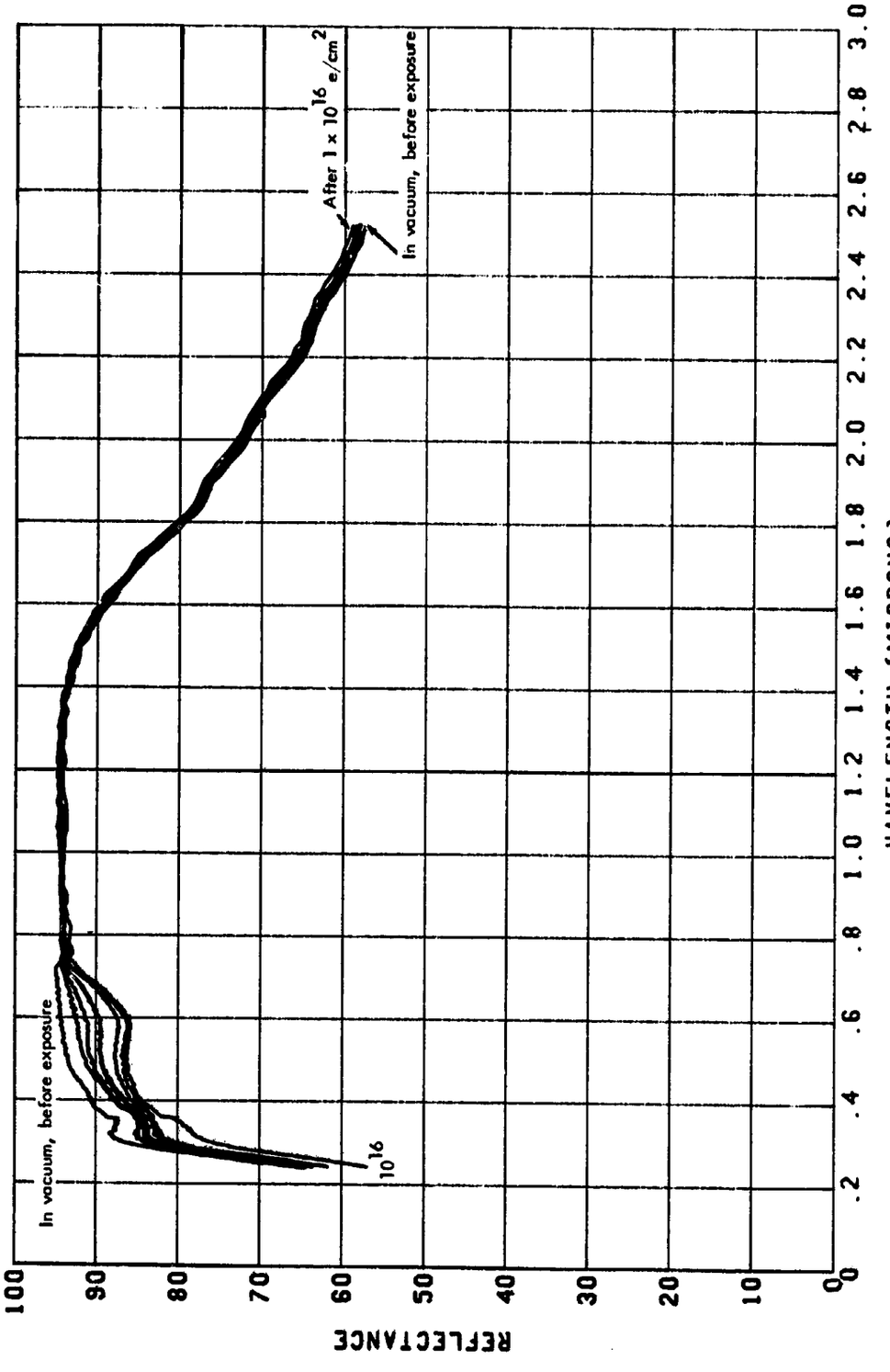

FIGURE 43.

IN SITU EFFECTS OF 40-KEV PROTONS ON THE REFLECTANCE OF NASA-GODDARD ALUMINUM OXIDE-POTASSIUM SILICATE [D3]

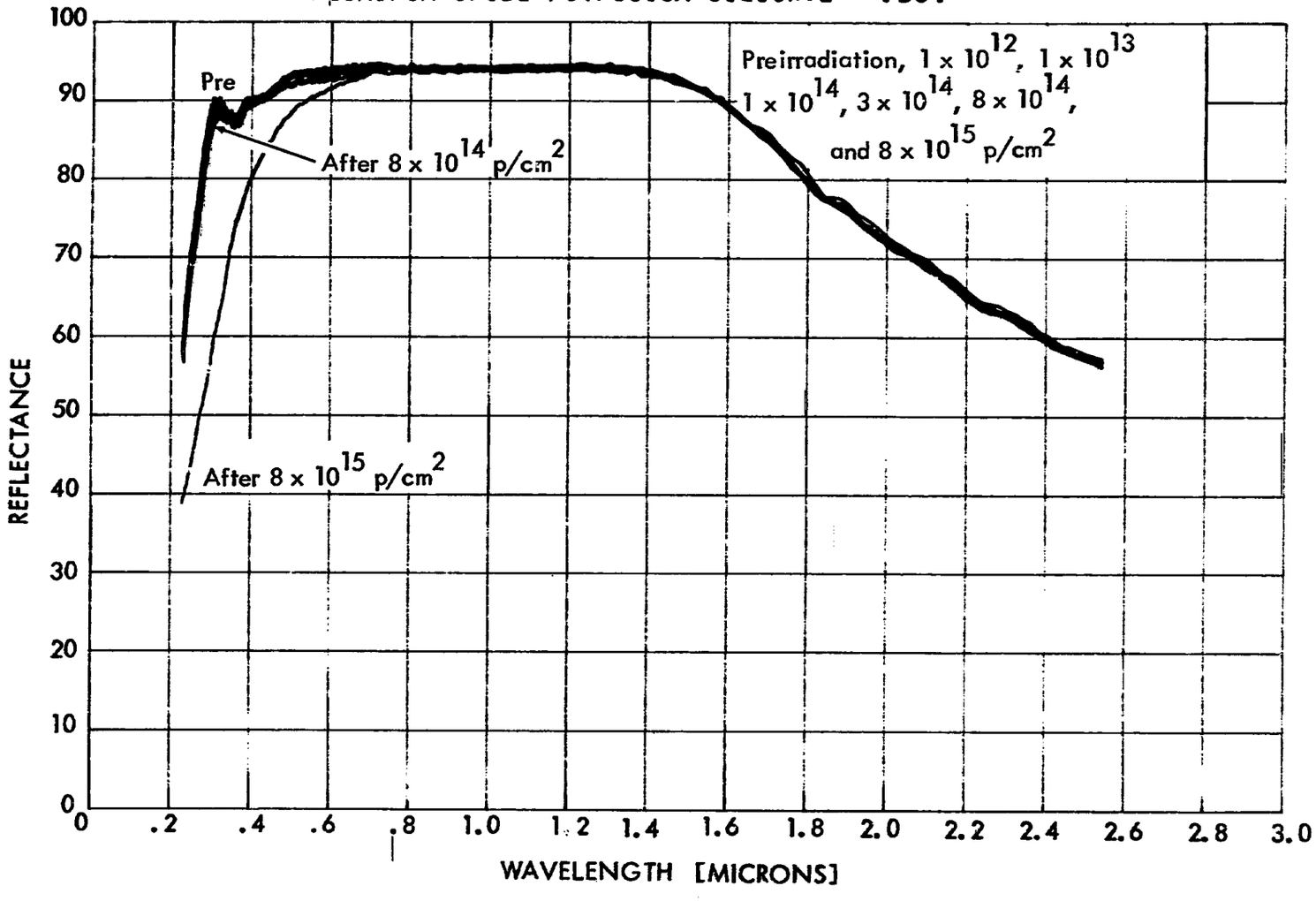

FIGURE 44.

IN SITU EFFECTS OF 40-KEV PROTONS ON THE REFLECTANCE OF NASA-GODDARD ZINC OXIDE-METHYL SILICONE [8]

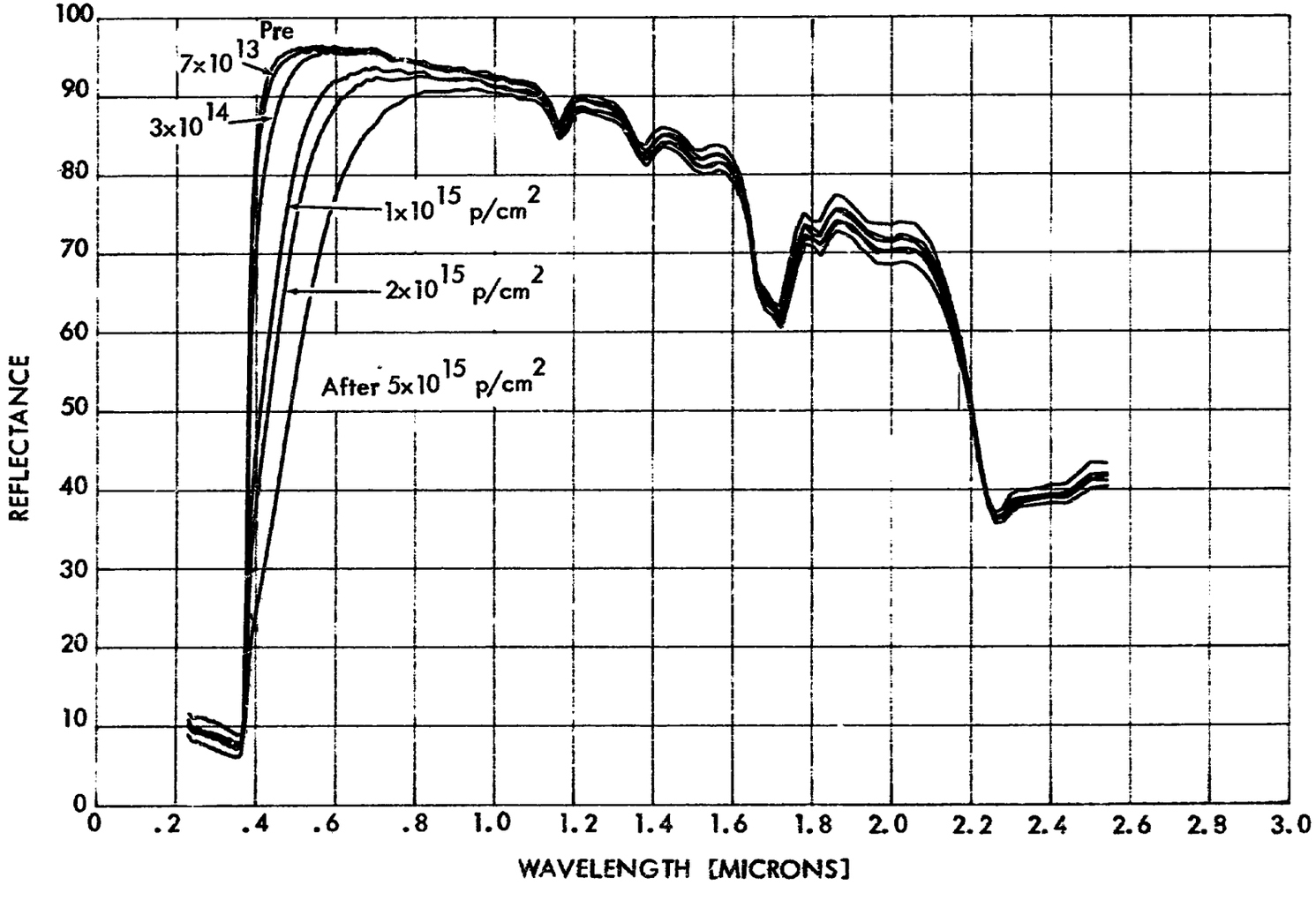

FIGURE 45.

IN SITU EFFECTS OF 40-KEV PROTONS ON THE REFLECTANCE OF NASA-GODDARD LEAFING ALUMINUM--MIXED PHENYLATED SILICONES [I]

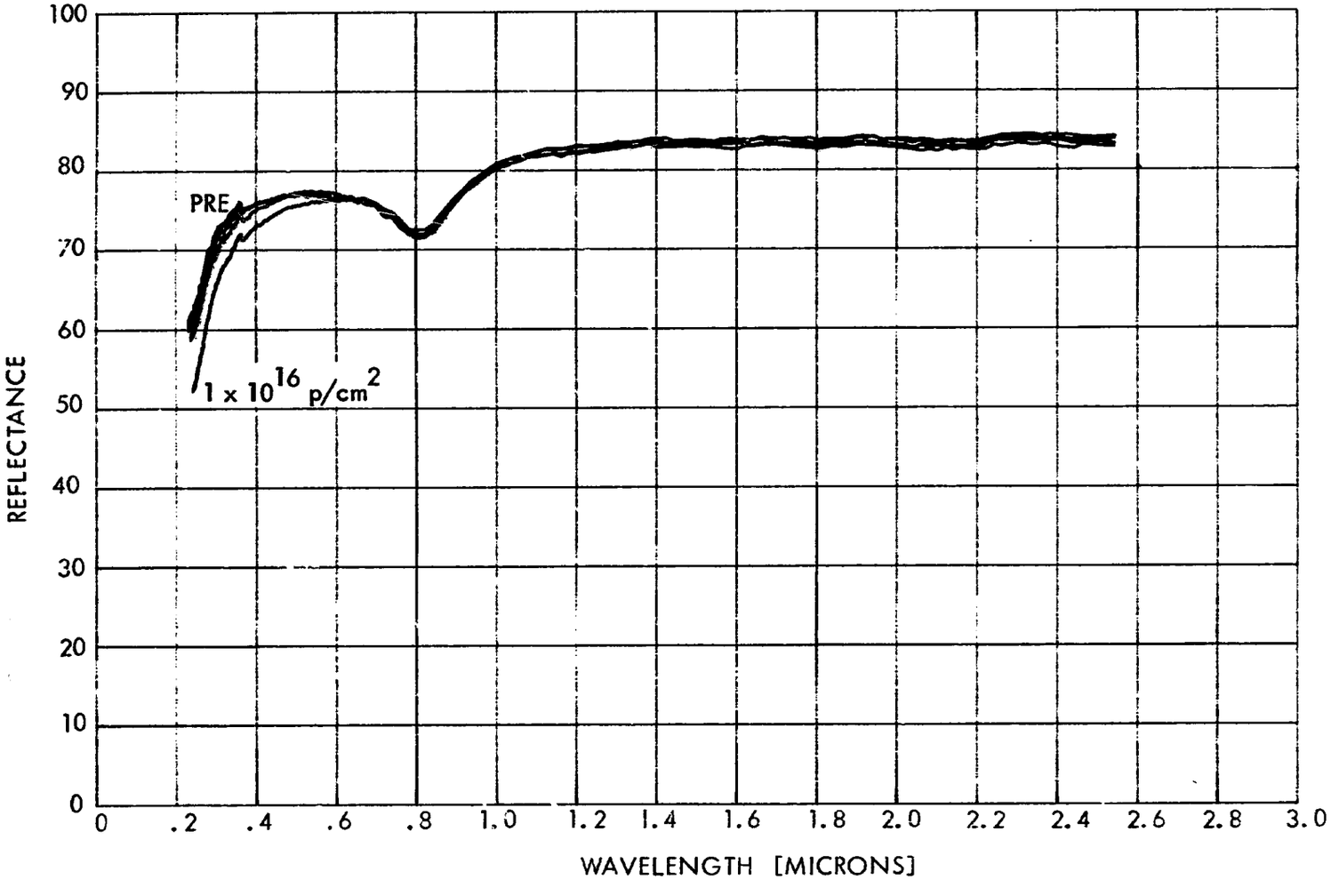

FIGURE 46.

IN SITU EFFECTS OF 40-KEV PROTONS ON THE REFLECTANCE OF NASA-GODDARD VAPOR-DEPOSITED ALUMINUM ON LACQUERED ALUMINUM SUBSTRATE [J]

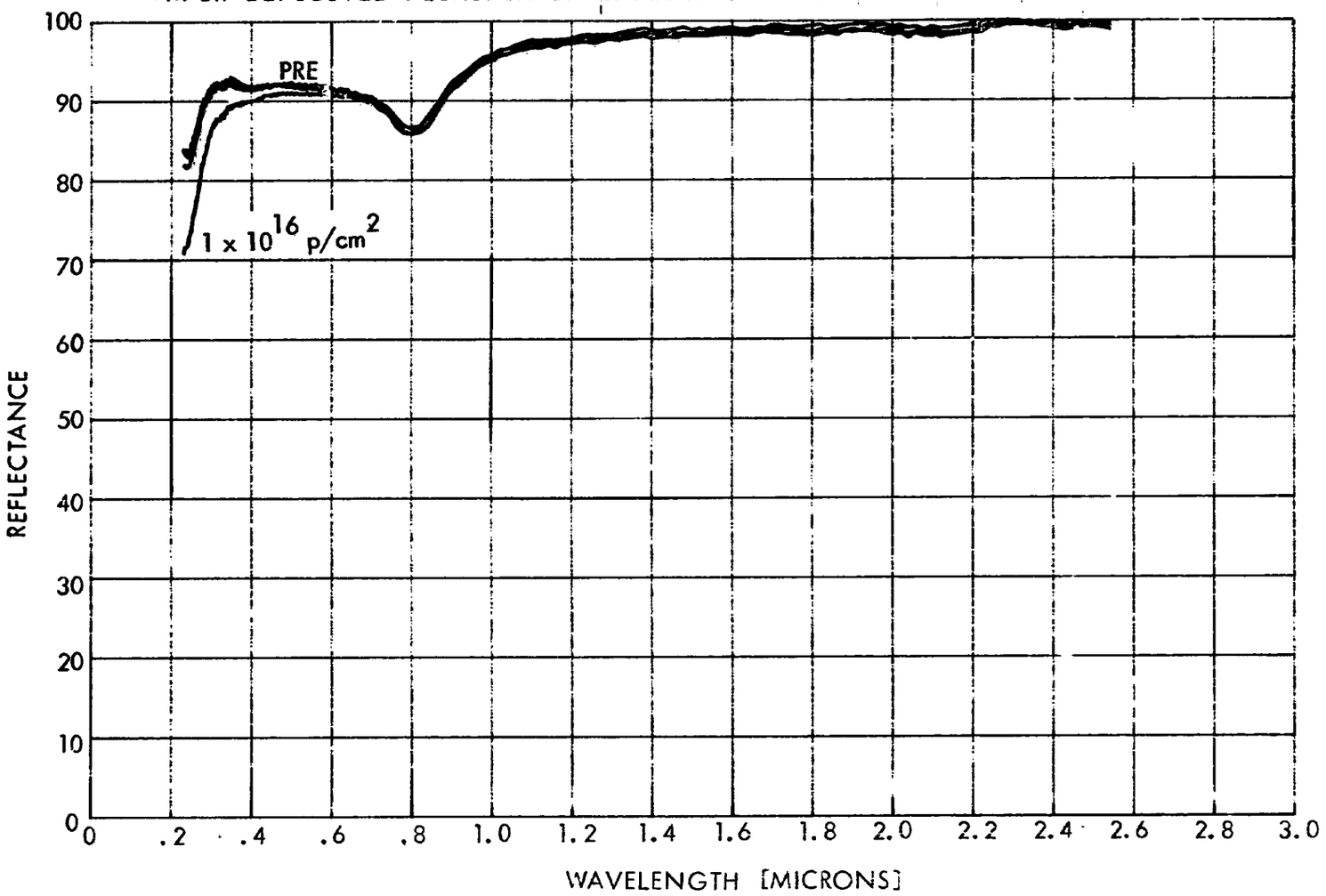

FIGURE 47.

IN SITU EFFECTS OF 40-KEV PROTONS ON THE REFLECTANCE OF NASA-GODDARD BUFFED AND VAPOR-DEGREASED ALUMINUM SUBSTRATE [K]

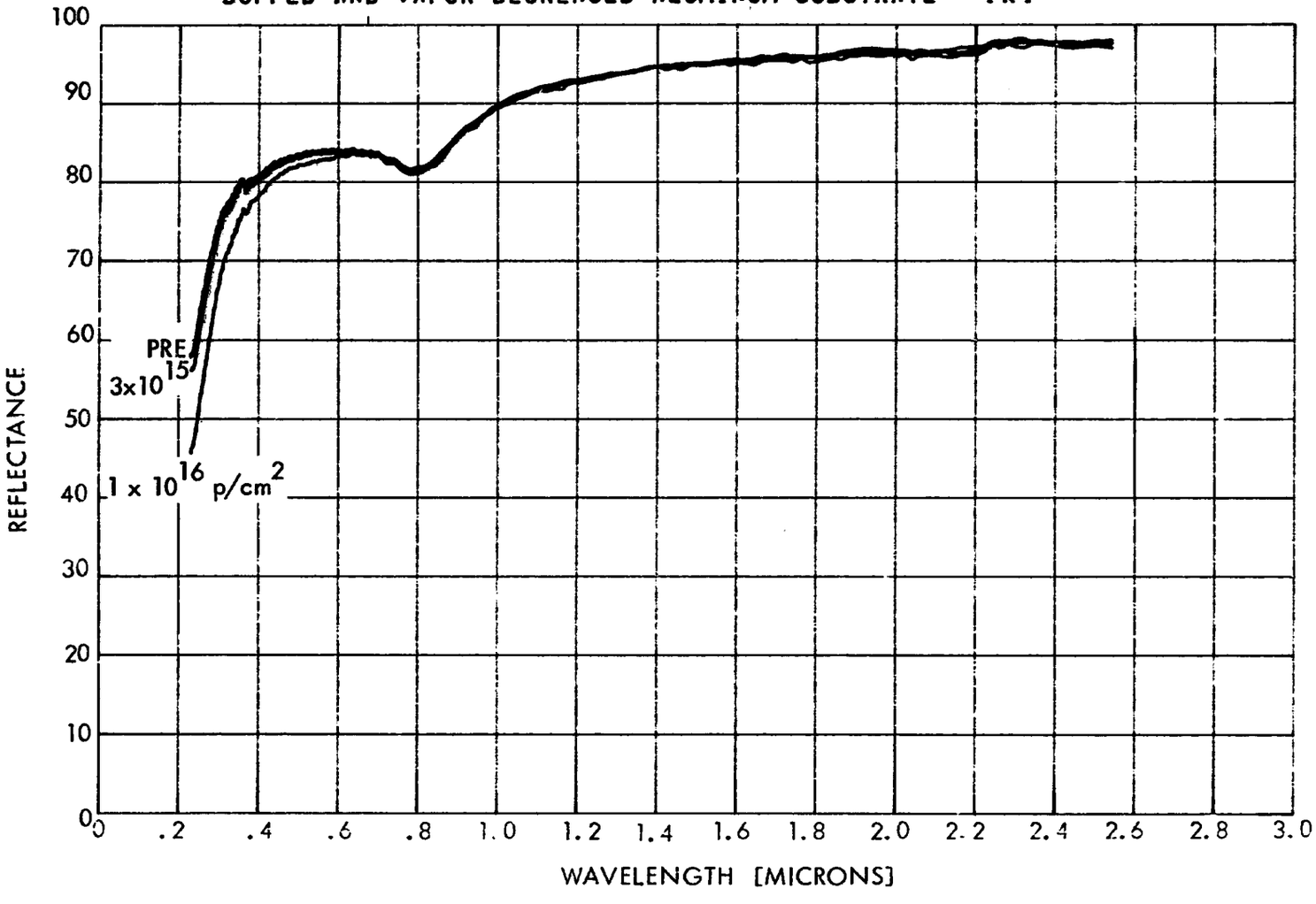

FIGURE 48.

IN SITU EFFECTS OF 40-KEV PROTONS ON THE REFLECTANCE OF NASA-GODDARD VAPOR-DEPOSITED ALUMINUM OXIDE ON ALUMINUM [G]

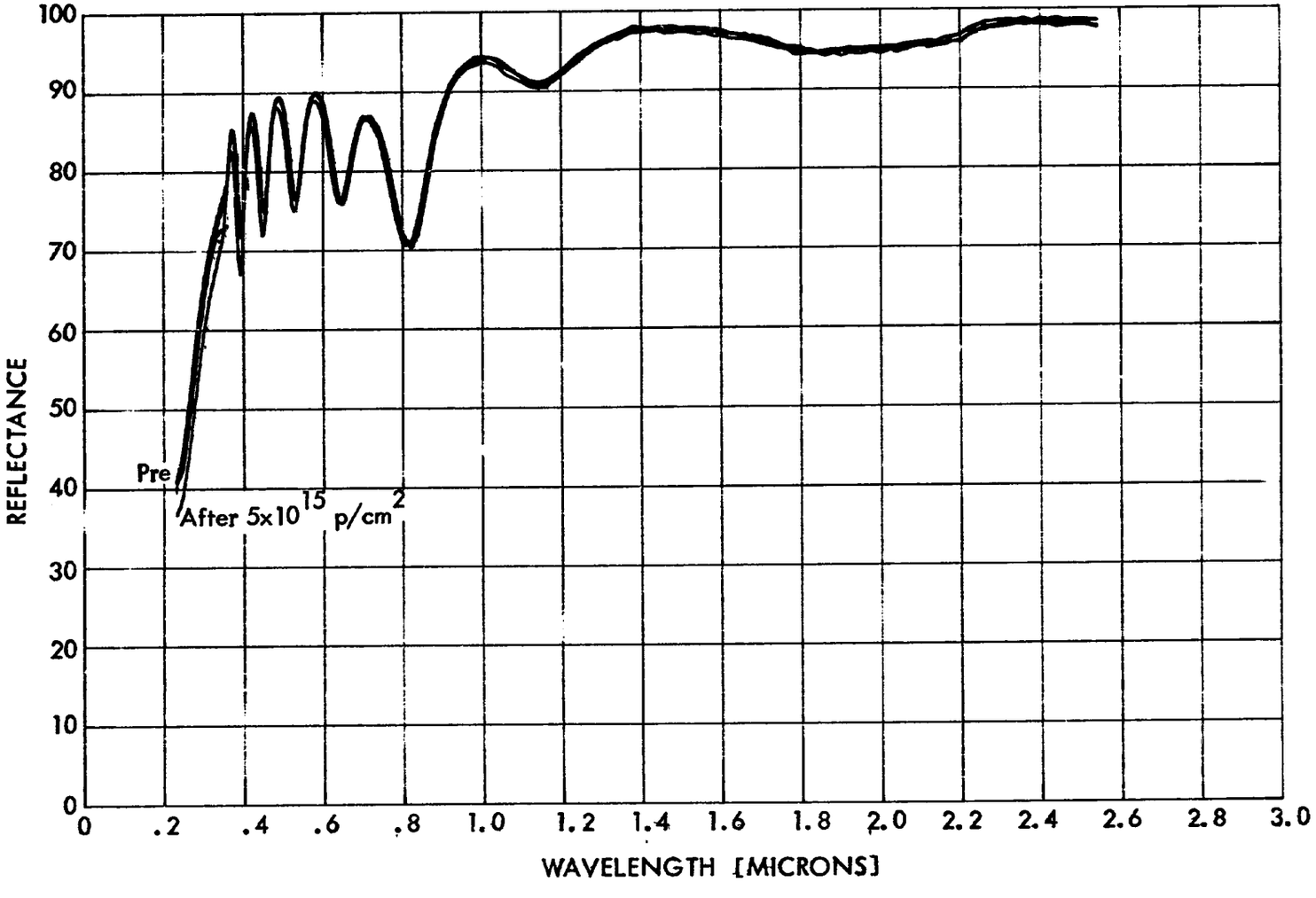

FIGURE 49.

IN AIR/IN VACUUM REFLECTANCE PROPERTIES OF NASA-GODDARD SILVERED 2-MIL TEFLON (TS-2)

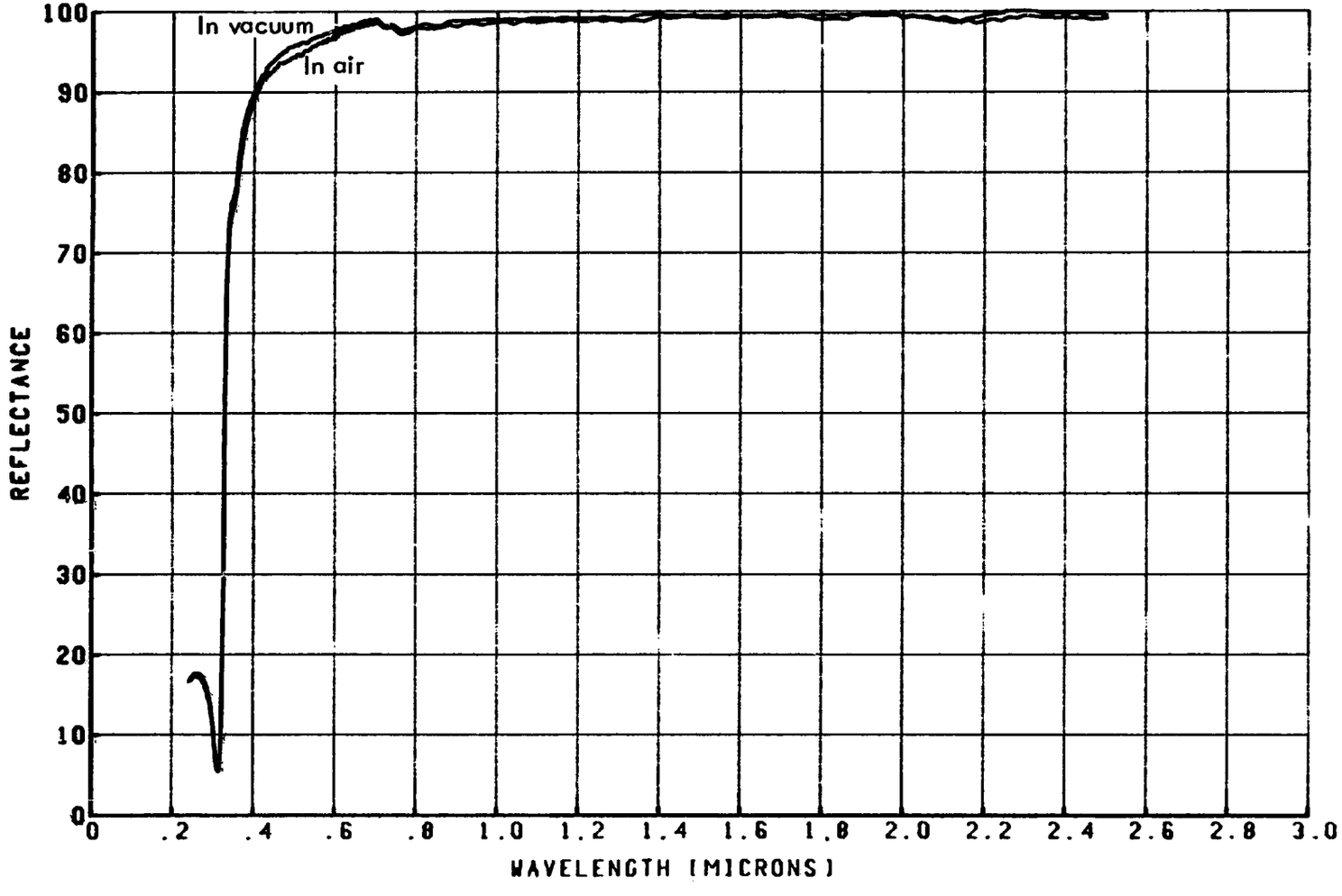

FIGURE 50.

IN AIR/IN VACUUM REFLECTANCE PROPERTIES OF NASA-GODDARD SILVERED 5-MI TEFLON (TS-5)

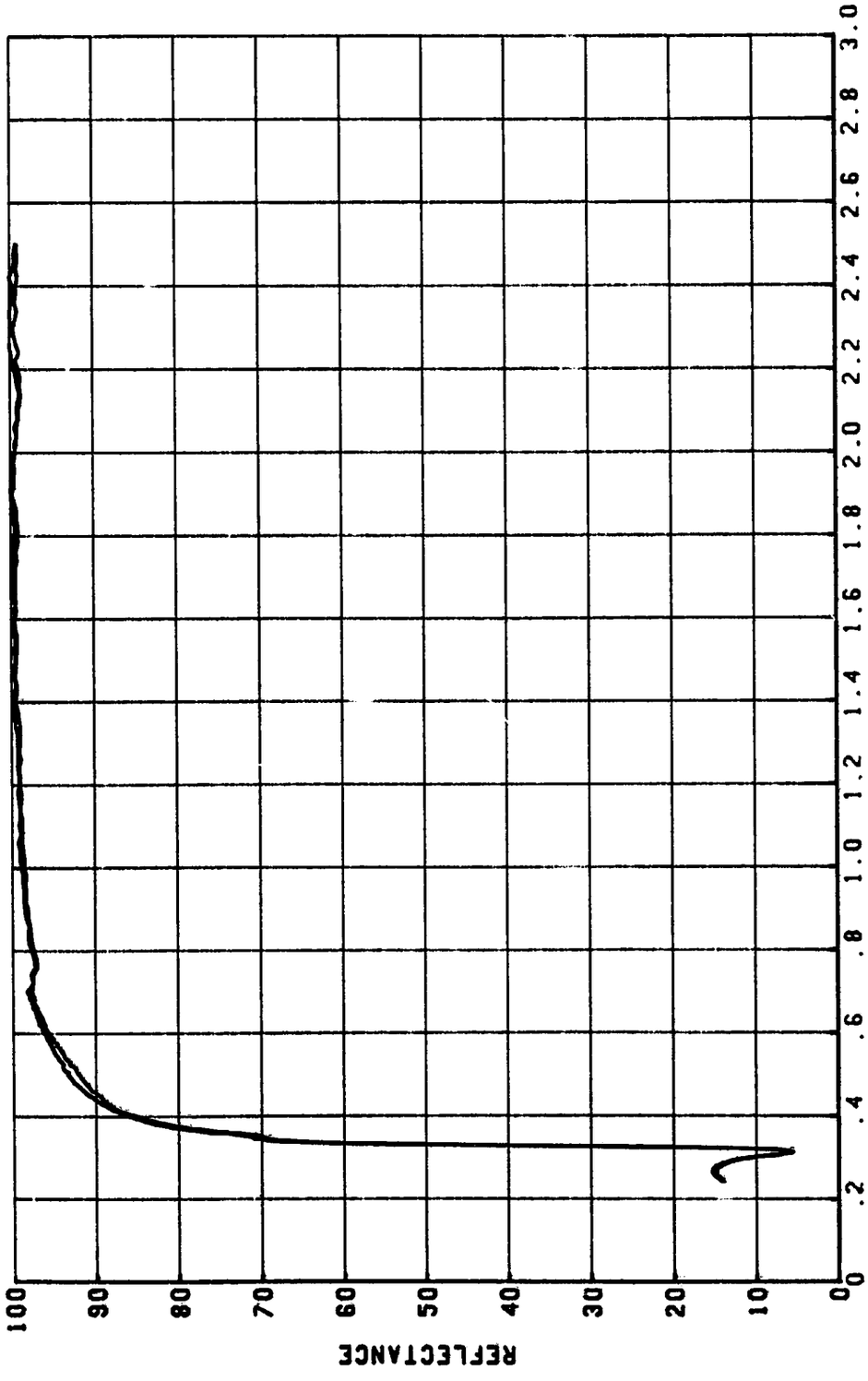

FIGURE 51.
IN AIR/IN VACUUM REFLECTANCE PROPERTIES OF NASA-GODDARD SILVERED 10-MIL TEFLON (TS-10)

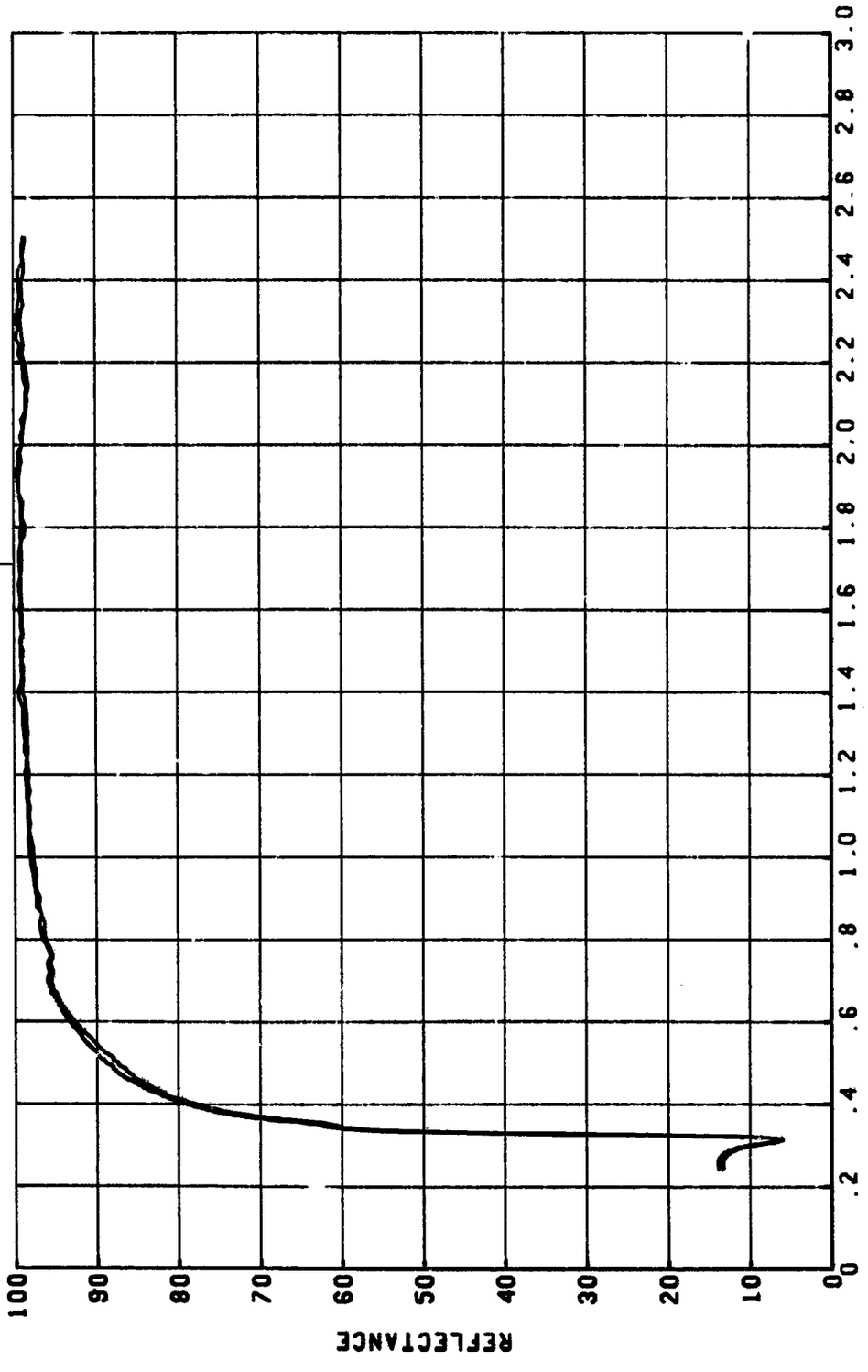

FIGURE 52.

IN AIR/IN VACUUM REFLECTANCE PROPERTIES OF NASA-GODDARD ALUMINIZED 2-MIL TEFLON (TA-2)

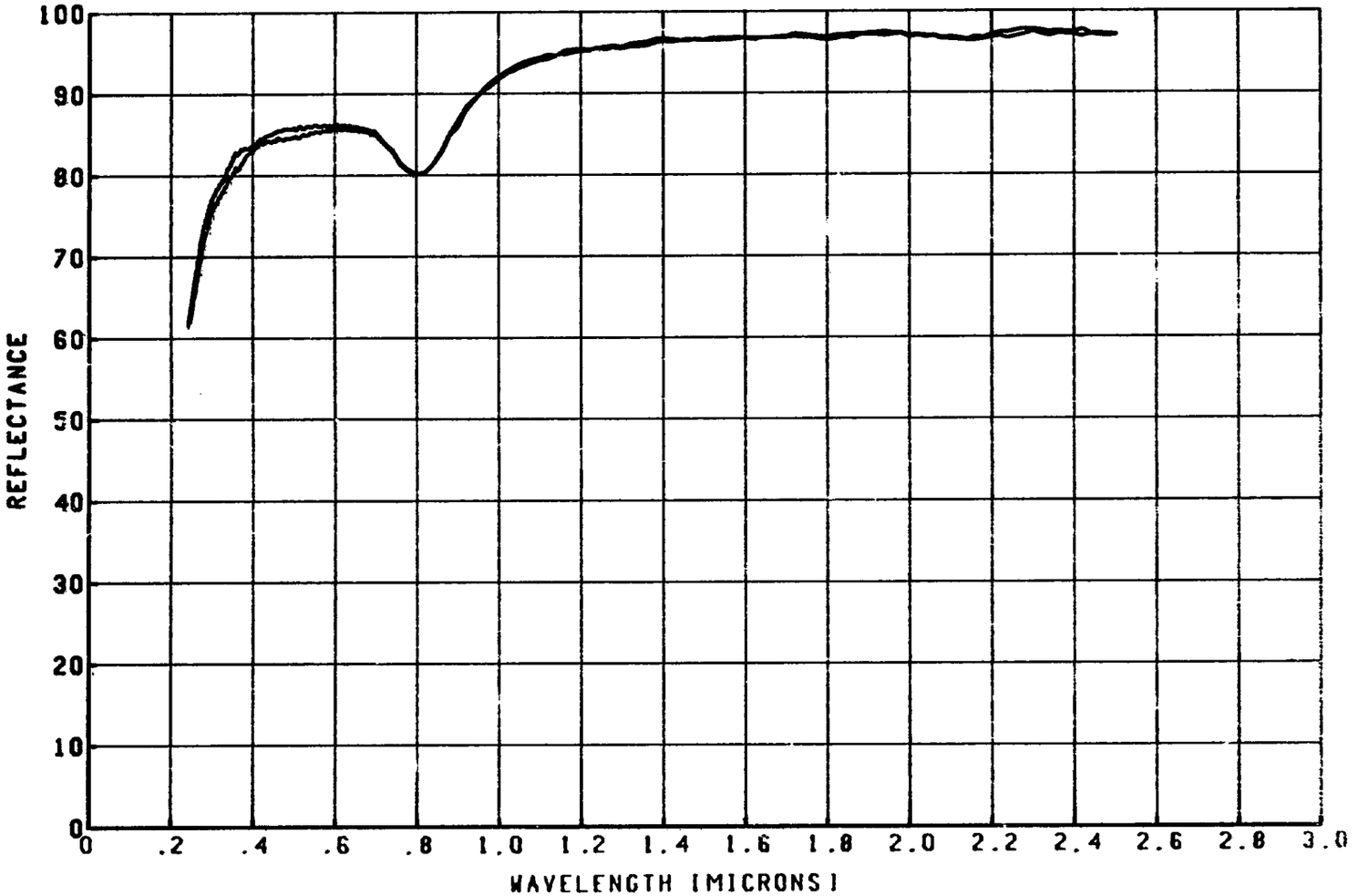

FIGURE 53.

IN AIR/IN VACUUM REFLECTANCE PROPERTIES OF NASA-GODDARD ALUMINIZED 5-MIL TEFLON [TA-5]

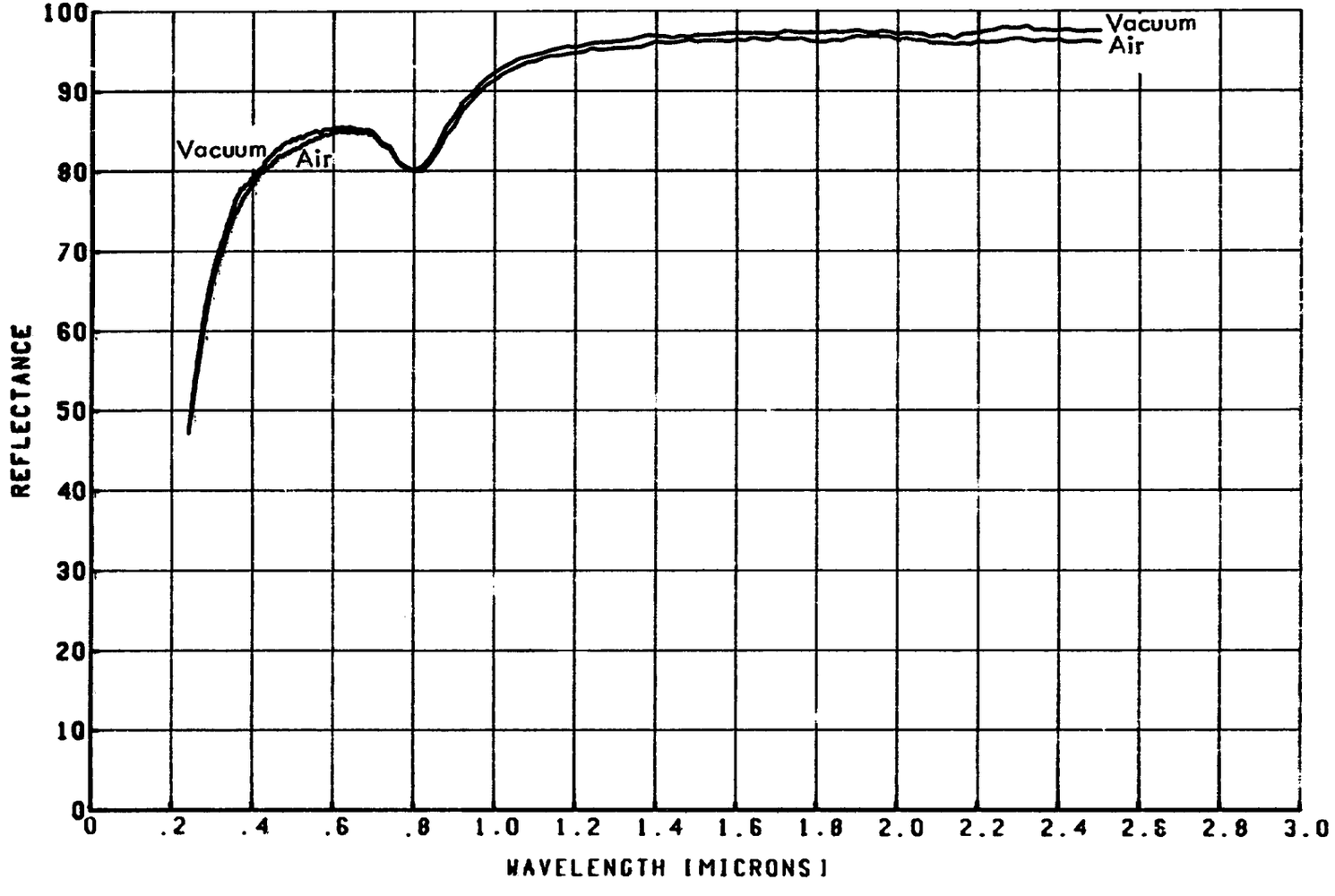

FIGURE 54.
IN AIR/IN VACUUM REFLECTANCE PROPERTIES OF NASA-GODDARD
ALUMINIZED 10-MIL TEFLON (TA-10)

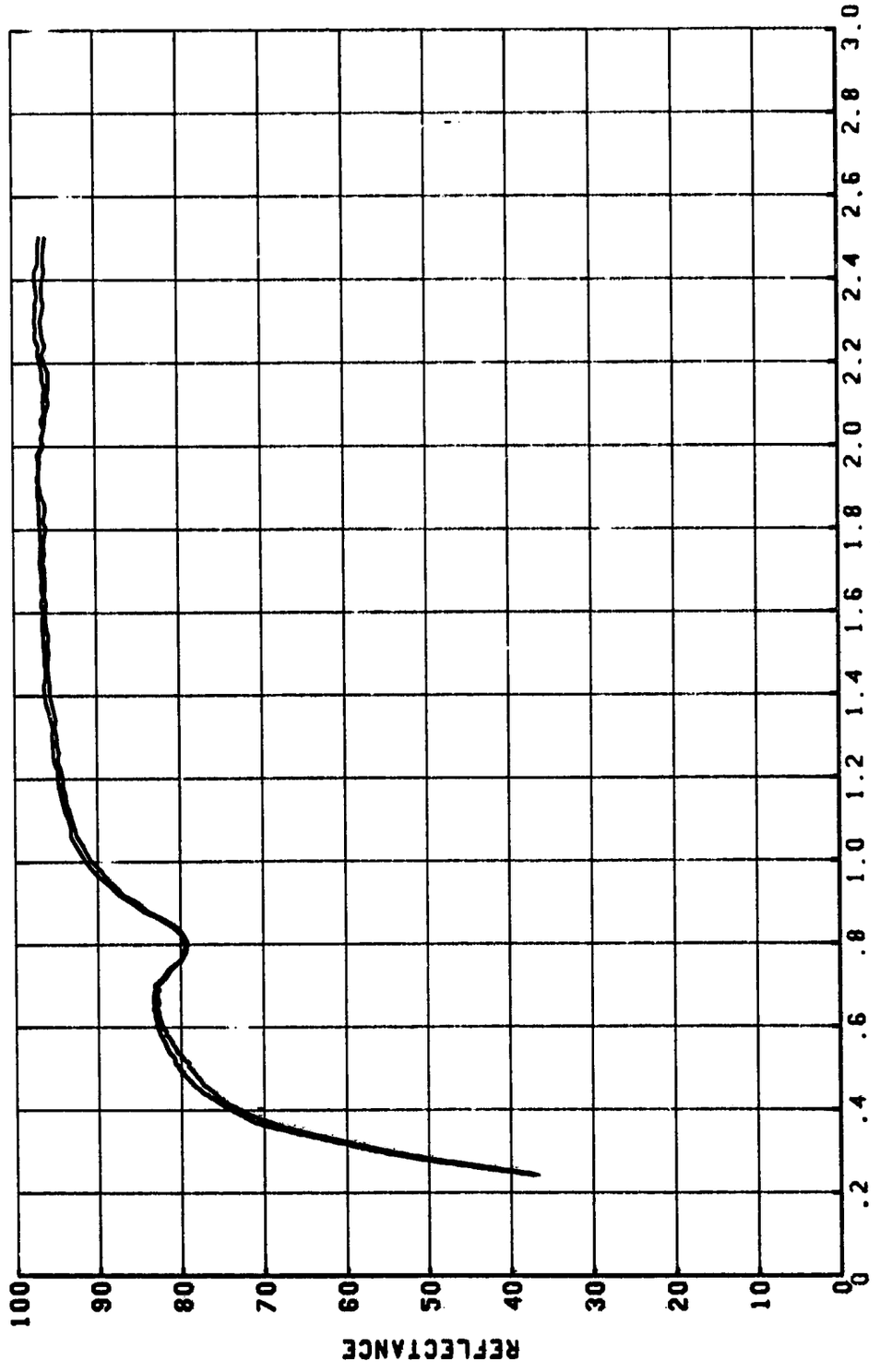

FIGURE 55.

IN AIR/IN VACUUM REFLECTANCE PROPERTIES OF NASA-GODDARD 0.15 MIL ALZAK [23]

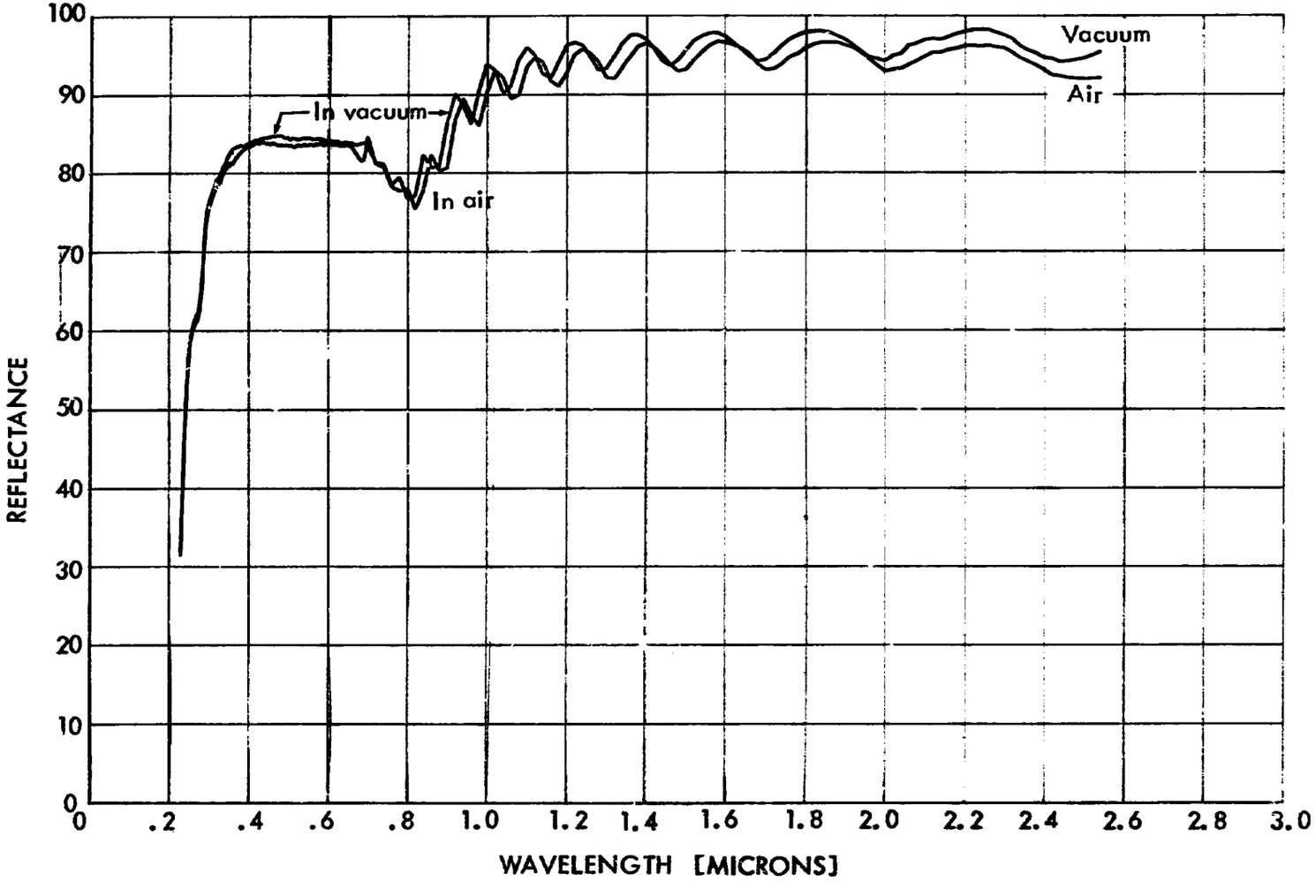

FIGURE 56.

IN AIR/IN VACUUM REFLECTANCE PROPERTIES OF NASA-GODDARD 0.22-MIL ALZAK [24]

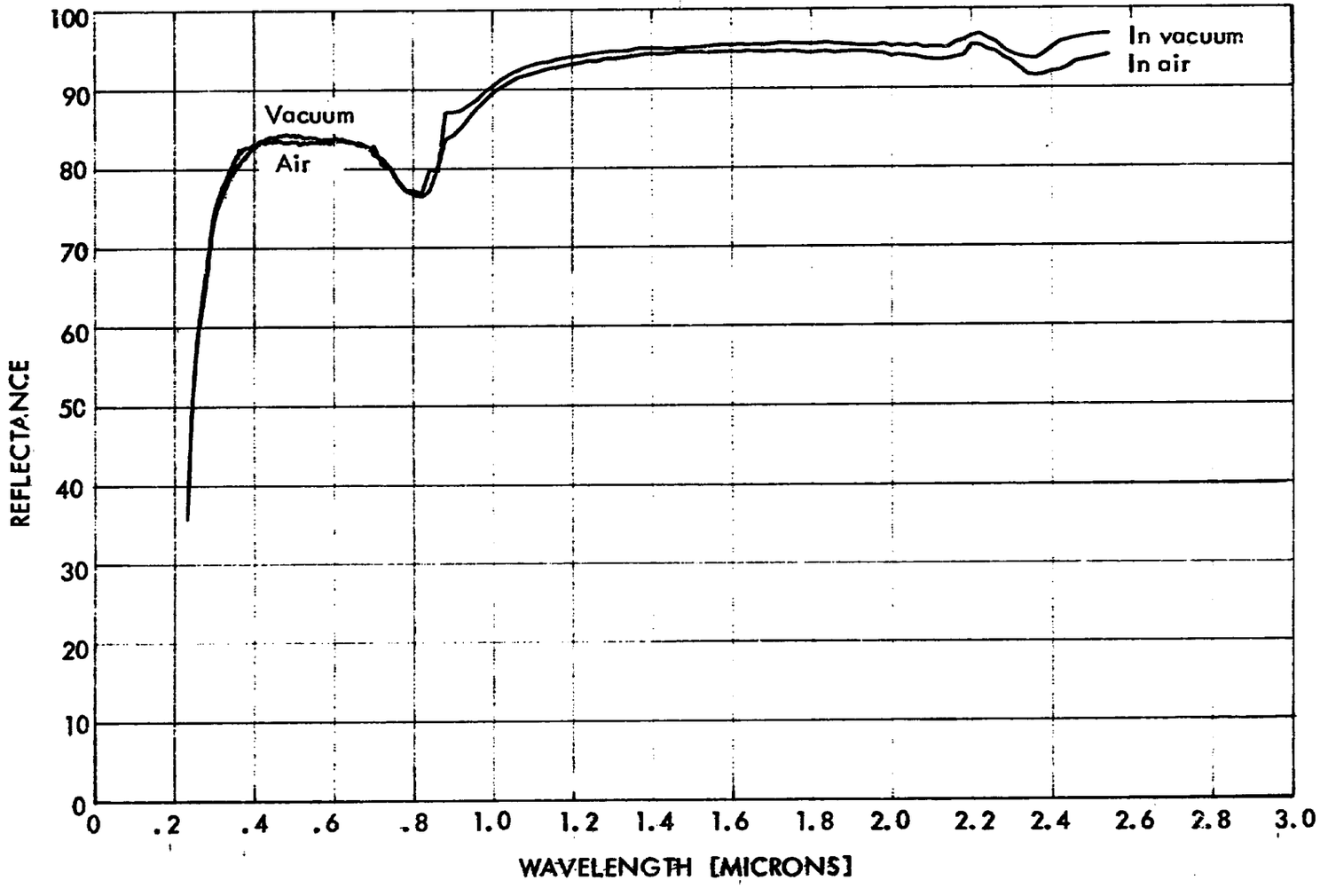

FIGURE 57.

IN AIR/IN VACUUM REFLECTANCE PROPERTIES OF NASA-GODDARD 0.34-MIL ALZAK [25]

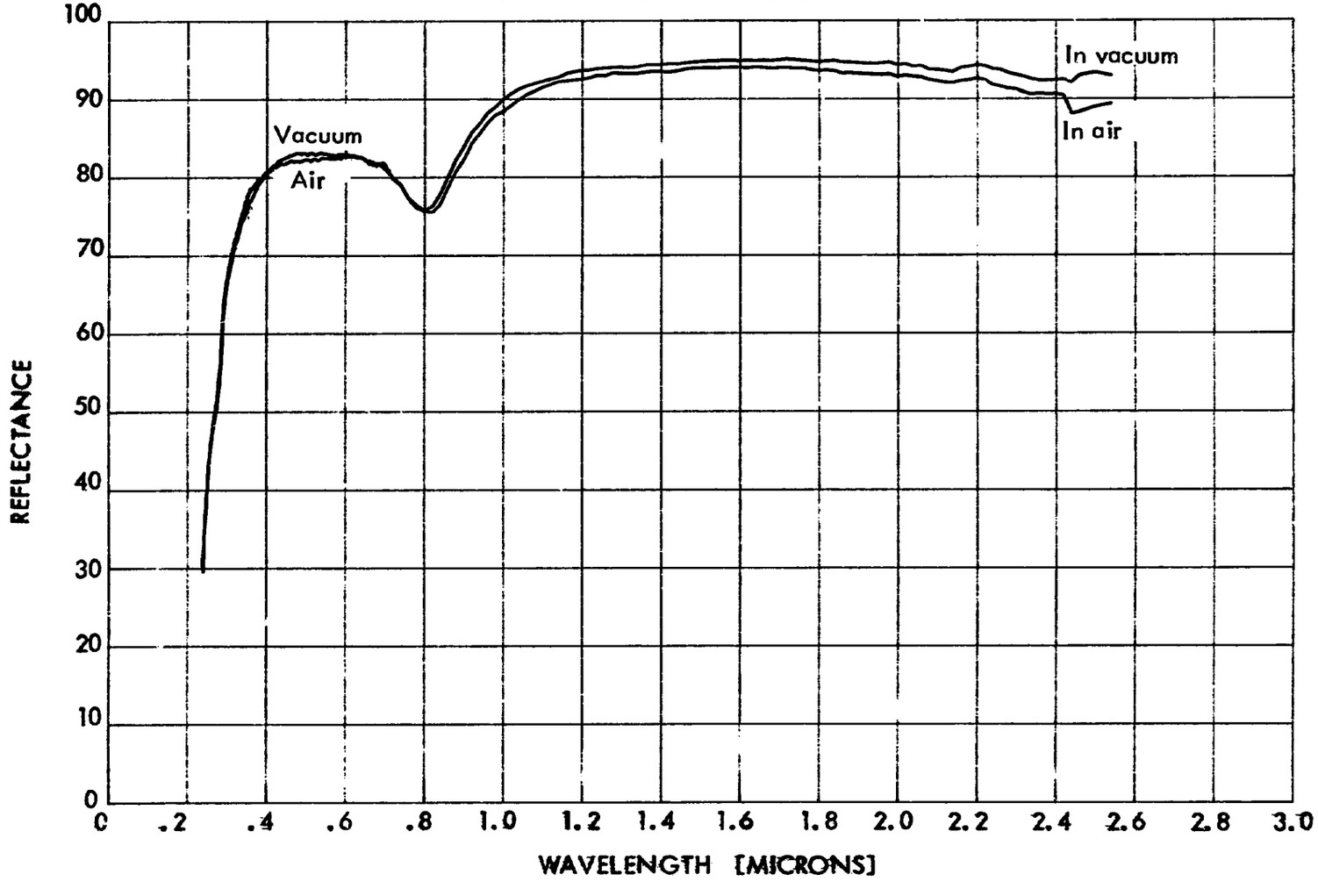

FIGURE 58.

IN AIR/IN VACUUM REFLECTANCE PROPERTIES OF NASA-GODDARD SILICON OXIDE EVAPORATED ONTO ALUMINUM [H]

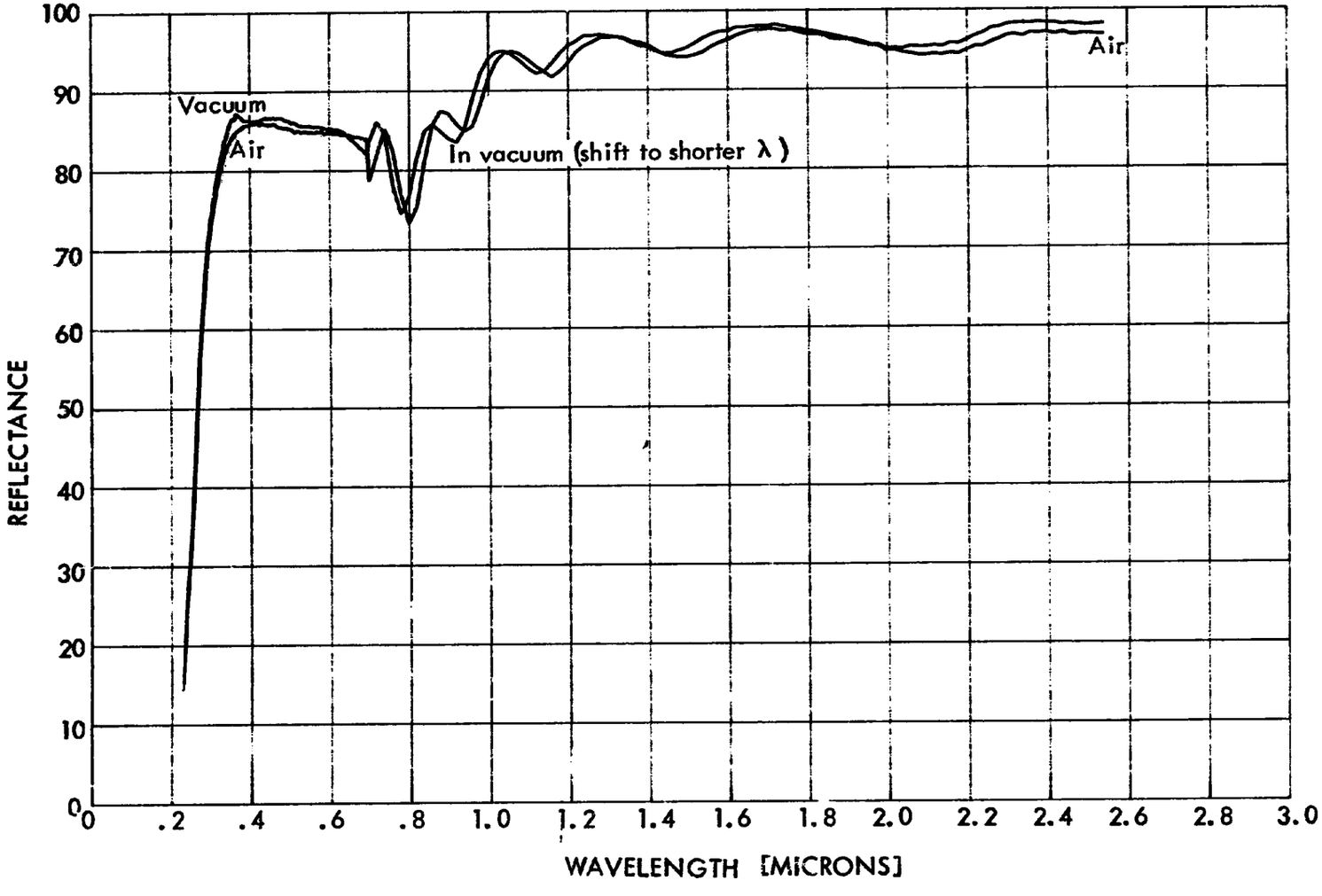

FIGURE 59.

IN AIR/IN VACUUM REFLECTANCE PROPERTIES OF NASA-GODDARD TYPE H KAPTON FILM (N)

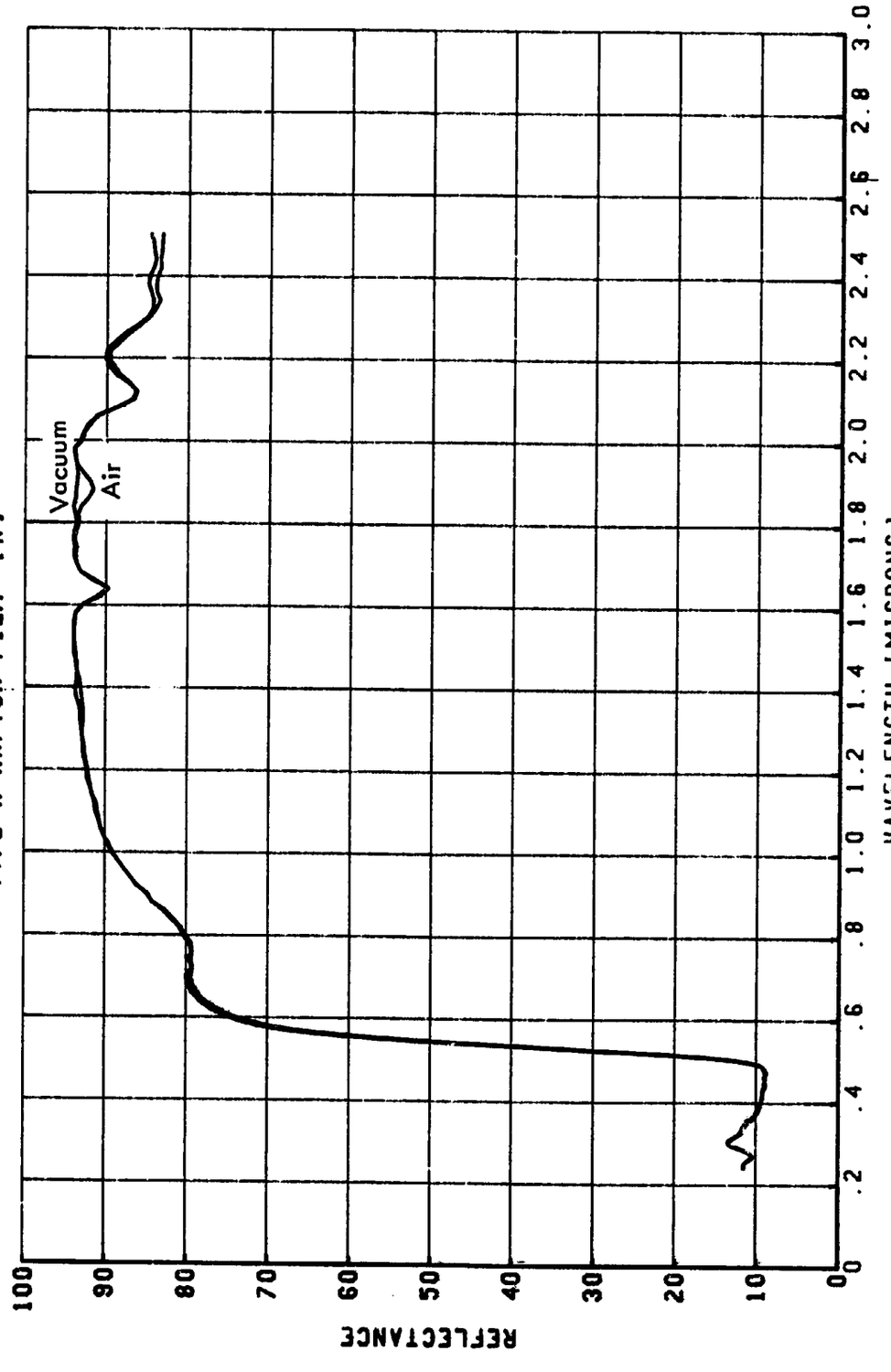

FIGURE 60.

IN AIR/IN VACUUM REFLECTANCE PROPERTIES OF NASA-GODDARD TREATED ZINC OXIDE—METHYL SILICONE (SERIES 101-7, R)

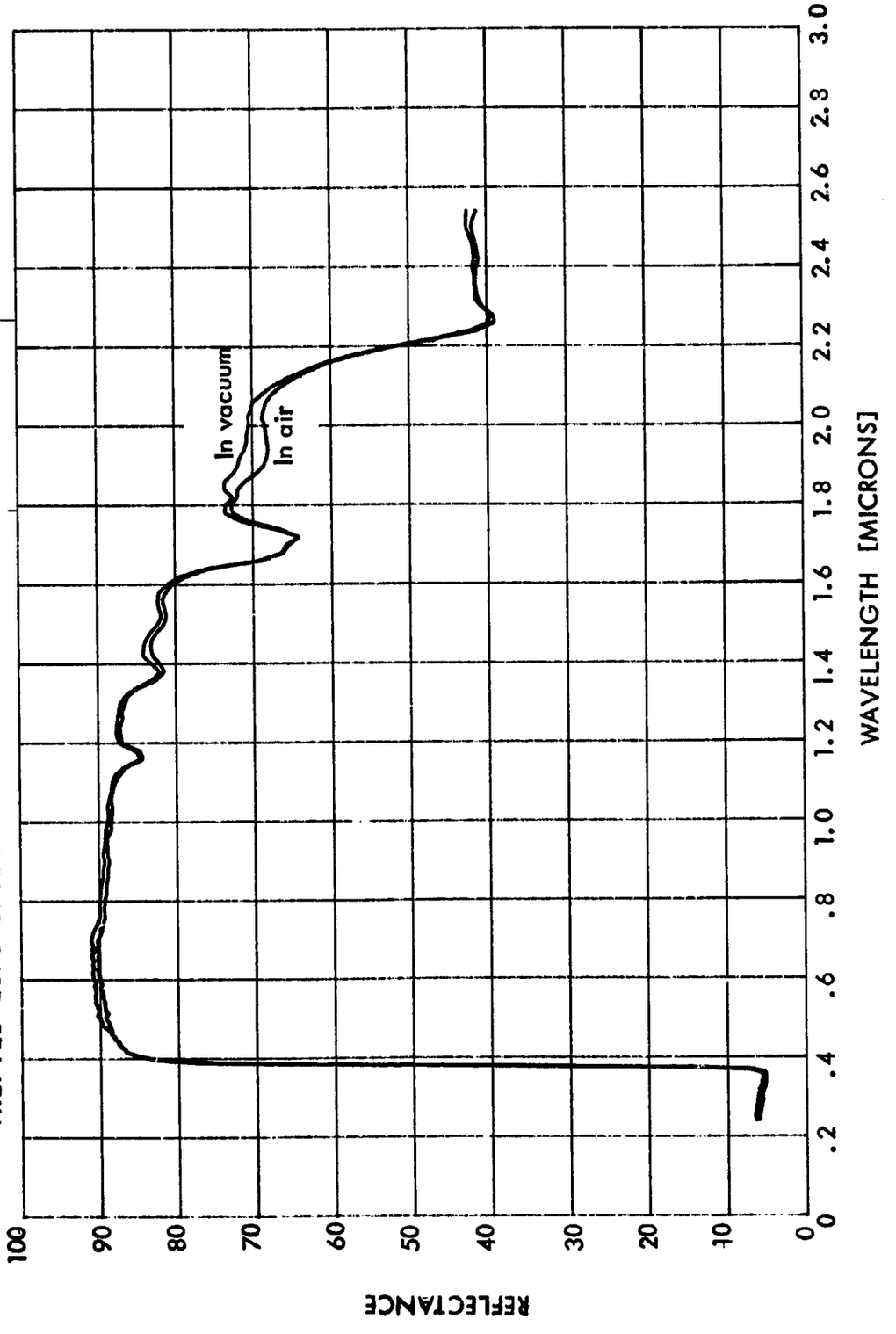

FIGURE 61.

IN AIR/IN VACUUM REFLECTANCE PROPERTIES OF NASA-GODDARD TREATED ZINC OXIDE — METHYL SILICONE [S-13G TYPE M]

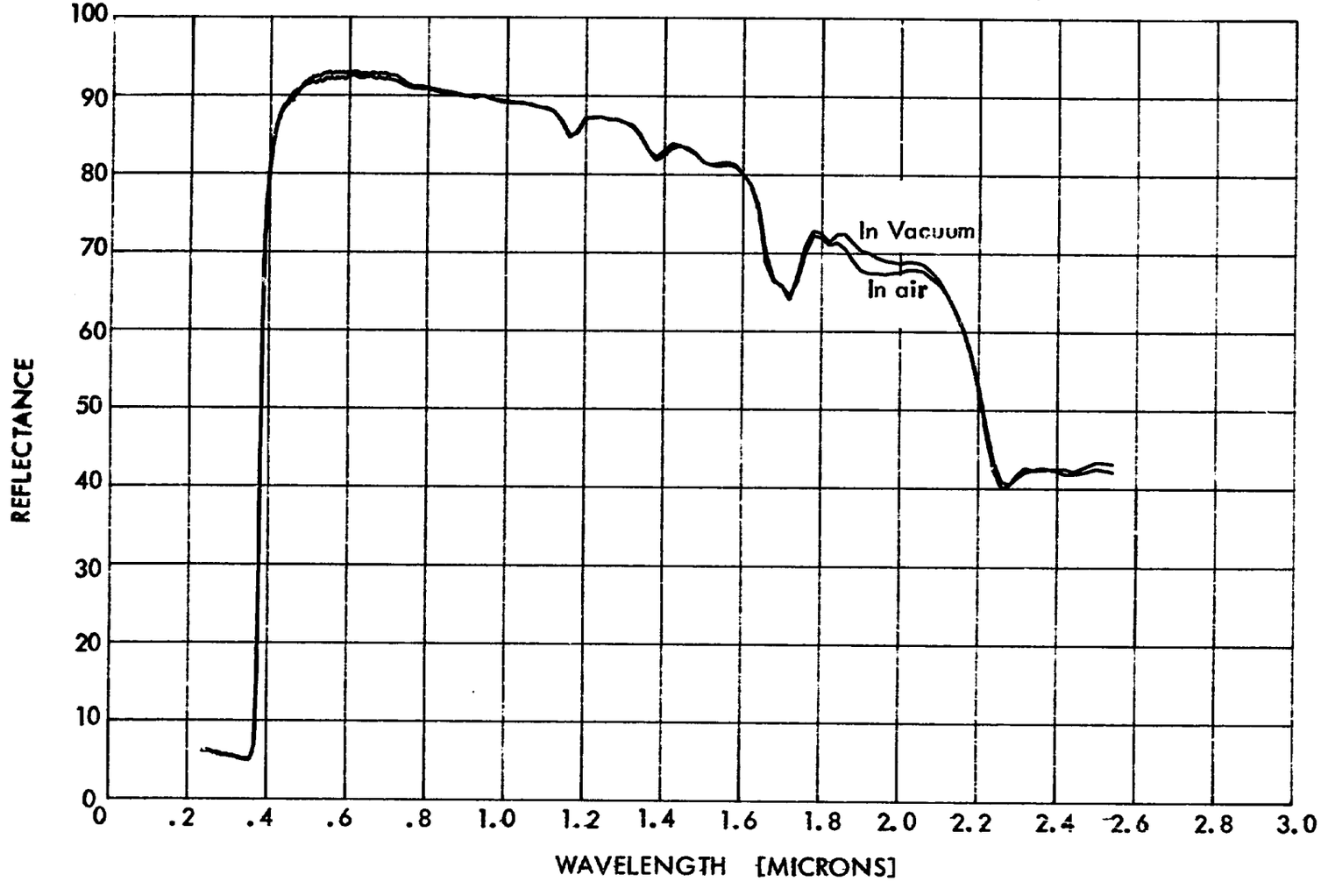

FIGURE 62.

IN AIR/IN VACUUM REFLECTANCE PROPERTIES OF NASA-GODDARD ANATASE TITANIUM DIOXIDE — METHYL SILICONE [L1]

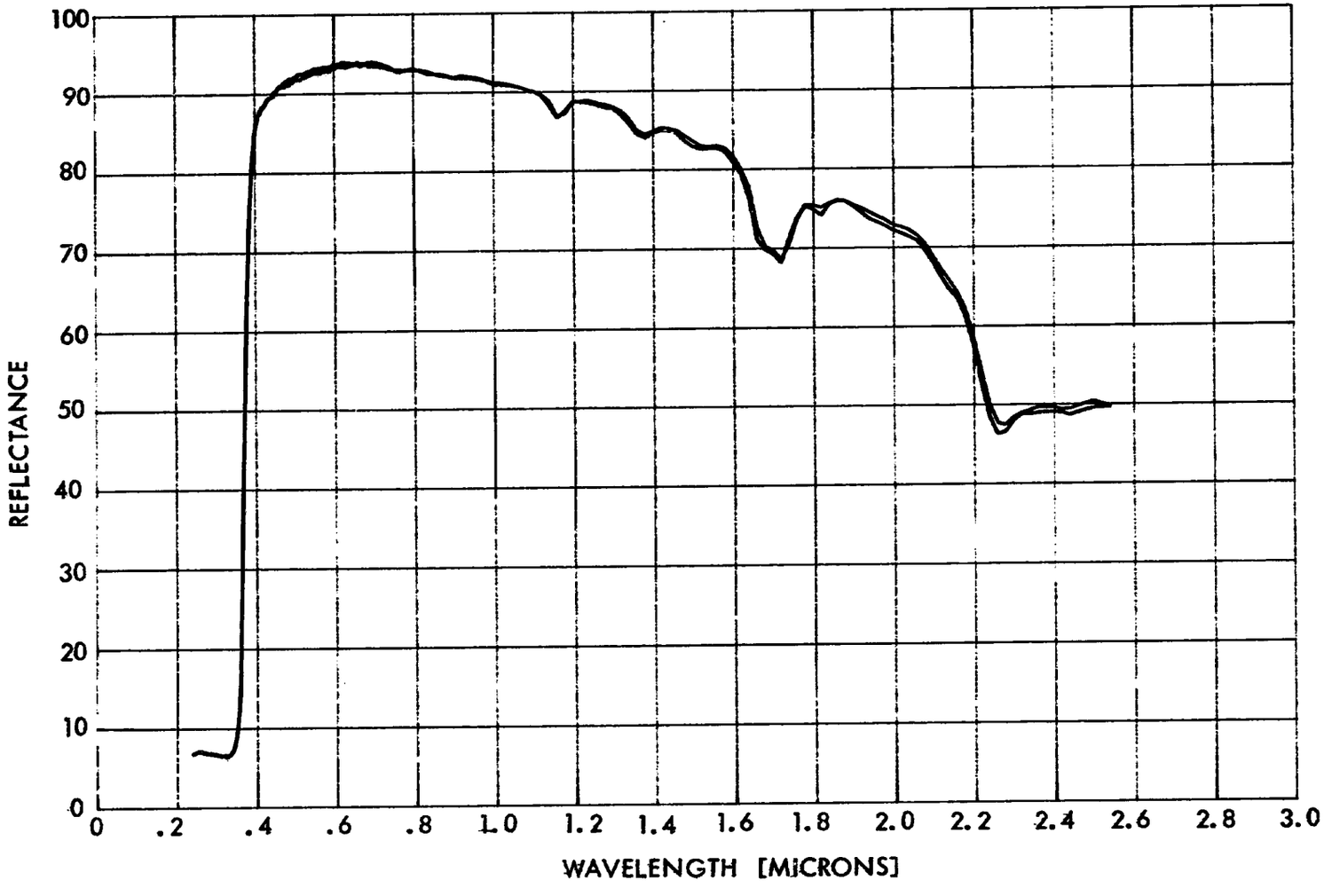

FIGURE 63.

IN AIR/IN VACUUM REFLECTANCE PROPERTIES OF NASA-GODDARD
RUTILE TITANIUM DIOXIDE—METHYL SILICONE [0]

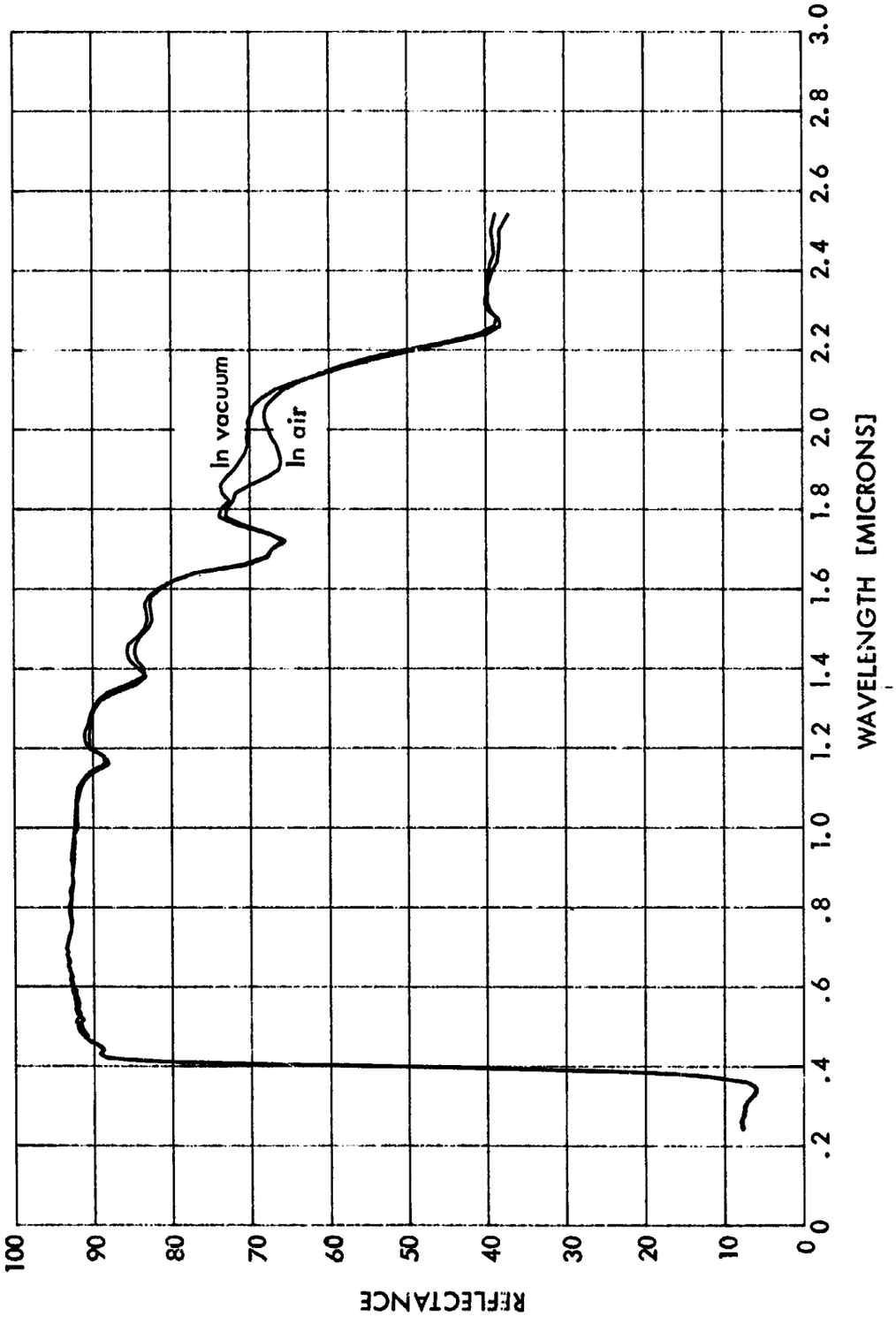

FIGURE 64.

IN AIR/IN VACUUM REFLECTANCE PROPERTIES OF NASA-GODDARD RUTILE TITANIUM DIOXIDE/ALUMINUM OXIDE — POTASSIUM SILICATE [E3]

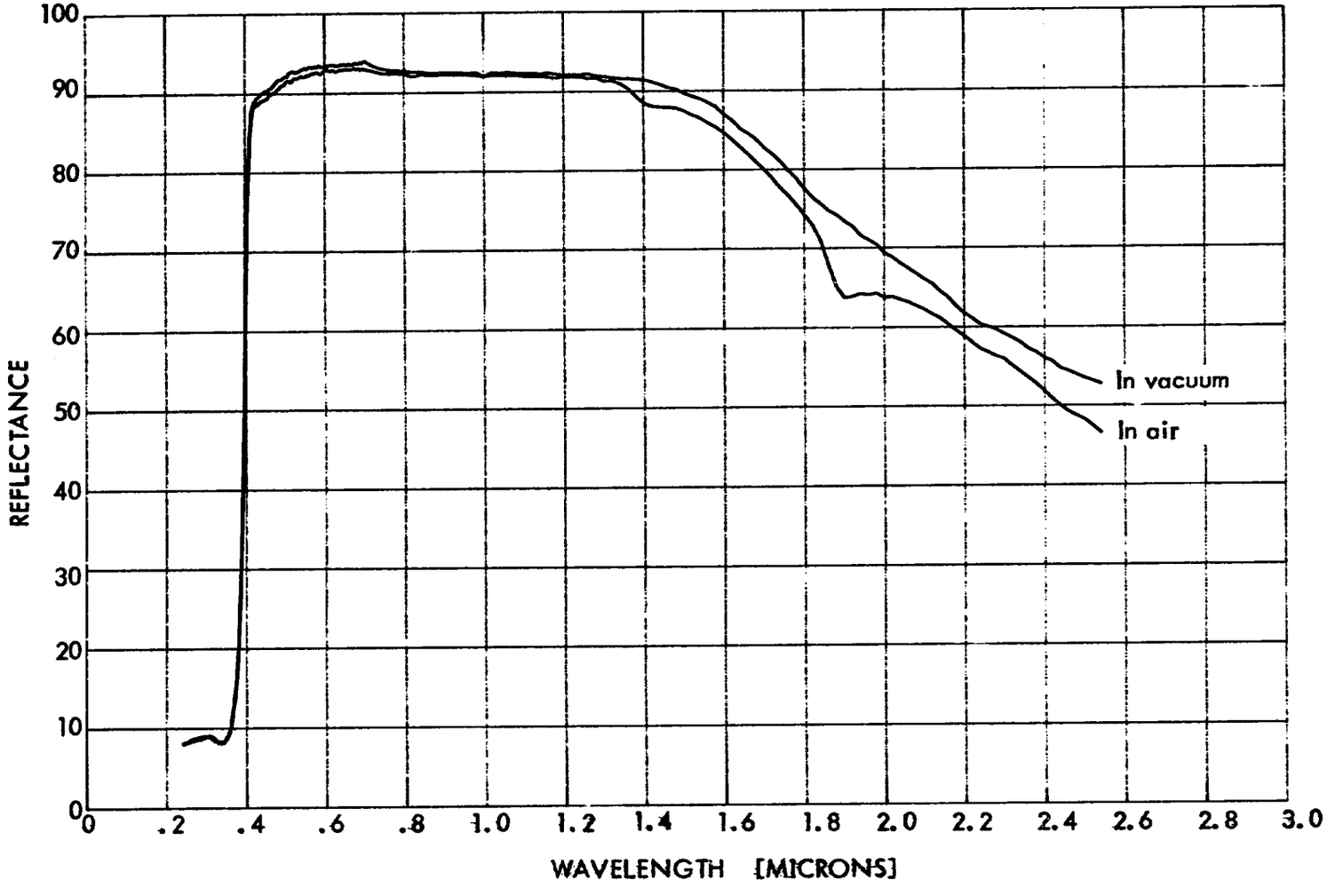

FIGURE 65.
IN AIR/IN VACUUM REFLECTANCE PROPERTIES OF NASA-GODDARD
ZINC OXIDE/ALUMINUM OXIDE — POTASSIUM SILICATE [F3]

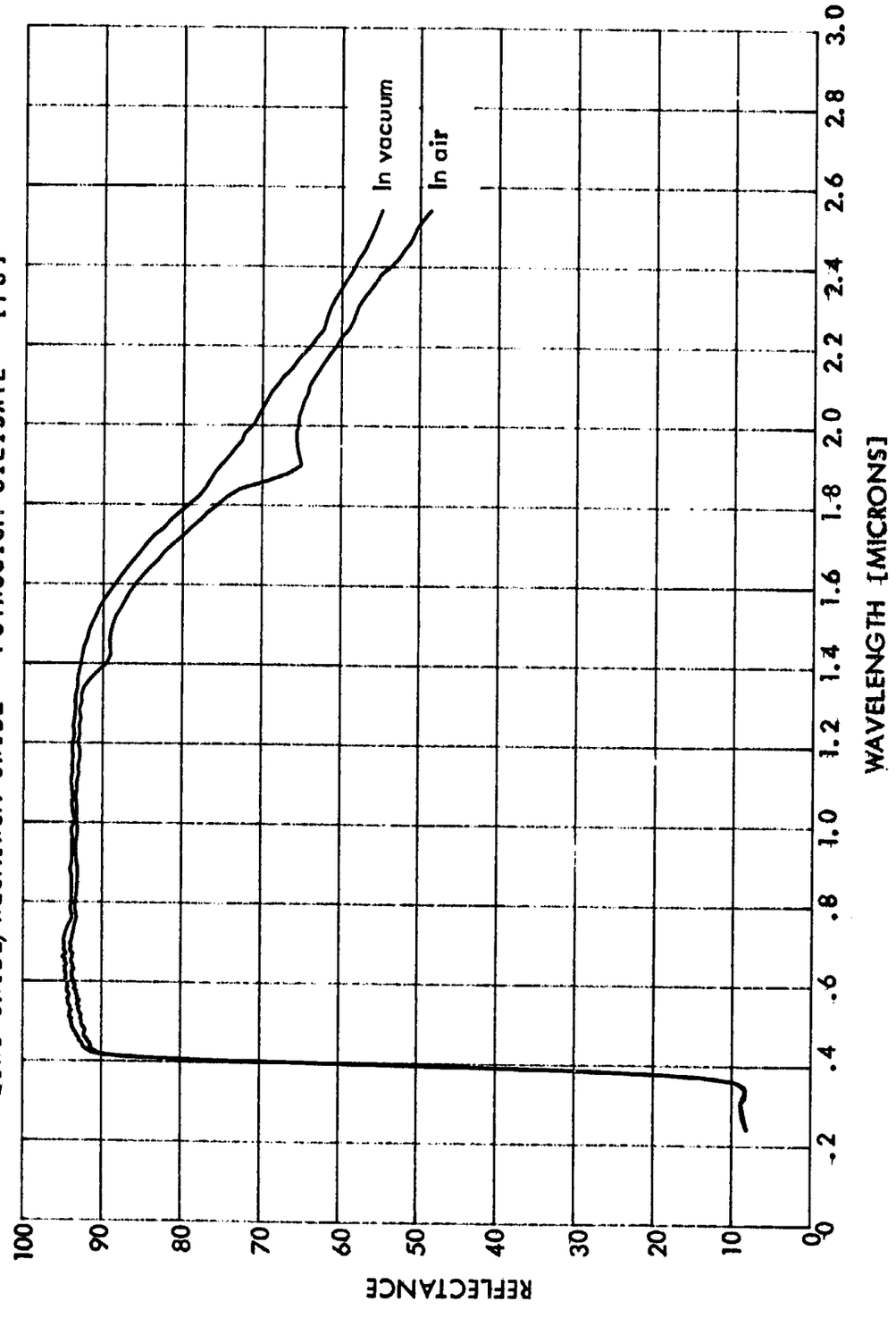

FIGURE 66.

IN AIR/IN VACUUM REFLECTANCE PROPERTIES OF NASA-GODDARD ALUMINUM OXIDE — POTASSIUM SILICATE [D3]

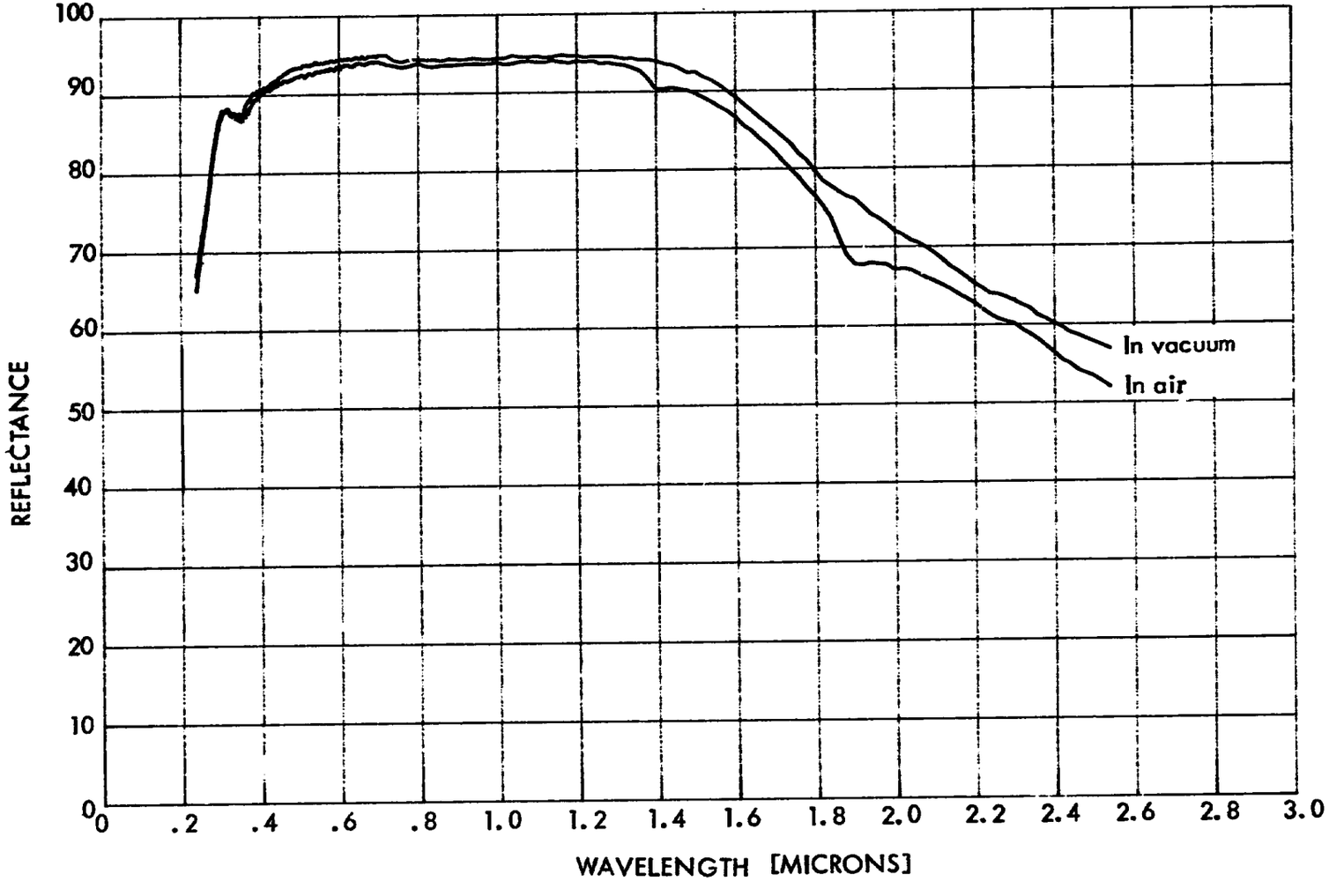

3.0 NEW TECHNOLOGY

The research performed under Contract NAS5-11219 has been reviewed for the purpose of uncovering potential reportable New Technology items. The review activities have considered the results of each study by itself, and the correlation of those results with knowledge of the various coatings already available. To the best of our knowledge, there is no New Technology to report.

4.0 CONCLUSIONS AND RECOMMENDATIONS

The in situ results and findings of this program are definitive enough to allow certain conclusions to be reached, and certain recommendations to be made.

4.1 CONCLUSIONS

1. Among the metallized Teflon coatings studied, the 2-mil materials offer superior initial solar absorptance characteristics and reasonably good stability during particle irradiation. Where lowest solar absorptance is required, and surface conformability is not a problem during application, these coatings (especially 2-mil silvered Teflon) should supplant earlier coating developments.

2. Vapor-deposited aluminum overcoatings (Al_2O_3 in type G and SiO_2 in type H) are more stable under exposure than are the anodized aluminum materials studied (Alzak).

3. Aluminum oxide pigment in a potassium silicate binder is the only white diffuse coating studied that is reasonably stable during particle irradiation. In contrast, solar absorptance more than doubles as a result of particle exposure of some of the other white diffuse coatings studied.

4. The spectral reflectance degradation characteristics of the coating materials studied may be classified into four types: (1) absorption band edge damage, (2) short wavelength damage, and (3) broad-band damage (damage in all three of these cases being manifested with about the same spectral character by protons and electr · alike); and (4) visible-region proton damage and infrared-region electron damage. Proton-induced damage at shorter wavelengths dominates in the specular materials comprising the first two damage classifications, whereas electron-induced damage at longer wavelengths tends to dominate in the diffuse coatings that constitute the other two damage categories.

5. These damage classifications can be related to the absorption of energy from the sun (or that used in making measurements) as a function of distance into a coating, and are related to electron and proton radiation penetration depths.

4.2 RECOMMENDATIONS

1. A temperature study should be initiated. The parameters of particle energy and types would be the same as those employed in this and previous work, and the influence of sample or coating temperature during exposure and measurement would be studied over a range from elevated to cryogenic levels.

2. A proton energy study should be continued, using selected sample temperatures as expected in space. Proton energy range would encompass that of primary concern for space applications.

3. Combined particle-ultraviolet radiation exposures should be conducted to evaluate synergistic effects in the coatings being studied, and by this better simulation improve the predictions of thermal control coating performance in space use.

4. The importance of measuring coating emittance as well as solar absorptance in situ should be studied analytically and evaluated experimentally during electron, proton, and ultraviolet radiation exposures. Experimental results from this and earlier programs indicate that reflectance-changing effects of electrons and protons do not stop at 2.5μ (the current in situ wavelength limit and end of the wavelength region important for the determination of solar absorptance). Rather these effects seem to extend to longer infrared wavelengths important for the determination of coating emittance.

REFERENCES

1. Fogdall, L.B., and Cannaday, S.S., "Dependence of Thermal Control Coating Degradation Upon Electron Energy", Final Report for NASA-Goddard Contract NAS5-11164; Boeing Document D2-126114-1, May, 1969.

2. Fogdall, L.B., Cannaday, S.S., and Brown, R.R., "Electron Energy Dependence for In-Vacuum Degradation and Recovery in Thermal Control Surfaces", Progress in Astronautics and Aeronautics: Thermophysics: Applications to Thermal Design of Spacecraft, Volume 23, Academic Press, New York, 1970.

3. Fogdall, L.B. and Cannaday, S.S., "In Situ Electron, Proton, and Ultraviolet Radiation Effects on Thermal Control Coatings". Final Report for NASA-Goddard Contract NAS5-9650; Boeing Document D2-84118-9. January, 1969.